

# Regional crop yield forecasting using probabilistic crop growth modelling and remote sensing data assimilation

**Promotor:**

Prof. dr. sc. nat. M.E. Schaepman  
Hoogleraar Geo-Informatiekunde mbav Remote Sensing,  
Wageningen Universiteit (Nederland)

**Co-promotoren:**

Drs. P.J.J.F. Torfs  
Universitair hoofddocent bij de Leerstoelgroep Hydrologie  
en Kwantitatief Waterbeheer, Wageningen Universiteit (Nederland)

Dr. ir. S. de Bruin

Universitair docent bij het Laboratorium voor Geo-Informatiekunde  
en Remote Sensing, Wageningen Universiteit (Nederland)

**Promotiecommissie:**

Prof. dr. ir. H. van Keulen – Wageningen Universiteit (Nederland)  
Prof. dr. ir. B.J.J.M. van den Hurk – KNMI (Nederland)  
Prof. dr. C.J. Tucker – University of Maryland (USA)  
Dr. A.J. Challinor – University of Leeds (UK)

Dit onderzoek is uitgevoerd binnen de onderzoekschool SENSE  
'Netherlands Research School for the Socio-Economic and Natural  
Sciences of the Environment'

# Regional crop yield forecasting using probabilistic crop growth modelling and remote sensing data assimilation

Allard de Wit

Proefschrift  
ter verkrijging van de graad van doctor  
op gezag van de rector magnificus  
van Wageningen Universiteit  
Prof. dr. M.J. Kropff  
in het openbaar te verdedigen  
op vrijdag 19 oktober 2007  
des namiddags te vier uur in de aula

Allard de Wit

Regional crop yield forecasting using probabilistic crop growth modelling  
and remote sensing data assimilation

Thesis Wageningen University, Wageningen 2007.  
With summaries in English and Dutch.

ISBN 978-90-8504-709-4

*Aan mijn ouders,  
voor alle kansen en steun die ze mij gegeven hebben*



# Voorwoord

Mijn eerste kennismaking met het onderwerp van mijn proefschrift gaat terug tot 1995 toen ik als afstudeervakker ging werken bij het toenmalige DLO Staring Centrum. Na een korte periode werkzaam te zijn geweest bij de Meetkundige Dienst van Rijkswaterstaat, ben ik in 1997 in dienst getreden bij het DLO Staring Centrum waar ik eerst enige jaren gewerkt heb aan het Landelijk Grondgebruiksbestand Nederland (LGN). In 2001 heb ik de ontwikkeling van LGN overgedragen en ben ik samen met collega's weer gaan werken aan regionale toepassing van gewasgroeimodellen en remote sensing voor oogstvoorspellingen.

Terugkijkend op deze periode van meer dan 10 jaar concludeer ik dat ik met veel plezier gewerkt heb aan een groot aantal projecten op het gebied van remote sensing, GIS, gewasgroeimodellen, geostatistiek en landgebruik waarvan de resultaten in meer of mindere mate hebben bijgedragen aan mijn proefschrift. Enerzijds is er het voordeel dat je, als onderzoeker in dienstverband, aan een proefschrift kunt werken zonder de druk van een deadline van vier jaar. Anderzijds is het soms moeilijk om voldoende prioriteit te geven omdat er zo veel andere zaken (projecten, voorstellen, vergaderingen, reizen en administratie) om aandacht vragen. Dat het mij uiteindelijk gelukt is om een proefschrift te voltooien is dan ook mede dankzij de inbreng en steun van een aantal mensen die ik hierbij wil bedanken.

Ten eerste de geestelijk vader van CGMS en de toepassing daarvan op regionale schaal: Kees van Diepen. Dit proefschrift bouwt direct voort op het werk van Kees en zonder zijn inhoudelijke kennis en inzet had ik nooit zo ver kunnen komen. Daarnaast ben ik hem zeer erkentelijk voor zijn bereidheid om de administratieve last op zich te nemen van een aantal grote projecten. Hierdoor stelde hij mij in staat om me op de inhoud te richten en de resultaten te produceren die deels in dit proefschrift zijn opgenomen.

Mijn promotor en co-promotoren, Michael Schaepman, Sytze de Bruin en Paul Torfs wil ik bedanken voor de wetenschappelijke ondersteuning die nodig is om een proefschrift te voltooien. Michael heeft bovendien de gave om zeer snel de lacunes in mijn teksten te kunnen vinden, waardoor ik op efficiënte wij-

ze een verzameling artikelen heb kunnen combineren tot een proefschrift. Sytze en Paul zijn onmisbaar geweest bij het uitwerken van de (geo)-statistische details die belangrijk zijn bij het berekenen en interpreteren van de resultaten in hoofdstukken 4 & 5. Peter Troch wil ik bedanken voor zijn hulp en ideeën ten aanzien van data assimilatie.

Hendrik Boogaard heeft mij wegwijs gemaakt in de praktische kanten van CGMS en de achterliggende database en heeft een belangrijke bijdrage geleverd aan hoofdstukken 2 & 3. De hulp van Joost Wolf, Henk van der Ham en Daniël van Kraalingen t.a.v. allerhande inhoudelijke en praktische zaken over WOFOST en ORACLE mag niet onvermeld blijven. Verder wil ik Bart van den Hurk bedanken voor zijn bereidheid om mij gebruik te laten maken van de ELDAS datasets waarop hoofdstukken 3 & 4 deels gebaseerd zijn.

Gerard Nieuwenhuis en Jandirk Bulens wil ik bedanken voor de ruimte die ik heb gekregen om het in dit proefschrift beschreven onderzoek uit te voeren. Bij het bijeenbrengen van de onderdelen die tezamen mijn proefschrift vormen, ben ik begeleid door Maja Kooistra. De hulp van Maja is onmisbaar geweest bij het formuleren van projecten waarvan ik de resultaten in mijn proefschrift heb kunnen gebruiken. De strakke layout van dit proefschrift is voor een belangrijk deel te danken aan Arend Ligtenberg wiens LaTeX stijl ik heb hergebruikt en de mooie omslag is verzorgd door mijn zus: Leonie de Wit.

The help of Klaus Scipal and Wolfgang Wagner from the Institute of Photogrammetry and Remote Sensing of the Vienna University of Technology is acknowledged for providing the SWI dataset and the rapid answers to questions from my side.

Ten slotte wil ik Marlies bedanken voor de morele steun de afgelopen maanden. Hoewel je zelf zegt dat het je ‘is meegevallen’ heb ik toch minder tijd en aandacht geschonken dan ik normaal zou hebben gedaan. Ik hou van jou en ik zie de toekomst met jou en Geert met vertrouwen tegemoet.



# Abstract

Information on the outlook of yield and production of crops over large regions is essential for government services dealing with import and export of food crops, for agencies playing a role in food relief, for international organisations with a mandate in monitoring the world food production and trade, as well as for commodity traders. In Europe, such information is provided by the MARS (Monitoring Agriculture with Remote Sensing) Crop Yield Forecasting System operated by the Joint Research Centre. An important component in the MARS Crop Yield Forecasting System is the so-called Crop Growth Monitoring System (CGMS). This system employs the WOFOST crop growth model to determine the influence of soil, weather and management on crop yield with a spatial resolution of  $50 \times 50$  km grid. Aggregated CGMS results are used as predictors for crop yield at the level of EU member states.

CGMS is being applied successfully within the framework of the MARS crop yield forecasting system. Nevertheless, there are large uncertainties related to applying WOFOST over large areas such as poorly known sowing dates and soil parameters, application of irrigation and the effect of drought due to limited weather station density. This thesis focuses on developing and testing methods for quantifying and reducing uncertainty in crop model simulations with a focus on reducing the uncertainty related to drought. The uncertainty in crop model simulations is quantified through the variability within an ensemble of models, while it is reduced by combining crop model simulations with satellite-derived information through an ensemble Kalman filter (EnKF). A key aspect in this approach is that the uncertainty of the different components of the system can be estimated. The ultimate goal is to improve the accuracy and timeliness of regional crop yield forecasts.

It was demonstrated that the uncertainty in the interpolated meteorological forcings is important, particularly the uncertainty in precipitation fields. Therefore, a method was developed to generate equiprobable realisations of precipitation inputs which can be used as input in the crop simulation model. It was demonstrated that the statistical properties of the precipitation field were reproduced reasonably well in the realisations, while the deviations from

the target statistics that were found are of minor importance for crop models.

Further, an ensemble Kalman filter was used to assimilated satellite observations of root-zone soil moisture for Spain, France, Germany and Italy over the period 1992–2000 for winter-wheat and grain maize. It was demonstrated that the assimilation of satellite observations lowered the error on a linear regression model between crop simulation model output and EUROSTAT winter-wheat yield statistics for 66% of the administrative regions. For grain maize the improvement was less evident because improved relationships could be found for 56% of the regions. At national level, the results of the regression only improved for Spain, but not for Germany, France and Italy. Although the results at national level were somewhat disappointing, it is encouraging that the results did improve for Spain where crop production is most affected by water limitation and thus the potential for improvement is greatest.

Finally, it was concluded that the developed approach is operationally feasible because the algorithms are applicable at continental scale, the satellite data applied will be available at least until 2018 and the method does not rely on site-specific data. Therefore, the approach presented in this thesis can be applied within the European MARS system and has the potential to provide improved crop yield indicators for crop yield forecasting in many areas with major agricultural production of rainfed crops.

# Contents

<b>Voorwoord</b>	<b>vii</b>
<b>Abstract</b>	<b>ix</b>
<b>1 Introduction</b>	<b>1</b>
1.1 Background . . . . .	1
1.2 Operational application of RS in crop models . . . . .	4
1.3 Use of remote sensing derived products in CGMS . . . . .	6
1.4 Scope and objectives . . . . .	8
1.5 Outline of this thesis . . . . .	9
<b>2 Using NOAA-AVHRR land surface temperature</b>	<b>11</b>
2.1 Introduction . . . . .	11
2.2 Models . . . . .	13
2.2.1 WOFOST crop simulation model . . . . .	13
2.2.2 Crop Growth Monitoring System . . . . .	14
2.3 Data . . . . .	15
2.3.1 NOAA-AVHRR data . . . . .	15
2.3.2 Weather station locations and variables . . . . .	16
2.3.3 Pan-European Land Cover Database . . . . .	16
2.4 Methods . . . . .	18
2.4.1 Comparing surface temperature to air temperature . . . . .	18
2.4.2 Correction and aggregation of surface temperature . . . . .	18
2.4.3 Temporal interpolation of the surface temperature . . . . .	20
2.4.4 Magnitude correction of the surface temperature . . . . .	22
2.4.5 CGMS model simulation approach . . . . .	23
2.5 Results . . . . .	24
2.5.1 Comparison with independent weather-stations . . . . .	24
2.5.2 Spatial distribution of the temperature sums . . . . .	24
2.5.3 Crop simulation results . . . . .	26
2.6 Conclusions and discussion . . . . .	30

<b>3</b>	<b>Spatial resolution of precipitation and radiation</b>	<b>33</b>
3.1	Introduction . . . . .	33
3.2	Methodology . . . . .	35
3.2.1	The crop simulation model . . . . .	35
3.2.2	The Crop Growth Monitoring System . . . . .	35
3.2.3	Study area . . . . .	36
3.2.4	Soil and weather inputs . . . . .	37
3.2.5	High resolution precipitation and radiation inputs . . . . .	39
3.2.6	Setup of the experiment . . . . .	39
3.3	Results . . . . .	41
3.3.1	Comparison of CGMS and ELDAS fields . . . . .	41
3.3.2	Uncertainty of simulated crop yields . . . . .	42
3.3.3	Scaling of crop yield simulation results . . . . .	45
3.3.4	Results at national level and influence on the crop yield forecast . . . . .	45
3.4	Discussion . . . . .	50
3.5	Conclusions . . . . .	52
<b>4</b>	<b>Representing uncertainty in precipitation fields</b>	<b>53</b>
4.1	Introduction . . . . .	53
4.2	Data . . . . .	57
4.2.1	CGMS meteorological database . . . . .	57
4.2.2	ELDAS precipitation data . . . . .	58
4.2.3	Exploratory analyses of ELDAS and CGMS databases . . . . .	58
4.3	Method . . . . .	62
4.3.1	Conceptual modelling . . . . .	62
4.3.2	Normal score transformation . . . . .	63
4.3.3	Variogram modelling . . . . .	64
4.3.4	Simulation of residual fields . . . . .	65
4.3.5	Evaluation of precipitation realisations . . . . .	66
4.3.6	Probabilistic crop yield forecasting . . . . .	66
4.4	Results . . . . .	68
4.4.1	Distribution of precipitation residuals . . . . .	68
4.4.2	Variogram modelling . . . . .	69
4.4.3	Precipitation realisations . . . . .	72
4.4.4	Probabilistic crop yield forecasting . . . . .	80
4.5	Discussion . . . . .	80
4.6	Conclusions . . . . .	82

<b>5</b>	<b>Data assimilation with the ensemble Kalman filter</b>	<b>87</b>
5.1	Introduction . . . . .	87
5.2	Spatially distributed probabilistic crop growth model . . . . .	90
5.2.1	The crop growth model . . . . .	90
5.2.2	Spatial implementation of crop growth simulations . . . . .	90
5.2.3	The ensemble Kalman filter . . . . .	91
5.3	Study area . . . . .	92
5.4	Data and methods . . . . .	93
5.4.1	Deterministic crop, soil and weather inputs . . . . .	93
5.4.2	Probabilistic weather inputs . . . . .	94
5.4.3	Satellite derived soil water index (SWI) . . . . .	94
5.4.4	Influence of ensemble size . . . . .	95
5.4.5	Crop yield forecasting experiment setup and initialisation . . . . .	96
5.4.6	Spatial aggregation of simulation results . . . . .	96
5.4.7	Evaluation of model performance . . . . .	97
5.5	Results . . . . .	99
5.5.1	Impact of ensemble size . . . . .	99
5.5.2	Analyses of filter innovations . . . . .	103
5.5.3	Yield forecasting performance . . . . .	111
5.6	Discussion and conclusions . . . . .	114
<b>6</b>	<b>Conclusions</b>	<b>125</b>
6.1	Introduction . . . . .	125
6.2	Synthesis . . . . .	126
6.3	Reflection . . . . .	129
6.4	Priorities and further research . . . . .	132
	<b>References</b>	<b>146</b>
	<b>Extended summary</b>	<b>147</b>
	<b>Samenvatting</b>	<b>151</b>
	<b>Curriculum vitae</b>	<b>155</b>
	<b>Selected publications</b>	<b>157</b>



# List of Figures

2.1	The location of selected weather stations over western Europe. .	17
2.2	A schematic overview of the processing steps that were applied to the daily AVHRR images in order to obtain the average surface temperature for each CGMS grid cell. . . . .	20
2.3	Two examples of scatter plots between the maximum air temperature obtained from weather station ( $T_a^{max}$ ) and the area-averaged surface temperature obtained from NOAA-AVHRR ( $T_0$ ). .	21
2.4	Development of cumulative surface temperature ( $T_0$ ) for five locations in 1996, using two different approaches to account for missing data: Interpolation using the maximum air temperature (dashed lines) and substitution of the monthly average surface temperature (solid line). . . . .	22
2.5	The difference ( $\sum T_a^{max} - \sum T_a^{sim}$ ) between the cumulative maximum air temperature ( $\sum T_a^{max}$ ) measured at six independent stations and the cumulative simulated maximum air ( $\sum T_a^{max}$ ) derived from the AVHRR data. . . . .	25
2.6	Histogram of the 1995 (A) and 1996 (B) cumulative temperature for the CGMS gridcells in Spain, obtained using classic CGMS approach (thin line) and the satellite CGMS approach (thick line). . . . .	25
2.7	Spatial patterns of the yearly temperature sums that were derived from observed weather and AVHRR-derived surface temperature for 1995 and 1996. Each map is plotted as a 1/8 quantile map, where each legend interval represents 12.5% of the total data. . . . .	26
2.8	Histograms of the 1995 (A) and 1996 (B) CGMS simulated potential biomass for winter-wheat using the classic CGMS approach (thin line) and the satellite CGMS approach (thick line). .	27

2.9	Simulated potential green leaf area index for winter-wheat (A) and sunflower (B) during 1995 and 1996 for a CGMS grid cell near Zaragoza. Classic CGMS approach drawn as solid lines, satellite CGMS approach drawn as dashed lines . . . . .	29
2.10	Histograms of the 1995 (A) and 1996 (B) CGMS simulated potential biomass for sunflower using the classic CGMS approach (thin line) and the satellite CGMS approach (thick line). . . . .	30
3.1	Overview of the study area showing the NUTS0 regions (thick black country borders), the NUTS1 regions (grey provincial borders), the 50 × 50 km CGMS grid (black square grid) and the 10 × 10 km grid (grey square grid). . . . .	38
3.2	Scatter plot between water-limited yield storage organs (yield) at 50-km grid level obtained from the CGMS-Standard and CGMS-ELDAS- 50 experiments for winter-wheat (A) and grain maize (B). . . . .	44
3.3	Scatter plot between water-limited yield storage organs (yield) at NUTS1 level obtained from the CGMS-Standard and CGMS-ELDAS-50 experiments for winter-wheat (A) and grain maize (B). . . . .	45
3.4	Scatter plot between water-limited yield storage organs (yield) obtained from the CGMS-ELDAS-50 experiment and the average water-limited yield storage organs obtained from the CGMS-ELDAS-10 experiment for winter-wheat (A) and grain maize (B). Error bars are plus and minus one standard deviation. . . . .	47
3.5	Time evolution of the yield forecast for grain maize in Germany for the year 2000. The thick line is the official yield for the year 2000 as reported by the European Statistical Office (EUROSTAT). The dotted lines are plus and minus one standard deviation of the de-trended EUROSTAT yields over the period 1990–1999. . . . .	49
3.6	Time evolution of the yield forecast for grain maize in France for the year 2000. The thick line is the official yield for the year 2000 as reported by the European Statistical Office (EUROSTAT). The dotted lines are plus and minus one standard deviation of the de-trended EUROSTAT yields over the period 1990–1999. . . . .	50



4.1	Root Mean Squared Error of daily precipitation values in the CGMS database versus the ELDAS reference dataset for the period 1-October-1999 until 31-December-2000. The black skewed rectangles represent CGMS grids that were removed from the analyses based on a slope criterion. . . . .	60
4.2	Scatter plot of precipitation residuals (ELDAS - CGMS) versus CGMS precipitation amounts. . . . .	61
4.3	Flow diagram of the ensemble simulation approach. . . . .	67
4.4	Histograms of precipitation residuals for selected CGMS precipitation intervals. Continuous lines represent the normalised histogram for the period 1-January-2000 until 31-December-2000. Dashed lines represent the normalised histogram for per the period 1-October-1999 until 31-December-1999. . . . .	70
4.5	Spatial variograms of the normal score transformed residuals for selected dates (dashed lines; 1 <sup>st</sup> , 11 <sup>th</sup> , 21 <sup>st</sup> of each month) and weighted average variogram of all selected dates (thick continuous line). . . . .	71
4.6	Temporal variograms of the normal score transformed residuals for selected CGMS grids. . . . .	72
4.7	Comparison of model-induced indicator variograms (continuous line) and observed indicator variograms for different quantiles ( $p$ ) of the normal score transformed residuals. . . . .	73
4.8	Quantile-Quantile plots of precipitation quantiles for precipitation time-series of three selected grids in South-Spain (30032), South-France (43044) and C-Germany (59051): ELDAS precipitation sequence vs. CGMS precipitation sequence (figure A, C & E) and ELDAS precipitation sequence vs. 100 realised precipitation sequences (figure B, D & F). . . . .	75
4.9	Variograms of the ELDAS precipitation data (continuous line) and simulated precipitation fields (symbols; five realisations). . . . .	76
4.10	Dry-spell lengths from the CGMS and ELDAS precipitation datasets and dry-spell lengths for 25 precipitation simulations, for six representative sites. . . . .	77
4.11	Wet-spell lengths from the CGMS and ELDAS precipitation datasets and wet-spell lengths for 25 precipitation simulations, for six representative sites. . . . .	78
4.12	Comparison of a single precipitation realization, the CGMS input precipitation field and the ELDAS reference precipitation field. . . . .	79

4.13	Crop yield forecast during the growing season in 2000. Thick black line is the official reported yield by EUROSTAT, the blue line represents the deterministic yield forecast and the dotted lines represent the influence of uncertainty in precipitation on the yield forecast. Density plots indicate the shape of the yield forecast ensemble at three moments during the growing season.	83
5.1	Overview of the study area (greyed area) including country borders, provincial borders (NUTS1) and 50 × 50 km CGMS grid.	92
5.2	$R^2$ values of a series of regression models (one per dekad) between reported EUROSTAT yield of winter-wheat for Spain and WOFOST simulated total crop biomass of winter-wheat over the period 1992–2000. One series is based on the trend in the statistics only (marked as ‘f(trend only)’) and the second series using both the trend and the WOFOST simulation results (marked as ‘f(trend + WOFOST)’). The residual error of the regression model with the lowest error is plotted as a percentage of mean crop yield.	98
5.3	Temporal evolution of ensemble mean and variance for grids 30032 and 54041.	102
5.4	Maps of yearly total soil moisture innovations for grain maize simulations for the campaigns 1993 and 1999.	105
5.5	Maps of yearly total soil moisture innovations for winter-wheat simulations for the campaigns 1993 and 1999.	106
5.6	Temporal patterns of the soil moisture innovations for grain-maize simulations for four selected grids over the period 1992–2000.	107
5.7	Temporal patterns of the soil moisture innovations for winter-wheat simulations for four selected grids over the period 1992–2000.	108
5.8	Distribution of normalised filter innovations (thick line) and a standard normal distribution (thin line).	109
5.9	Soil moisture climatology for WOFOST simulations (mean 0.229, SD 0.047) and Soil Water Index (mean 0.207, SD 0.045).	110
5.10	Distribution of normalised innovations for normal observation variance (left) and inflated observation variance (right).	111
5.11	Normalised regression performance for winter-wheat and grain maize.	112

- 
- 5.12 Spatial distribution of regression results for NUTS1 (A) and NUTS2 (B) regions for winter-wheat. Bar charts in the maps give a relative indication of the residual error on the regression between EUROSTAT statistics for the trend-only, the EnKF experiment and the classic experiment. Regions are coloured according to the best performing system. . . . . 113
- 5.13 Spatial distribution of regression results for NUTS1 (A) and NUTS2 (B) regions for grain maize. Bar charts in the maps give a relative indication of the residual error on the regression between EUROSTAT statistics for the trend-only, the EnKF experiment and the classic experiment. Regions are coloured according to the best performing system. . . . . 115



# List of Tables

2.1	Regression parameters and correlation coefficient derived from an empirical relationship between $T_0$ and $T_a^{max}$ . . . . .	23
3.1	Summary of experiments and related scales and input data. . . .	41
3.2	Summary statistics of the differences between the CGMS and ELDAS databases (CGMS minus ELDAS) for radiation and precipitation averaged over all CGMS grids. . . . .	42
3.3	Summary statistics of the crop yield at 50×50 km grids obtained by the CGMS-Standard and CGMS-ELDAS-50 experiments. . . .	43
3.4	Summary statistics of the simulated crop yield at NUTS1 level of the CGMS-Standard and CGMS-ELDAS-50 experiments. . . .	46
3.5	Results from a linear regression between water-limited yield storage organs of the CGMS-ELDAS-50 experiment (50 × 50 km) and the water-limited yield storage organs of the CGMS-ELDAS-10 experiment (10 × 10 km). CGMS-ELDAS-10 results are averaged over the CGMS-ELDAS-50 grid. The intercept of the regression is assumed to be zero. . . . .	46
3.6	Simulation results obtained by the CGMS-Standard and CGMS-ELDAS-50 experiments at the end of the growing season aggregated to the national level for France and Germany. . . . .	48
3.7	$R^2$ values describing the results from the regression between the official yield statistics as reported by the European Statistical Office (EUROSTAT) and the crop yield indicators derived from the Crop Growth Monitoring System (CGMS) over the period 1990–1999. . . . .	48
4.1	Confusion matrix of precipitation intervals in the ELDAS and CGMS databases for the year 2000. Numbers are given as a percentage of the column total. . . . .	84

4.2	Confusion matrix of precipitation intervals in the ELDAS databases versus 25 realizations for the year 2000. Numbers are given as a percentage of the column total. . . . .	85
5.1	Estimates of RMSE on ensemble average and ensemble variance of volumetric soil moisture estimates throughout the growing season. Simulations were carried out for grain maize for five grids located in southern Spain (30032), northern Spain (40036), southern France (43044), northern France (54041) and central Germany (59061). . . . .	101
5.2	Residual error (% of mean yield) on the relationship between regional simulated biomass values and the EUROSTAT regional crop yield statistics for winter-wheat. . . . .	118
5.3	Residual error (% of mean yield) on the relationship between regional simulated biomass values and the EUROSTAT regional crop yield statistics for grain maize. . . . .	120

# Chapter 1

## Introduction

### 1.1 Background

In 1988 the Council of Ministers of the European Union (EU) decided to set up a project to improve the provision of agricultural statistics which are necessary to manage the large budgets involved in the European Common Agricultural Policy (CAP). This project has become known as the MARS project (Monitoring Agriculture by Remote Sensing) and it comprised different activities such as regional crop inventories, satellite-based rapid crop area estimates, assessment of foreign agricultural production and an agricultural information system (Council of the European Community, 1988).

The agricultural information system activity focused on providing early crop yield forecasts for the EU countries and used two approaches for providing indicators for crop yield prediction. The first approach used indicators derived from low resolution (1-km) sensors such as NOAA's AVHRR sensor (Advanced Very High Resolution Radiometer) onboard POES (Polar Operational Environmental Satellite). Daily AVHRR imagery were recorded, stored and processed into 10-day composites. Crop growth indicators such as surface temperature or Normalised Difference Vegetation Index (NDVI) were derived that could help in characterizing the growing season and quantifying the crop yield (Sharman, 1992).

The second approach focused on developing an agrometeorologic system employing crop growth models to estimate crop yield. For this purpose, weather data from weather stations were interpolated to a  $50 \times 50$  km grid and the WOFOST crop growth model (WOrld FOod STudies) was applied to each grid. The simulation results per crop type were stored in a database and spatially aggregated to administrative regions in order to be used as predictors for crop yield forecasting. This system has become known as the Crop Growth

Monitoring System (CGMS) (Diepen, 1992; Vossen and Rijks, 1995; Genovesi, 1998).

Despite the initial focus on the use of remote sensing techniques for crop yield forecasting within the MARS project, it was gradually recognized that remote sensing derived indicators played a minor role in forecasting of crop yield in Europe, as Vossen and Rijks (1995, page 5) state: *“Although remote sensing techniques are presently being turned into operational tools for crop acreage inventories, land utilisation assessment and low resolution vegetation condition monitoring, they do not permit yet, for various reasons, the quantitative prediction and assessment of regional or national mean crop yields within the E.U.”*

Vossen and Rijks (1995, pages 5 & 108) also mention several reasons for the relatively poor performance of using optical, low resolution satellite data for crop yield forecasting in Europe:

- Land cover in Europe is highly fragmented and interpretation of low resolution data is therefore often ambiguous because it represents most often a mixture of several land cover types;
- Lack of consistent time-series of remote sensing data due to persistent cloud cover, sensor calibration problems or satellite mission continuity. This renders regression analyses on time-series of remote sensing derived indicators for yield forecasting problematic;
- The non availability of proven models to relate satellite information to quantitative yield estimates on a regional scale. This is related to the lack of sensitivity of commonly used remote sensing indicators (e.g. NDVI) in much of Europe due to the high crop production levels and the relatively small year-to-year variability.

Except for a lack of sensitivity for some regions and crop types, the agrometeorologic approach employed within CGMS does not suffer from the above-mentioned drawbacks: The interpretation of results is straightforward because specific crops can be modelled and the results can be easily compared with statistical data. Moreover, the results are available and consistent over long time-series due to a long-term record of meteorological observations available. As a result, the approach for quantitative crop yield prediction within the MARS project gradually shifted towards an agrometeorologic approach, while remote sensing derived indicators were merely used as qualitative descriptors of the growing season.

Although the Crop Growth Monitoring System was originally envisaged as a backup system in case of unavailability of satellite data (Kees van Diepen, pers. comm.), it has become the backbone of the MARS crop yield forecasting



system. Since 1994, CGMS operationally monitors crop growth in the European Union, Eastern-Europe, Anatolia and the Maghreb. Its main purpose is to provide information on weather indicators and crop status during the growing seasons and to provide objective forecasts of crop yield on the level of EU member states early in the crop growth season (see <http://www.marsop.info>).

After the initial MARS project phase (1988–1994), the Crop Growth Monitoring System has been improved incrementally on a number of aspects over the last 15 years:

- CGMS has been implemented for the EU12 and then gradually extended towards EU15, the Central European countries, Eastern Europe up to the Ural mountains, Turkey and the Maghreb;
- In parallel with the spatial extension, the network of weather stations has been extended and densified so that the system could profit from improved interpolated meteorologic fields;
- Operational aspects of the system have been gradually improved and integrated into an automated processing chain covering the full cycle from ingestion of weather to the forecasting of crop yield and the automated production of maps, charts and tables;
- Improvements in database technology and processing speed have greatly improved the ability to interactively query the database and generate maps and tables on-the-fly using a dedicated client application or a website.

Despite the success of CGMS in an operational framework and the technological improvements listed above, the thematic approach in CGMS is still largely similar to what was developed within the MARS project. Few improvements have been made to the original WOFOST modelling concept and some of the key uncertainties related to applying WOFOST on the regional scale have not been resolved. Examples of these uncertainties are the generally unknown within-season sowing dates, the uncertainty in the effect of drought due to limited weather station density and poorly known soil parameters, the lack of information about irrigation and the weighting of individual simulation results to administrative regions (Vossen and Rijks, 1995, pages 105–109).

Moreover, the deterministic modelling approach which is currently implemented in CGMS is not capable of accounting for uncertainties and quantifying their influence on the crop yield forecast. Remote sensing has often been mentioned as a means to resolve some of the uncertainties mentioned, but the use of remote sensing in crop models has its own set of challenges which will be outlined in the following section.

## 1.2 Application of remote sensing in crop growth models in an operational context

Crop yield forecasting applications applied over large areas and relying on a spatially distributed crop growth model are typically confronted with large uncertainty in the spatial distribution of soil properties and initial soil conditions, crop parameters and meteorologic forcings (Hansen and Jones, 2000). Within the crop growth model, this uncertainty influences the simulation of two important physiological processes: 1) the simulation of the crop canopy development which determines light interception and, when combined with temperature data, the potential for photosynthesis; 2) the simulation of moisture content in the soil which determines the actual evapotranspiration and reduction of photosynthesis as a result of drought stress. Improving the simulation of these two processes by using remotely sensed observations has been a field of intense research and an overview will be given in relation to operational application in yield forecasting systems.

Research on improving the simulation of crop canopy development has mostly focused on the use of sequences of high spatial resolution satellite imagery (20-30 m) to either recalibrate crop model parameters such as the emergence date, or to integrate the observations in a model using a forcing or updating approach (Bach and Mauser, 2003; Boegh et al., 2004; Bouman, 1995; Guérif and Duke, 2000; Maas, 1988; Moulin et al., 1998; Prevot et al., 2003; Schneider, 2003). Although results demonstrated that many crop model states (e.g. simulated biomass, leaf area index, yield) could be improved using satellite observations, such methods have proven difficult to be applied in crop yield forecasting applications operating at regional to continental scales.

The main reason for this slow adoption is the disparity in scales between the process (crop growth on fields often as small as 1 hectare) and the type of observing system that can be used operationally and economically over large areas with high temporal frequency (satellite sensor observations with a spatial resolution ranging from 250 m to 1 km). Given the relatively coarse spatial resolution of such satellite sensors, in many parts of the world the instantaneous field of view (IFOV) covers a mixture of various land cover types, making it difficult to estimate the value of crop states (assessed through LAI or biomass) for specific crops. Some studies attempted to cope with the sub-pixel heterogeneity directly (De Wit, 1999; Fischer, 1994; Moulin et al., 1995), while others attempted to unmix a coarse resolution signal into its underlying spectral components (Cherchali et al., 2000; Faivre and Fischer, 1997). The general drawback of these approaches is that they rely on the availability of

ancillary data (e.g. land cover/crop maps) which are usually not available over large areas for the current growing season.

A few studies describe yield forecasting results obtained by integrating coarse resolution satellite observations in crop simulation models at regional scales over areas with relatively homogeneous land cover. For example, Doraiswamy et al. (2005) used Leaf Area Index derived from MODIS 250m observations over Iowa (U.S.) to recalibrate crop model parameters, while Mo et al. (2005) used Leaf Area Index derived from NOAA-AVHRR as a forcing variable in a crop model for the North China Plain. Their results demonstrate that crop yield estimates improve when satellite observations are used to update or force a crop model. Nevertheless, these techniques can only be applied over regions with homogeneous land cover and a limited number of crop types. These studies also recognise that the results deteriorate in areas with complex land cover patterns where the satellite sensor signal consists of a mixture of many crop types.

Considerable work has also been carried out on the estimation of vegetation evapotranspiration or soil moisture by satellite thermal infrared observations with the aim of improving estimates of drought stress or water use (Courault et al., 2005; Oliso et al., 2005). Although promising semi-operational results have been demonstrated (Bastiaanssen and Ali, 2003; Roebeling et al., 2004), the use of these kind of observations in crop models remains very limited (Oliso et al., 2005). Besides the scale issues outlined before, other factors which limit operational application play a role, such as that no generally accepted operational systems have been available to routinely estimate actual evapotranspiration over large areas using satellite observations.

Additional to the thematic issues outlined above, it is also appropriate to state that remote sensing often has not delivered a convincing operational scenario that would justify the investments needed for operational implementation. Satellite missions often consist of a single or a few satellites being launched with no warranties on data continuity beyond the expected lifetime of the satellite (e.g. LandSat 7 ETM+, VGT on SPOT4/5 and MODIS on TERRA/AQUA). The exceptions here are the operational meteorological satellites such as the geo-stationary satellites (MeteoSat first and second generation, GOES, etc.) and their polar orbiting counterpart the NOAA-AVHRR. In the near future the NOAA-AVHRR type of satellites will be succeeded by the METOP and NPOESS satellites of the Joint Polar System (JPS) developed jointly by NOAA and EUMETSAT. Both the polar orbiting and geostationary systems managed by EUMETSAT have a mandate until 2018 and provide near-realtime data products for various operational services.

### 1.3 Use of remote sensing derived products in CGMS

Despite the challenges in the use of remote sensing listed in the previous section there are key uncertainties in regional crop modelling (section 1.1) where advantage could be taken from remote sensing products. However, for any sustainable operational use of remote sensing derived products in CGMS it is thus necessary to focus on the products that can be delivered by the geostationary and polar orbiting meteorological satellites.

Two products derived from geostationary satellites that can be used directly in CGMS are estimates of radiation and rainfall (Beyer et al., 1996; Grimes et al., 2003). Although these products can be used to improve the quality of CGMS meteorologic inputs, they are merely replacements of existing meteorological products and their implementation is a technical issue rather than a scientific challenge. Next, there is a range of biophysical products that can be derived from new optical instruments on the geostationary and polar orbiting satellites such as SEVIRI onboard MSG (Camacho de Coca et al., 2003) or in the near future VIIRS on NPOESS. These products will be useful for qualitative monitoring of the growing season, but have an inappropriate spatial resolution as was argued already in section 1.2.

A third product that will become available from the METOP satellites are soil moisture estimates derived from scatterometer measurements over land (Hasenauer et al., 2006). These soil moisture measurements are instantaneous measurements of the upper few centimeters only and therefore not directly useful for a crop model which needs root zone soil moisture and operates in daily time-steps. However, methods exist to derive a so-called soil water index (SWI) which is representative of the root-zone soil moisture (Ceballos et al., 2005; Wagner et al., 1999; Wagner et al., 2003).

Within CGMS, soil moisture is currently the only factor which limits the potential production, while its estimation is still one of the key uncertainties in the application of WOFOST on the regional scale (section 1.1). Therefore, the SWI product could potentially improve the soil water balance and increase the predictive capabilities of CGMS in terms of crop yield. An additional advantage of the SWI product is that a global archive is available over the period 1992–2000 based on observations of the scatterometer instruments onboard the European Radar Satellites (ERS1/2). This ensures that time-series of simulation results can be compared with time-series of regional crop yield statistics.

The spatial resolution of the SWI product derived from METOP is in the order of  $25 \times 25$  km. This resolution is even lower than the products derived from the low resolution optical sensors and it is therefore impossible to derive crop

specific estimates of root-zone soil moisture. However, two particular aspects of soil moisture make the resolution aspect less critical compared to products derived from low resolution optical sensors. First of all, in contrast to biophysical variables (e.g. LAI, biomass) or actual evapotranspiration, soil moisture is derived independently from the plant canopy and the retrieval process is therefore less influenced by the particular arrangement of land cover/crop patches within the resolution cell. In fact, the algorithms for soil moisture retrieval aim to remove all vegetation influence from the scatterometer signal before estimates of soil moisture can be made (Wagner et al., 1999).

Secondly, the spatial correlation length of variability in soil moisture is not only depending on local interactions between the land surface and the soil, but for a large part also on atmospheric patterns (rainfall, temperature, radiation) operating on spatial scales with a much larger spatial correlation length. Moreover, it has been shown that with increasing depth of the soil layer the atmospheric patterns become dominant in describing the spatial variability of the soil moisture fields, while the temporal variability is strongly reduced (Vinnikov et al., 1996; Vinnikov et al., 1999). This makes the root-zone soil moisture estimates derived from SWI more suitable for use in a crop model running at daily time-steps.

After having identified suitable satellite derived data products, appropriate methods must be selected to combine the model output and observation through an assimilation procedure. Various approaches are available to assimilate satellite observation in crop models (section 1.2). However, the operational character of the system puts some constraints on the type of data assimilation that can be applied. First of all, the assimilation approach should be robust in order not to compromise the operational system when satellite observations are not available, for example due to sensor or telecommunications failure. Secondly, the data assimilation procedure must be able to ingest satellite observations on-the-fly as the growing season progresses. These requirements are most easily met by using a sequential data assimilation approach. Particularly the ensemble Kalman filter (EnKF) is one of the more attractive algorithms because the structure of many crop models lends itself well for implementation in the EnKF and the state vector in crop models is relatively small (Dorigo et al., 2006)

One of the conditions for successfully applying the ensemble Kalman filter is that the uncertainty on the model states (in terms of co-variance) can be properly estimated. This means that the factors that cause the uncertainty in the model states must be properly represented during model initializing and simulation. Within this thesis, it is assumed that the influence of uncertainty in weather is the major factor (Aggarwal, 1995; Easterling et al., 1998; Mathe-Gaspar et al., 2005; Mearns et al., 2001) which determines the uncertainty on

the modelled soil moisture (Syed et al., 2004).

## 1.4 Scope and objectives

The thematic limitations of CGMS outlined in section 1.1 combined with the thematic and operational limitations of remote sensing derived products (sections 1.2 and 1.3) have led to the following overall objective of this thesis:

*Providing a basis for probabilistic crop growth modelling and remote sensing data assimilation for improved regional crop yield forecasting.*

More specifically, this thesis will address:

- Exploring the uncertainties related to the spatial and temporal variability of the main meteorologic forcings necessary for running a crop growth model (temperature, radiation, precipitation);
- Modelling of the uncertainty in precipitation inputs using a stochastic approach on a spatial and temporal scale which is consistent with the needs of regional crop growth modeling;
- Developing a probabilistic framework for crop growth modelling coupled to an ensemble Kalman filter for assimilation of remote sensing derived observations;
- Applying the developed probabilistic framework in a case study and demonstrating the improvements in the relationships between model output and crop yield statistics through the assimilation of soil moisture estimates.

Additionally, the components in this study have been carried out with the following constraints in mind:

- No algorithms or methods have been used in this study which cannot be applied and calibrated in an operational context (e.g. locally derived relationships between NDVI and LAI).
- All satellite data products that have been used in this study can provide frequent global coverage and are operated by an organisation with a long-term mandate;
- The results of this study do not depend in any way on local ancillary data (e.g. detailed land cover or crop maps) which often impedes scaling up the results from field to region.

## 1.5 Outline of this thesis

The core of this thesis (Chapters 2–5) is based on a series of four peer-reviewed journal papers. Each chapter is introduced separately by stating its research goals and by outlining its relationship with other relevant work.

Chapter 2 explores the use of AVHRR-derived surface temperature as a replacement for interpolated maximum air temperature in a spatial crop monitoring and yield forecasting system (Wit et al., 2004). Chapter 3 describes the effect of uncertainty in the CGMS radiation and precipitation estimates on the crop simulation results and yield forecast (Wit et al., 2005). This work is carried out by comparing the output from the standard CGMS system with the results obtained from using a high resolution precipitation and radiation database as input. Furthermore, the spatial scaling behaviour of CGMS is analysed with regard to precipitation and radiation inputs.

Chapter 4 builds on chapter 3 by developing a method to capture the uncertainty in the CGMS precipitation patterns through a stochastic approach (Wit et al., 2007). The method treats the CGMS precipitation field as a first guess for the true precipitation field and uses an additive error model to generate many equiprobable realisations. Together, this ensemble of realisations characterises the uncertainty in the precipitation field and it is demonstrated how such an ensemble can be used to characterise the uncertainty on the crop yield forecast.

Chapter 5 presents results obtained from a spatially distributed probabilistic version of the WOFOST crop growth model coupled to an ensemble Kalman filter (Wit and Diepen, 2007). We used this framework to assimilate coarse resolution satellite microwave sensor derived soil moisture estimates for correcting errors in the water balance of the WOFOST model caused by uncertainty in rainfall or model initialisation. The results of this work are validated by determining whether this approach results in improved relationships between model output and crop yield statistics for administrative regions.

Finally, Chapter 6 concludes this thesis with a summary and discussion of the main findings and suggestions for further work.





## Chapter 2

# Using NOAA-AVHRR estimates of land surface temperature for regional agrometeorological modelling\*

### 2.1 Introduction

During the last decade agrometeorological crop simulation models have been used to provide information on soil/crop conditions at the scale of fields and regions (Bouman et al., 1996). The application domain of these models is diverse and includes: yield risk and yield variability analyses, crop yield forecasting, crop rotation analyses and the effect of climate change on crop growth (Hoogenboom, 2000; Supit et al., 1994). Moreover, a relatively new range of applications for agrometeorological models has been developed by including the spatial domain in agrometeorological modelling.

Traditionally, agrometeorological models have been developed using daily meteorological input data measured at specific sites; the model outputs therefore are site-specific. If the spatial dimension is to be included in the agrometeorological modelling system, then spatially representative values of various model parameters (i.e. crop parameters, soil parameters and sowing dates) need to be gathered as well as spatially representative meteorological input data. Usually this is (partly) accomplished by linking the crop model with a GIS (Hartkamp et al., 1999). The use of a GIS facilitates handling spatio-

---

\*Chapter based on: Wit, A.J.W d., Boogaard, H. and Diepen, C.A. v.: 2004, Using NOAA-AVHRR estimates of land surface temperature for regional agrometeorological modelling, *International Journal of Applied Earth Observation and Geoinformation* 5(3), 187–204

temporal information both in input as well as model output. Furthermore, the GIS can be used to derive some crop model parameters like soil type and slope from digital soil maps and elevation models. The GIS itself does not fulfil the task of finding spatially representative meteorological input data, because the weather variables measured at weather stations represent 'point' information.

Various approaches exist to tackle the fact the weather stations are often widely spaced. One can simply assume that point observations are representative for a larger area. Usually this is not a valid assumption depending on the size of the area and factors like orography, the dimension and pathway of rainstorms, land cover and micro-climate. If data from a network of weather stations is available, one can interpolate the weather variables between the stations before running the crop model (Carbone, 1993; Voet et al., 1994). The other option is to run the model with the site-specific weather variables and interpolate the results after the simulation (Bindi and Maselli, 2001). The handling of the spatial component of meteorological input data is currently one of the main concerns in spatial agrometeorological modelling (Hoogenboom, 2000).

The solutions that were described above all assume that meteorological variables can only be obtained through weather stations. Two alternatives exist that can be of great relevance to spatial agrometeorological modelling systems. The first alternative is to obtain input data through a weather forecasting model such as the one operated by the European Centre for Medium Range Weather-Forecasting (ECMWF). The ECMWF weather forecasting model provides weather variables on a 0.25-degree grid, which is a much higher density compared to most meteorological networks. A second advantage is that large time-series of simulated weather variables are becoming available through for example the ERA15 and ERA40 projects (<http://www.ecmwf.int/research/era/>). However, a complete discussion on the use of simulated weather variables is beyond the scope of this paper.

The second alternative involves the use of satellite sensor observations to estimate meteorological variables. In this respect, temperature and solar radiation are particularly interesting. Temperature can be derived from a variety of satellite platforms that carry thermal scanners, while operational procedures have been developed for determining daily solar radiation from Meteosat observations (Beyer et al., 1996). The use of satellite sensor observations has a number of advantages:

- The spatial density of the satellite sensor observations is far greater than any meteorological network.
- Satellite sensor observations have the advantage that data can be gathered at the actual location where the crop is growing.

- The data are readily available and data from many sensors can be downloaded through the internet without cost.

Besides these advantages of satellite sensor data, also some disadvantages have to be taken into account:

- Often a large effort is required to process satellite sensor data into useful information.
- The overpass time and frequency can be limiting factors.
- The presence of cloud cover complicates obtaining continuous time-series of surface temperature estimates.

The objective of this study is to evaluate the use of AVHRR-derived temperature as a substitute for interpolated maximum air temperature in a spatial crop monitoring and yield forecasting system; the Crop Growth Monitoring System (Vossen and Rijks, 1995). First, a short introduction to the WOFOST crop simulation model and the Crop Growth Monitoring System (CGMS) is given; the ancillary data are described and the processing steps are documented that were applied to a two-years set of daily NOAA-AVHRR data. Next, the AVHRR-derived temperature estimates are validated against measurements of maximum air temperature from weather stations and the spatial patterns of the temperature sums are visualised. Furthermore, the crop model results are evaluated and compared with the standard CGMS approach (Diepen, 1992; Vossen, 1995; Vossen and Rijks, 1995). Finally some conclusions on the use of AVHRR-derived surface temperature in CGMS are presented.

## 2.2 Models

### 2.2.1 WOFOST crop simulation model

The WOFOST (WOrld FOod STudies) crop simulation model (Diepen et al., 1989; Supit et al., 1994) is a mechanistic crop growth model that describes plant growth by using light interception and CO<sub>2</sub> assimilation as growth driving processes and by using crop phenological development as growth controlling process. The WOFOST model can be applied in two different ways: (1) a potential mode, where crop growth is purely driven by temperature and solar radiation and no growth limiting factors are taken into account. (2) A water-limited mode, where crop growth is limited by the availability of water. The

difference in yield between the potential and water-limited mode can be interpreted as the effect of drought. Currently, no other yield-limiting factors (nutrients, pests, weeds, farm management) are taken into account.

In the WOFOST model, temperature exerts influence on many different aspects of plant growth and development. First of all, temperature influences the duration of the successive growth stages, and hence on the duration of the total growth cycle because the length of each growth stage is defined by the summation of the daily effective temperature. Daily effective temperature is a function of the daily average temperature and is calculated by linear interpolation between a crop-specific base temperature, below which no phenological processes take place, and a crop-specific maximum temperature, beyond which phenological activity does not increase. Higher temperatures lead to faster ageing of the crop and shortening of successive growth stages.

Moreover, temperature influences the life span of green leaves, the maintenance respiration and the photosynthetic capacity. For example, when temperature increases, the maintenance requirements of the crop increase, leading to a lower net growth, even if the photosynthetic capacity of the crop remains at the same level. The highest potential biomass production is therefore obtained when the weather is cool and sunny throughout the year.

### 2.2.2 Crop Growth Monitoring System

The Crop Growth Monitoring System has been developed for crop monitoring and yield forecasting in the European Union and consists of a weather, soil and crop database, the WOFOST crop simulation model and a GIS (Diepen, 1992; Vossen, 1995; Vossen and Rijks, 1995). Within the framework of the MARS (Monitoring Agriculture with Remote Sensing) project at JRC (Joint Research Centre) Ispra (Italy), CGMS monitors from 1994 onward the agricultural production in Europe, Anatolia and the Maghreb with a spatial resolution of  $50 \times 50$  km and a temporal resolution of one day.

Within CGMS three operational levels can be distinguished:

1. interpolation of weather variables to a  $50 \times 50$  km grid;
2. simulation of crop growth and;
3. forecasting of crop yield.

At the first level weather data are interpolated from weather stations to centres of climatic grid cells. These grid cells are assumed to be homogeneous regarding the weather. Each grid cell receives values for temperature, radiation, air humidity and wind speed as the average from suitable surrounding

weather stations. Determination of the most suitable weather stations takes place on the basis of the so-called “meteorological distance” (Voet et al., 1994). This meteorological distance is a virtual distance which is not only based on the true distance between the grid cell and the weather station, but also on factors like altitude, distance to coast and the existence of climate barriers (e.g. mountain ridges, water bodies) between the grid cell and the weather station. In case of rainfall a grid cell receives the value of the weather station with the smallest meteorological distance from the grid cell.

At the second level, the actual crop modelling is carried out. For this purpose, data from the European soil map (King et al., 1995) are used as input in the calculation of the water balance. Soil moisture contents at different pressure heads (saturation, field capacity, wilting point) determine the water retention of the soil. Besides the hydrologic soil characteristics, the soil map is used to estimate the suitability of soils for different crops. The climatic grid and the soil map are combined in an overlay procedure that results in a number of unique simulation units: combinations of climatic grid cell and soil type. For these simulation units the potential and water-limited crop growth are simulated with the WOFOST crop growth model.

At the third level, CGMS aggregates the daily biomass values per simulation unit into dekadal values per administrative unit. The CGMS model outputs are gathered for time-series of 15 to 20 years and are regressed against the historic known values of crop yields for each administrative unit.

## 2.3 Data

### 2.3.1 NOAA-AVHRR data

The AVHRR sensor (Advanced Very High Resolution Radiometer) onboard NOAA's (National Oceanic and Atmospheric Administration) POES (Polar Operational Environmental Satellite) satellites records radiation reflected and emitted by the land surface at spectral intervals centered at 0.63, 0.91, 3.7, 11 and 12  $\mu\text{m}$  with a spatial resolution of 1.1 by 1.1 km at nadir. At each overpass the sensor scans a 2400 km wide strip of the Earth. Due to the characteristics of its Sun synchronous orbit each NOAA-AVHRR sensor scans the entire Earth at least two times a day. The tracks of the NOAA satellite do not repeat on a daily basis, although the local solar time of the satellite's passage is essentially unchanged for any latitude.

For this study, a dataset from the AVHRR sensor onboard the NOAA-14 satellite has been used which overpasses western Europe between 13.00 and 14.00 local solar time. This dataset contains daily images and spans almost

two years, starting at February 1<sup>st</sup> 1995 and ending at November 28<sup>th</sup> 1996. The dataset covers an area that is bounded by the 10<sup>th</sup> meridian west and 5<sup>th</sup> meridian east. In the north-south direction it covers an area starting in East Anglia and The Netherlands (54° N) in the north to Morocco in the extreme south (30° N).

The pre-processing of the AVHRR data was carried out at the Free University of Berlin (Koslowsky, 2003; Koslowsky et al., 2001) and consisted of registering the data to a geographic co-ordinate system and calibrating the AVHRR channels to top-of-atmosphere (TOA) reflectance (channels 1,2,3) and TOA brightness temperature (channels 4,5). The pre-processing chain also provided ancillary information like cloud masks, Normalised Difference Vegetation Index (NDVI) and broadband albedo.

### **2.3.2 Weather station locations and variables**

The CGMS database contains daily meteorological observations from a large number of weather stations in Europe. To compare surface temperature data obtained from the AVHRR sensor with the observed air temperature, daily weather variables including minimum/maximum air temperature, wind speed, precipitation and cloud cover were extracted from the database for 11 weather stations over western Europe (Figure 2.1). Most of these weather stations are located in major agricultural production areas.

### **2.3.3 Pan-European Land Cover Database**

The PELCOM database (Pan-European Land COVer Monitoring) is based on classifications of monthly NDVI composites that were derived from NOAA-AVHRR observations (Mücher et al., 2000). The goal of the PELCOM project was to establish a 1-km Pan-European land cover database with a consistent classification methodology. The nomenclature of the database discriminates eight classes that are divided into various subclasses depending on the region of interest. The purpose of the database is to meet the demands of environmental and meteorological models for reliable and accurate land cover data at a European scale.

The accuracy and reliability of the PELCOM database varies significantly between classes and also between different regions in the database (Mücher et al., 2001). Furthermore different methods of validation result in different estimates of accuracy and reliability. During this study the PELCOM database has been used to identify areas with agricultural land cover. The validation of the PELCOM database has demonstrated that the PELCOM class 'arable land' is classified with an accuracy in the order of 80%.



Figure 2.1: The location of selected weather stations over western Europe.

## 2.4 Methods

### 2.4.1 Comparing surface temperature to maximum air temperature

Surface temperature and air temperature are two different physical quantities which are related through the exchange of energy fluxes near the Earth's surface. During daytime the surface temperature is normally higher than the air temperature because of the existence of a sensible heat flux induced by solar radiation. The physical relationship between the air temperature and the surface temperature is complex and depends on factors like moisture condition, radiation, vegetation density and micrometeorological conditions (Monteith and Unsworth, 1990). In this study we try to relate surface temperature to maximum daily air temperature. Maximum daily air temperature corresponds to the maximum air temperature measured during the day and is usually measured in the early afternoon. Surface temperature is defined as the surface temperature during the time of satellite overpass. For the NOAA-14 satellite, the time of overpass compares favourably with the period of maximum air temperature. Differences between the maximum daily air temperature and the AVHRR-derived surface temperature are thus caused by:

1. Differences between the estimated surface temperature and the true surface temperature due to assumptions in atmospheric corrections and emissivity.
2. Differences between the true surface temperature and the maximum air temperature measured at a weather station, due to the physical difference of the quantities that are being compared.
3. The distribution of vegetation and bare soil within the pixel and the effect of water stress on the vegetation canopy temperature.
4. Differences in the local time of the acquisition of the surface temperature and maximum air temperature.

Because these influences are difficult to separate we will apply an empirical model that is fitted using observations of maximum air temperature at weather stations.

### 2.4.2 Correction and aggregation of surface temperature

The NOAA-AVHRR channels 4 (10.5 – 11.5  $\mu\text{m}$ ) and 5 (11.5 – 12.5  $\mu\text{m}$ ) are sensitive to radiation emitted in the thermal part of the electromagnetic spec-



trum and are used to estimate the Earth's surface temperature. Before the surface temperature of the Earth can be determined it is necessary to minimise the effects of the Earth's atmosphere on the recorded signal. For this purpose, algorithms have been developed that can determine the atmospheric effects on the signal from slight differences in the observed brightness temperature in the AVHRR channels 4 and 5.

These so-called split-window algorithms were originally developed for determining sea surface temperature but have been extended to land applications as well. In this study a split-window algorithm developed by Sobrino et al. (1991) has been applied. This algorithm describes the split-window coefficients for a number of standard atmospheric conditions and a given emissivity of the Earth's surface in AVHRR channels 4 and 5. For the period of April to September the coefficients for the standard atmosphere 'mid-latitude summer' were used, all other months were corrected with the coefficients for 'mid-latitude winter'. More advanced split-window algorithms have been described in literature (Ouaidrari et al., 2002; Qin and Karnieli, 1999) but these algorithms require additional information like atmospheric water vapour distribution which was not available for this study.

A fixed surface emissivity of 0.95 was assumed for both AVHRR channels. This assumption is based on the work of Salisbury and D'Aria (1992) who demonstrated that the emissivity for different terrestrial materials is less variable within the 10.5 – 12.5  $\mu\text{m}$  AVHRR spectral window compared to the whole 8 – 14  $\mu\text{m}$  thermal atmospheric window. Therefore, an emissivity of 0.95 is a reasonable estimate. Another approach is to estimate emissivity from NDVI using an empirical relationship (Van de Griend and Owe, 1993). However, this approach provides an estimate of broadband (8 – 14  $\mu\text{m}$ ) emissivity, which is not representative for the emissivity in the AVHRR spectral bands.

The AVHRR sensor has a spatial resolution of 1.1 kilometre at nadir while CGMS monitors crop growth at a spatial resolution of 50 kilometres. To compensate for this scale difference, some form of aggregation must be applied to the surface temperature data. The most straightforward aggregation approach would be to take the average of all AVHRR pixels within each CGMS grid cell. This approach has the disadvantage that many pixels will be included that are not representative of crop growth conditions (urban areas, forests, mountains, etc.). Therefore, we decided to use the PELCOM land cover database to stratify the surface temperature images prior to aggregation. Only those pixels classified as 'arable land' in the PELCOM land cover database were selected.

The last step in the processing chain involves the influence of cloud cover. To exclude clouded pixels from the aggregation, the cloud masks supplied with the AVHRR images were used to select only cloud-free pixels. Figure 2.2 gives an overview of the processing steps that were carried out to obtain the average surface temperature per CGMS grid cell.

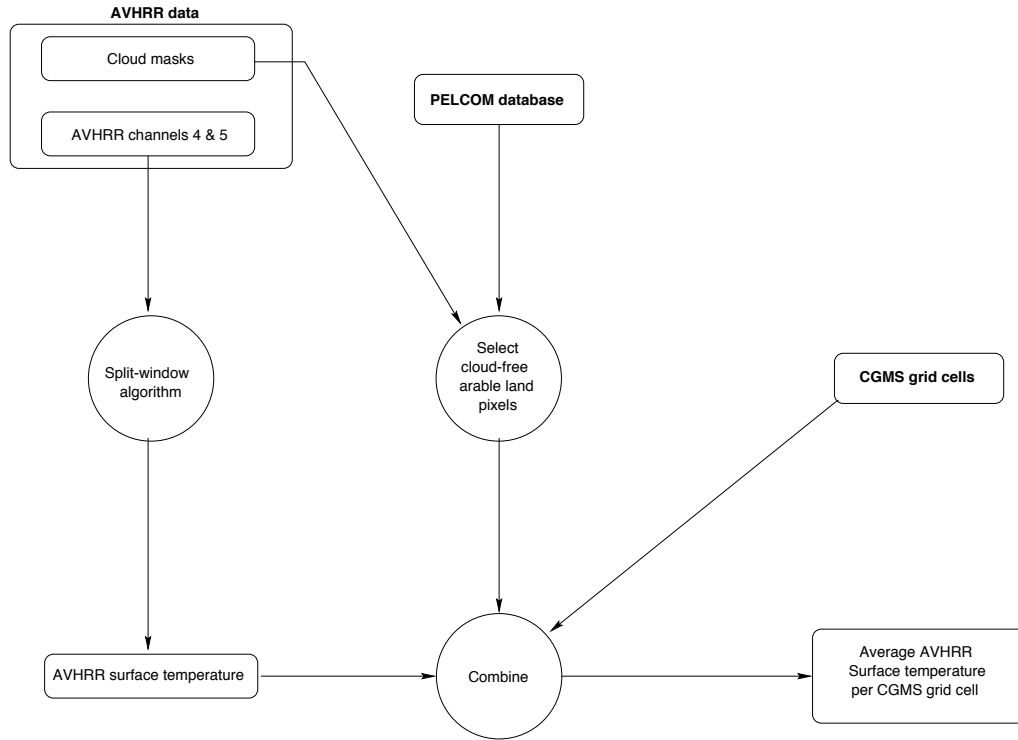


Figure 2.2: A schematic overview of the processing steps that were applied to the daily AVHRR images in order to obtain the average surface temperature for each CGMS grid cell.

### 2.4.3 Temporal interpolation of the surface temperature

A clear disadvantage of the use of temperature data from satellite sensors is the difficulty of obtaining continuous time-series of land surface temperature estimates due to the effect of cloud cover. One approach to estimate the land surface temperature on clouded overpasses is to derive a relationship between the surface temperature on cloud-free overpasses and the observed maximum air temperature at a weather station, because good relationships exist between surface temperature and maximum air temperature (figure 2.3). Next, this relationship can be used to estimate the surface temperature on clouded overpasses from the observed maximum air temperature.

The drawback is that this approach is only valid near a weather station. Therefore, we decided to use a second approach where we substitute the surface temperature on clouded overpasses with the monthly average surface temperature obtained from cloud-free overpasses. This approach is based on the following considerations:

- In the WOFOST crop model, the cumulative air temperature is driving

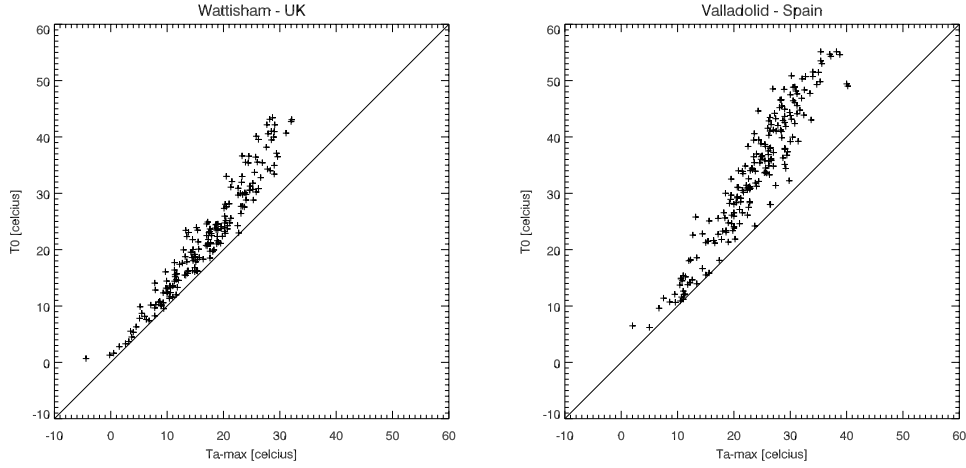


Figure 2.3: Two examples of scatter plots between the maximum air temperature obtained from weather station ( $T_a^{max}$ ) and the area-averaged surface temperature obtained from NOAA-AVHRR ( $T_0$ ).

the development stages of the crop. It is therefore important to obtain a correct development of the cumulative air temperature, while deviations in air temperature on a daily basis are permissible.

- We assume that we introduce little bias in the cumulative surface temperature when we substitute the monthly average surface temperature on clouded overpasses. One could argue that our approach always overestimates the surface temperature, because we are using estimates obtained on cloud-free overpasses to estimate surface temperature on cloudy overpasses when the surface temperature will be lower as a result of cloudiness. However, this cannot be solved in this study.
- The approach is fast and easy to implement, which is important when processing large datasets.

We selected five grid cells where a weather station provided the observed maximum air temperature and both approaches could be applied. The development of the cumulative surface temperature for both interpolation approaches demonstrates that differences are small (figure 2.4). For all locations, the relative differences at the end of the years are within 2% and the absolute differences through the season are smaller than 200 degrees.

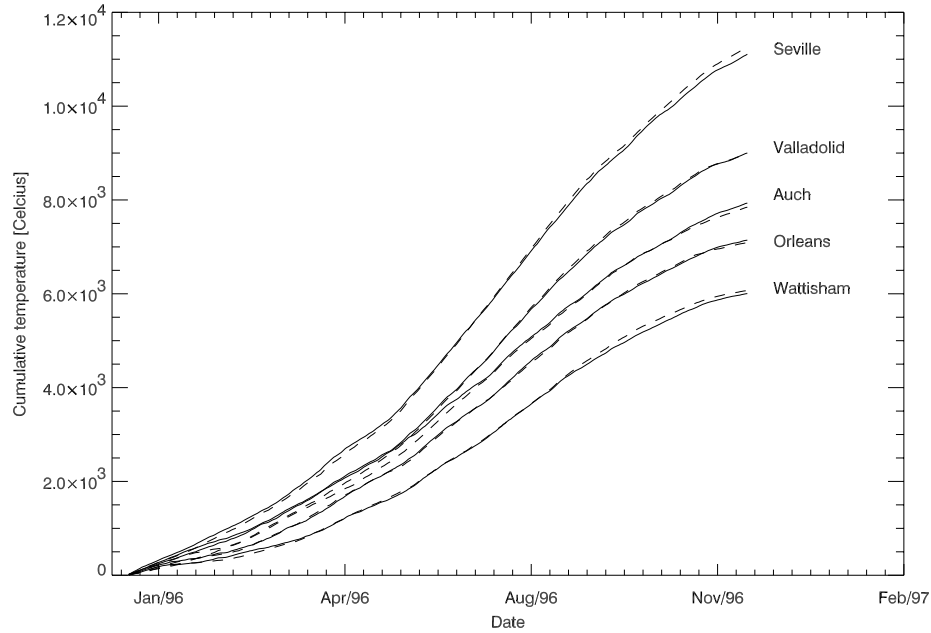


Figure 2.4: Development of cumulative surface temperature ( $T_0$ ) for five locations in 1996, using two different approaches to account for missing data: Interpolation using the maximum air temperature (dashed lines) and substitution of the monthly average surface temperature (solid line).

#### 2.4.4 Magnitude correction of the surface temperature

A final correction to the surface temperature data is necessary, because the AVHRR-derived surface temperature at overpass time is usually higher than the maximum air temperature measured during the day (figure 2.3). Without this correction, the temperature sums in the WOFOST model would be reached too early in the growing season and thus the simulated crop would develop too fast. We use a simple empirical model to apply this correction. The underlying assumption is that a single correction model can be used throughout the entire study area in order to convert surface temperature at overpass time to a simulated maximum air temperature. The empirical model was of the type:

$$T_0 = aT_a^{max} + bT_a^{max} \quad (2.1)$$

We assume that the relationship between surface temperature ( $T_0$ ) and observed maximum air temperature ( $T_a^{max}$ ) is almost linear at low air temperature, but the difference between  $T_0$  and  $T_a^{max}$  gets progressively larger at higher air temperature. We determined the model coefficients using the

*Table 2.1:* Regression parameters and correlation coefficient derived from an empirical relationship between  $T_0$  and  $T_a^{max}$ .

Year	Coefficient $a$	Coefficient $b$	$R^2$
1995	1.11855	1.06250	0.91
1996	1.10137	1.06973	0.90

observed maximum air temperature from 5 weather stations (Wattisham, Orleans, Auch, Valladolid and Seville) and the surface temperature of the CGMS grid cells where these weather stations were located.

Table 2.1 shows the model coefficients found and the correlation coefficients between the observed surface temperature and the surface temperature estimated from the observed maximum air temperature. The results illustrate that the correlation coefficient is high and the regression coefficients found for 1995 and 1996 are similar. We decided to use the coefficients derived from 1995 because the data that were obtained during the 1995 season cover a slightly larger temperature range.

#### 2.4.5 CGMS model simulation approach

Crop simulations for Spain were carried out using CGMS for two different crops (winter-wheat and sunflower) during the 1995 and 1996 growing seasons. One CGMS model run was carried out using the standard CGMS system, which derives the spatial weather variables by interpolation from weather stations. This approach will be herein referred to as the 'classic CGMS approach'. The second CGMS model run used the AVHRR derived temperature. This approach will be herein referred to as the 'satellite CGMS approach'.

The satellite CGMS approach differed from the classic CGMS approach on two aspects: First, the interpolated maximum air temperature for each grid cell was replaced with the simulated maximum air temperature derived from the AVHRR surface temperature. For January 1995, we had to use the interpolated maximum air temperature because no AVHRR images were available for this month.

Second, a simulated minimum air temperature replaced the measured minimum air temperature. The simulated minimum air temperature was derived by subtracting a daily long-term average temperature difference from the simulated maximum air temperature. This daily long-term average temperature

difference was calculated using the long-term record of weather variables in the CGMS weather database. For an operational procedure, the daily minimum air temperature might be derived from night-time AVHRR-observations but these were not available for this study.

## 2.5 Results

### 2.5.1 Comparison with independent weather-stations

We compared the simulated maximum air temperature ( $T_a^{sim}$ ) with the maximum air temperature ( $T_a^{max}$ ) measured at six independent weather stations. The results are plotted as the difference in the cumulative temperature ( $T_a^{max} - T_a^{sim}$ ) over the period 1 February 1995 to 28 November 1996 (figure 2.5). For the stations 'De Bilt', 'Cognac' and 'Grenoble' the differences are small and within 300 degrees over the entire period. For the stations 'Zaragoza' and 'Valencia' the maximum air temperature is overestimated leading to a difference in cumulative temperature of 1000 and 750 degrees. The most southern weather station at Albacete shows a strong overestimation of the maximum air temperature leading to a difference in cumulative temperature of 2700 degrees at the end of the two-year period.

### 2.5.2 Spatial distribution of the temperature sums

We calculated the yearly temperature sum in each CGMS grid cell in Spain for both the classic and the satellite CGMS approaches in order to analyse the distribution and the spatial patterns of the yearly temperature sum. The temperature sum for 1995 was calculated over the entire year, while the temperature sum for 1996 was calculated over the period from January 1<sup>st</sup> to November 28<sup>th</sup>. Therefore, the histograms of the temperature sum cannot be compared directly between 1995 and 1996 (figure 2.6a,b).

The histograms demonstrate that the temperature sums for the classic and the satellite CGMS approach are similar at the cool side of the histograms. However, at the warm side of the temperature histograms the satellite CGMS approach reaches higher temperature sums compared to the classic CGMS approach. These results confirm that the cumulative temperature is overestimated by the satellite CGMS approach. Note that the overall shapes of the histograms are similar for both approaches in 1995 as well as 1996.

We visualised the spatial patterns of the yearly temperature sums using 1/8 quantile maps, where each interval in the legend represents 12.5% of the total data (figure 2.7). A general north-south pattern exists of relatively

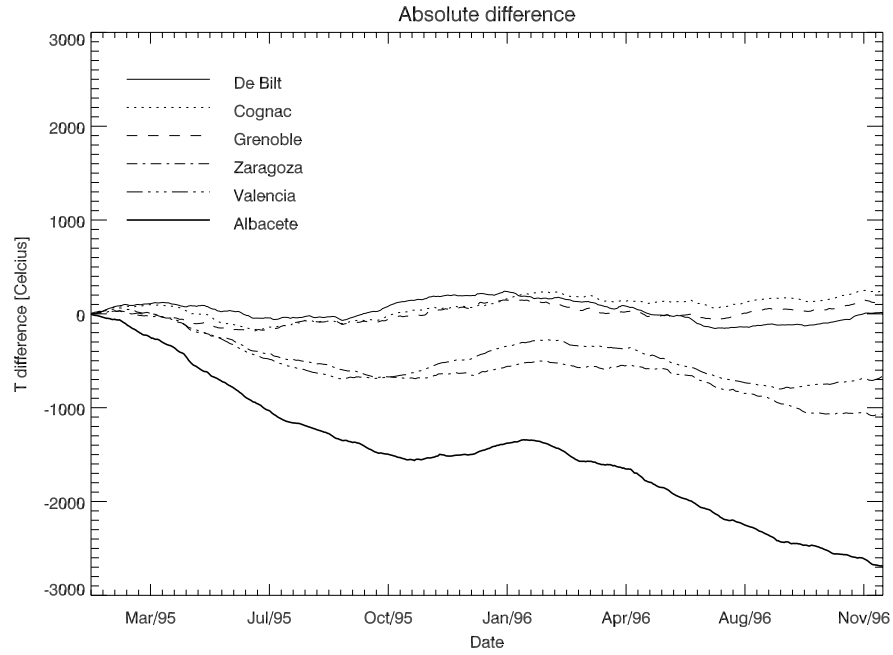


Figure 2.5: The difference ( $\sum T_a^{max} - \sum T_a^{sim}$ ) between the cumulative maximum air temperature ( $\sum T_a^{max}$ ) measured at six independent stations and the cumulative simulated maximum air ( $\sum T_a^{max}$ ) derived from the AVHRR data.

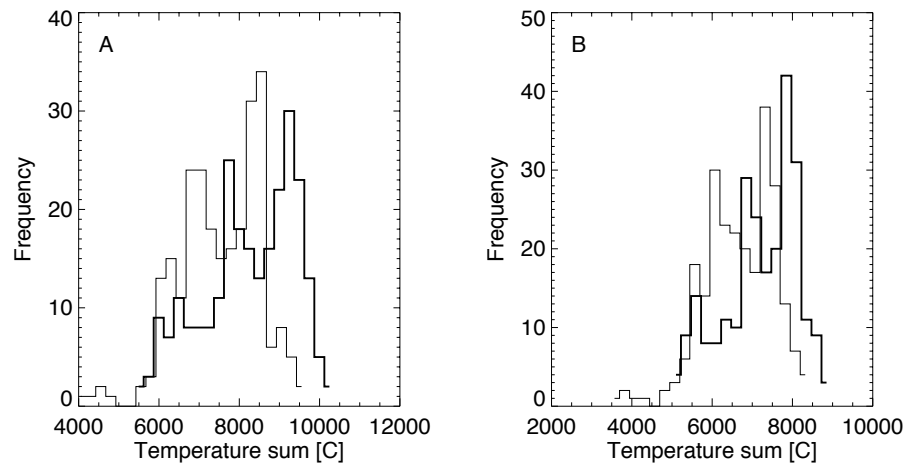


Figure 2.6: Histogram of the 1995 (A) and 1996 (B) cumulative temperature for the CGMS gridcells in Spain, obtained using classic CGMS approach (thin line) and the satellite CGMS approach (thick line).

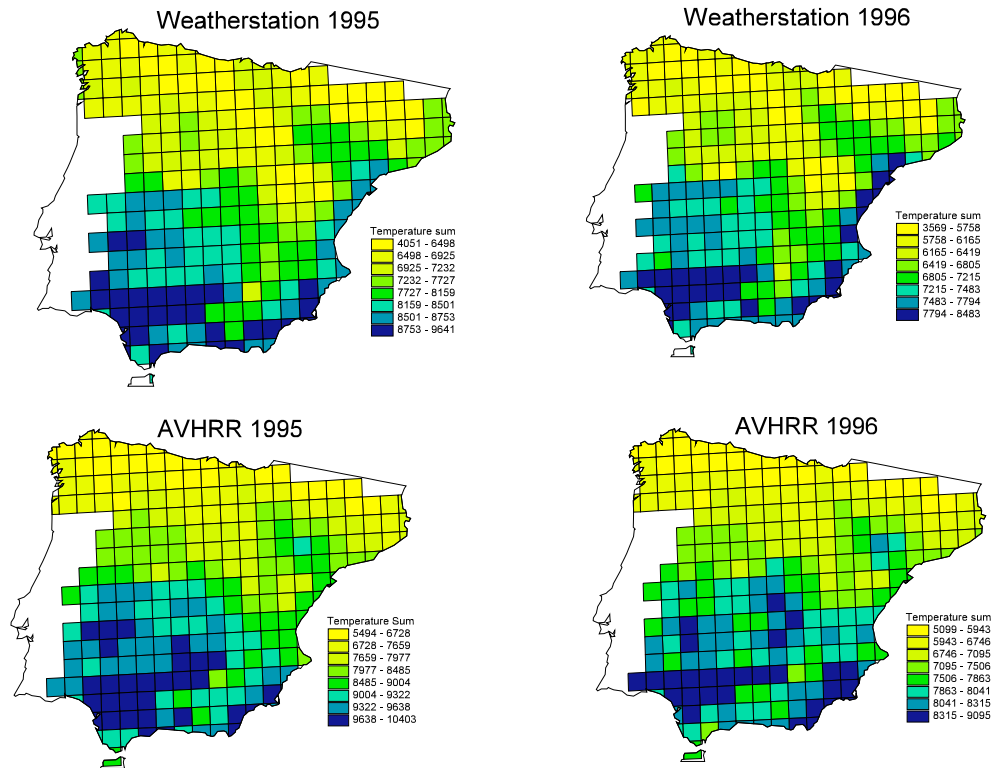


Figure 2.7: Spatial patterns of the yearly temperature sums that were derived from observed weather and AVHRR-derived surface temperature for 1995 and 1996. Each map is plotted as a 1/8 quantile map, where each legend interval represents 12.5% of the total data.

low temperature sums in north Spain to high temperature sums in southwest Spain. Also the relatively high temperature sums in the Ebro valley can be easily discriminated in both approaches, as well as the strip of high temperature sums along the Mediterranean coast. Differences in the spatial patterns can be found in the south-central parts of Spain (Extremadura en Sierra Morena). Given the fact that few weather stations are available in this area, it can be argued that the AVHRR-derived patterns are probably a better indication of the true spatial variability of the cumulative temperature than the interpolated spatial patterns.

### 2.5.3 Crop simulation results

Next, we compare crop simulation results from using the satellite and classic CGMS approaches. The WOFOST crop model generates a number of crop



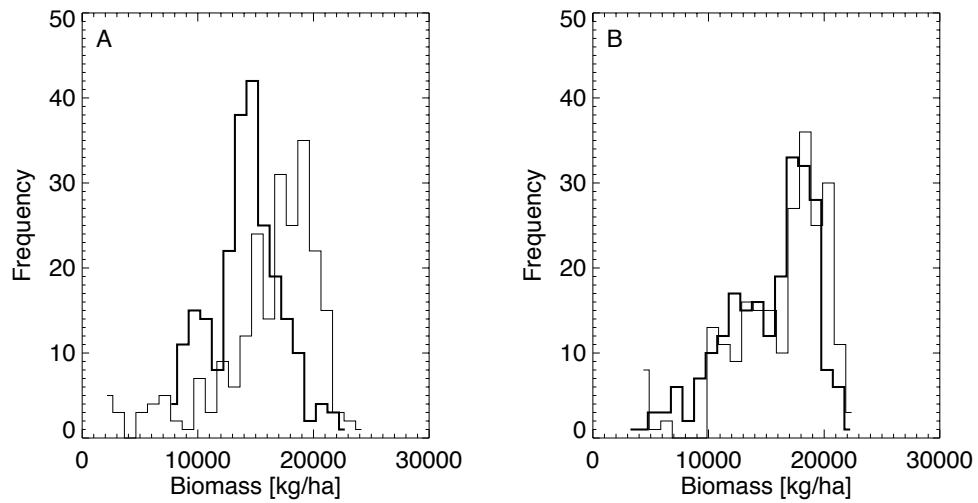


Figure 2.8: Histograms of the 1995 (A) and 1996 (B) CGMS simulated potential biomass for winter-wheat using the classic CGMS approach (thin line) and the satellite CGMS approach (thick line).

parameters that can be used for comparing the two approaches. We selected the potential biomass and the potential leaf area index because these parameters reflect the effect of differences in temperature, whereas the water-limited biomass and water-limited leaf area index are also influenced by the availability of water.

### Winter-wheat

The histograms for the total potential biomass at the end of the growing season show clear differences between the 1995 and 1996 growing seasons (figure 2.8a,b). For the classic CGMS approach the peaks of the distributions lie between 18,000 and 20,000 kg ha<sup>-1</sup> in 1995 as well as 1996 with an average biomass of 16,500 in 1995 and 16,800 kg ha<sup>-1</sup> in 1996. For the satellite CGMS approach the peaks of the distributions lie around 14,000 kg ha<sup>-1</sup> in 1995 and around 17,000 kg ha<sup>-1</sup> in 1996 with an average biomass of 14,600 kg ha<sup>-1</sup> in 1995 and 15,700 kg ha<sup>-1</sup> in 1996.

The development of the simulated potential LAI through time explains why the satellite CGMS approach yields lower biomass values. We selected a representative example of the simulated leaf area index near Zaragoza (figure 2.9a). This figure demonstrates that the ascending parts of the LAI curves are similar and the peak LAI values are nearly identical for both approaches in 1995 as well as 1996. However, for the satellite CGMS approach the de-

scending part of the LAI curve starts earlier compared to the classic CGMS approach. In 1995, the crop simulation for the satellite CGMS approach finishes three decades (i.e. 10-day periods) before the classic CGMS approach. In 1996, the satellite CGMS approach is only one decade ahead of the classic CGMS approach.

The early descent of the LAI curves for the satellite CGMS approach is caused by the higher temperature that was obtained with the satellite CGMS approach. Due to the higher temperature, the temperature sums in the crop model are reached earlier in the season and thus the model changes to a subsequent phenological stage earlier in the season. This effect is particularly evident in the last part of the growing season when temperatures are higher. The effect of the differences in LAI development on the biomass development is clear since the simulated plant acquires less time to assimilate and consequently less biomass can be accumulated.

### Sunflower

The histograms for the total potential biomass at the end of the growing season (figure 2.10a,b) demonstrate that large differences are present between the satellite and the classic CGMS approach for sunflower. For the classic CGMS approach the peaks of the distributions lie between 9,000 and 11,000 kg ha<sup>-1</sup> in 1995 as well as 1996 with an average biomass of 9400 kg ha<sup>-1</sup> in 1995 and 10,000 kg/ha in 1996. For the satellite CGMS approach the peaks of the distributions lie around 7,000 kg ha<sup>-1</sup> in 1995 as well as 1996 with an average biomass of 6400 kg ha<sup>-1</sup> in 1995 and 7400 kg ha<sup>-1</sup> in 1996. In both years the frequency distributions of the satellite CGMS approach are shifted towards lower biomass values. This is particularly evident in 1995 where the relatively 'peaked' distribution of the classic CGMS approach is in contrast with the flat distribution of the satellite CGMS approach with a high occurrence of grid cells with low biomass.

The temporal evolution of the simulated potential leaf area index shows a pattern similar to that of the simulated potential leaf area index of winter-wheat (figure 2.9b). The ascending parts of the LAI curves are nearly identical for the satellite and classic CGMS approaches, while the descending part of the LAI curve for the satellite CGMS approach is four decades (i.e. 10-day periods) ahead of the classic CGMS approach. However, the effect of the higher temperature is more extreme in the case of sunflower because the maximum LAI value reached during the satellite CGMS approach is roughly two-thirds of the maximum LAI value reached with the classic CGMS approach. Sunflower is grown three months later in the crop growth season than winter-wheat. Therefore the model simulations for sunflower in the satellite CGMS approach are more influenced by the overestimation of the maximum air temperature.

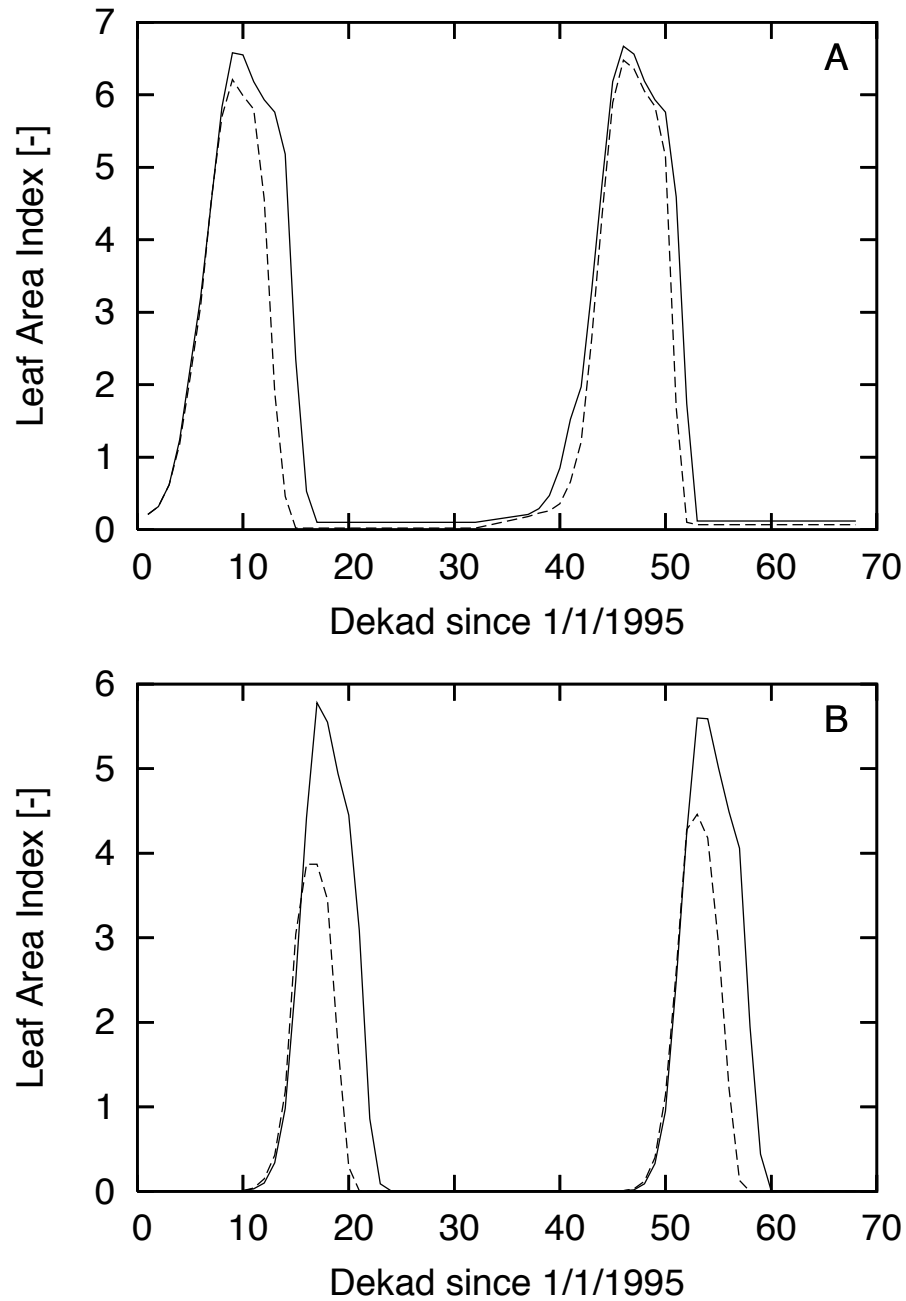


Figure 2.9: Simulated potential green leaf area index for winter-wheat (A) and sunflower (B) during 1995 and 1996 for a CGMS grid cell near Zaragoza. Classic CGMS approach drawn as solid lines, satellite CGMS approach drawn as dashed lines

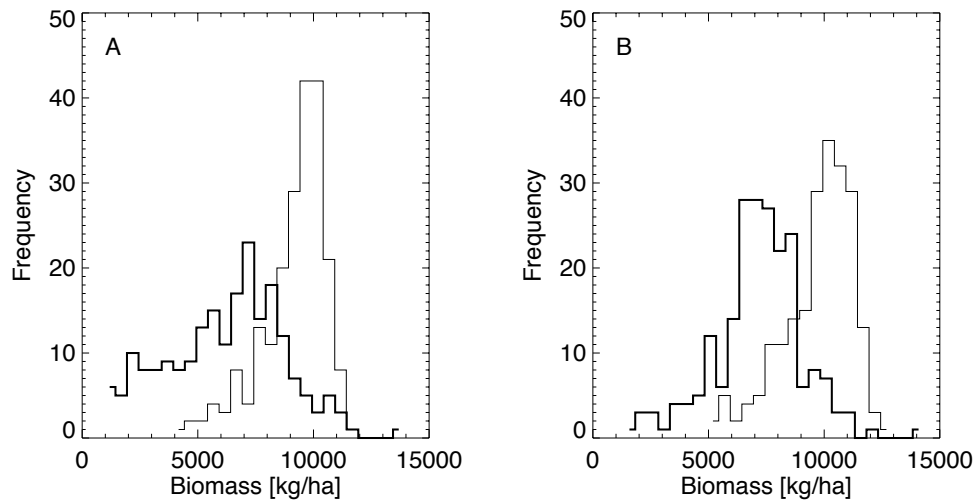


Figure 2.10: Histograms of the 1995 (A) and 1996 (B) CGMS simulated potential biomass for sunflower using the classic CGMS approach (thin line) and the satellite CGMS approach (thick line).

## 2.6 Conclusions and discussion

We have explored the use of AVHRR-derived surface temperature as a substitute for interpolated maximum air temperature in a spatial crop monitoring and yield forecasting system (CGMS). A processing chain was developed which derives estimates of surface temperature per CGMS grid cell from a two-year set of NOAA-AVHRR data, interpolates the missing values and converts the surface temperature estimates into a simulated maximum air temperature using a simple model and limited weather station data. Next, CGMS crop simulations were carried out for winter-wheat and sunflower using both interpolated maximum air temperature and simulated maximum air temperature. Our results can be summarised as follows.

We evaluated two approaches to account for missing data due to cloud cover (1) substituting the monthly average surface temperature (2) interpolation using a relationship with measured maximum air temperature. The two approaches lead to different estimates of surface temperature on cloudy days, but these differences are small when time-series of cumulative temperature are compared. We therefore conclude that, for regional agrometeorological purposes, substituting the monthly average surface temperature on days with missing surface temperature is an effective way of accounting for missing data.

A direct use of AVHRR-derived surface temperature in crop growth models is not possible because the surface temperature obtained from NOAA-AVHRR

is usually higher than the maximum air temperature measured at a meteorological station. We used a simple empirical model to correct for this difference and to convert the AVHRR-derived surface temperature into a simulated maximum air temperature. Validation of the simulated maximum air temperature with measured maximum air temperature from independent weather stations demonstrates that the differences in cumulative temperature are small for the northern weather stations (Netherlands, France) but the simulated maximum air temperature is systematically overestimated for the southern weather stations (Spain).

The histograms of the yearly temperature sums in Spain confirm that the simulated maximum air temperature is overestimated. Nevertheless, the 1/8 quantile maps demonstrate that the spatial patterns of the temperature sums for both approaches agree well. These results therefore indicate that AVHRR-observations of surface temperature can be used to obtain realistic spatial patterns of the temperature sum. However, a better correction of the surface temperature must be carried out in order to adjust the AVHRR-derived surface temperature to daily maximum air temperature.

When the simulated maximum air temperature is used as input in the crop growth monitoring system, the effects on the simulation of winter-wheat and sunflower are predictable. For both crops the overestimation of the temperature sums causes a shortening of the growing season and subsequently a lower accumulation of biomass at the end of the season. This effect is more pronounced for sunflower because this crop is grown later in the season.

The overall results of this research demonstrate that the AVHRR-derived surface temperature has good potential for use in regional agrometeorological systems. Future work along this line of research could consider a more quantitative analysis on the performance of surface temperature to predict air temperature at a particular location and compare it to the performance that is obtained by using interpolation from surrounding weather stations for that same location. This approach could be carried out by using co-kriging to interpolate air temperature measured at weather stations on the basis of AVHRR-derived surface temperature, thus combining the accuracy of point measurements with the spatial variability derived from AVHRR land surface temperature. Other potential extensions include the use of a climatic zonation in combination with a larger number of weather station observations. Hence, relationships between surface temperature and maximum air temperature could be derived for each climatic zone. Finally, the use of new thermal satellite sensors (i.e. TERRA-MODIS, ENVISAT-AATSR) could be investigated.



## Chapter 3

# Spatial resolution of precipitation and radiation: the effect on regional crop yield forecasts\*

### 3.1 Introduction

Agrometeorological crop simulation models are used operationally in many parts of the world for monitoring the effect of weather conditions on crop growth and for predicting crop yields from regional to continental scales (Challinor et al., 2004; Hansen et al., 2004; Nemecek et al., 1996; Thornton et al., 1997; Vossen and Rijks, 1995; Yun, 2003). The success of the crop yield forecasting application strongly depends on the crop simulation model's ability to quantify the influence of weather, soil and management conditions on crop yield and on the systems ability to properly integrate model simulation results over a range of spatial scales (Hansen and Jones, 2000).

Originally, agrometeorological models were developed during the 1970's and 1980's to simulate crop growth at point locations under well known conditions. Since then, these models have been applied in crop monitoring and yield forecasting systems at regional and continental scales with typical spatial resolutions of 25 to 100 km. At these scales, the conditions for crop growth are difficult to define due to the large spatial and temporal variability in weather, soil and crop management. Typically Geographical Information Systems (GIS) have been applied to derive spatially explicit input (Hartkamp et al., 1999). However, limitations in soil, weather and management data

---

\*Chapter based on: Wit, A.J.W. d., Boogaard, H.L. and Diepen, C.A. v.: 2005, Spatial resolution of precipitation and radiation: the effect on regional crop yield forecasts, *Agricultural and Forest Meteorology* **135**(1-4),156-168

cause a considerable uncertainty in all the components of large area yield forecasting systems (Hoogenboom, 2000; Russel and Gardingen, 1997). Currently, it is often unclear how these uncertainties propagate through the system given the non-linear behaviour of crop models and the aggregation errors that may occur when aggregating crop model outputs to larger regions (Hansen and Jones, 2000).

Considerable research into the effects of uncertainty in weather, soil and management on crop model outputs has been carried out by both the crop modelling and climate change research communities. The crop modelling community has focused on point and local scale studies in order to assess uncertainty in management (Bouman, 1994), soil (Pachepsky and Acock, 1998) and weather (Fodor and Kovacs, 2005; Nonhebel, 1994; Soltani et al., 2004) data as well as integrated approaches assessing combined uncertainty in weather and soil (Launay and Guérif, 2003) and uncertainty in model parameters (Aggarwal, 1995). These results generally show that the uncertainties in soil and weather data were the main drivers for the uncertainty in the model output. However, the local scale of these studies makes the results hardly representative of uncertainty in regional to continental scale crop yield forecasting systems.

Within the climate research community much research has been dedicated to quantifying the effects of climate change on crop yield and studying the response of crop models to the uncertainty in climate change scenarios derived from general circulation models (GCMs) at a range of spatial scales. These studies demonstrated that crop models are sensitive to the variability of precipitation and temperature inputs (Mearns et al., 2001; Semenov and Porter, 1995) and that the spatial scale of the weather inputs matters (Carbone et al., 2003; Mearns et al., 1999; Mearns et al., 2001). Furthermore, when aggregating model output to regional scale, weather becomes the dominant uncertainty while the soil strongly affects the spatial variance but having less effect on the mean aggregated yield (Easterling et al., 1998; Mearns et al., 2001). A limitation of these climate-related studies is that they focused primarily on the uncertainty in the GCM simulations, rather than the true weather patterns. Moreover, the spatial resolution of 'high resolution' climate change scenarios ( $0.5^\circ$ ) applied in these studies, can still be regarded as fairly low.

This study positions itself between the local to point scale crop modelling studies using observed data on the one side, and the regional climate change studies using simulated weather data on the other side. The objective is to quantify the influence of uncertainty in radiation and precipitation on (1) the crop simulation results at  $50 \times 50$  km grid level, (2) the spatially averaged crop simulation results at regional level and, (3) the national yield forecasts



for France and Germany through the growing season. Moreover, we evaluate the influence of averaging of radiation and precipitation values on the model output. These results are obtained by comparing output from an operational crop yield forecasting system (which uses interpolated meteorological variables from weather stations) with output obtained by integrating a high-resolution ( $0.2^\circ$ ) precipitation and radiation database into the system.

## 3.2 Methodology

### 3.2.1 The crop simulation model

To assess the effect of uncertainty in precipitation and radiation input, we used the WOFOST (WORld FOod STudies) crop simulation model (Diepen et al., 1989). WOFOST is a mechanistic crop growth model that describes plant growth by using light interception and  $\text{CO}_2$  assimilation as growth driving processes and by using crop phenological development as growth controlling process. The model can be applied in two different ways: 1) a potential mode, where crop growth is purely driven by temperature and solar radiation and no growth limiting factors are taken into account; 2) a water-limited mode, where crop growth is limited by the availability of water. The difference in yield between the potential and water-limited mode can be interpreted as the effect of drought. Currently, no other yield-limiting factors (nutrients, pests, weeds, farm management) are taken into account.

WOFOST and the other Wageningen crop models (Bouman et al., 1996; van Ittersum et al., 2003) have been applied and validated in temperate, Mediterranean, sub-tropical and tropical environments under different soil and management conditions. The WOFOST model is capable of simulating many crop types using crop specific parameter sets. Although validation has mainly been carried out at field scale, WOFOST was developed with regional applications in mind which has led to modest input requirements in terms of weather, soil and crop management. The model results are sensitive to weather, soil and management parameters as well as crop variety.

### 3.2.2 The Crop Growth Monitoring System

The Crop Growth Monitoring System (CGMS) allows regional application of WOFOST by providing a database framework which handles model input (weather, soil, crop parameters), model output (crop indicators such as total biomass and leaf area index), aggregation to statistical regions and yield forecasting (Boogaard et al., 2002; Diepen, 1992; Genovese, 1998; Vossen and

Rijks, 1995). CGMS is a typical example of a ‘simulate first – aggregate later’ type of system which implies that individual crop simulations are first carried out on the smallest spatial unit possible: a soil unit. In a subsequent step, simulations results are aggregated to grids or statistical regions by weighing on the relative area of the soil unit. The idea underlying this approach is that aggregation errors caused by non-linear response of crop models to inputs can be avoided as much as possible.

Yield forecasting in CGMS takes place at the level of European Union (EU) countries by searching for a relationship between CGMS crop indicators aggregated to national level and the crop yield statistics available from the European Statistical Office (EUROSTAT). It is assumed that crop yield for a region can be divided into three factors: mean yield, multi-annual trend (or technology trend) and residual variation (Vossen, 1992). CGMS uses a running time-series of yield statistics of at least nine years to determine a linear technology trend assuming that the trend is stable over this period. The time-series of crop simulation results are then used to explain the residual deviation. The system selects the best predictor out of four CGMS crop indicators (simulation results): potential yield biomass, potential yield storage organs, water-limited yield biomass and water-limited yield storage organs. Crop yield forecasting takes place by using the crop simulation results to predict the deviation from the technology trend already at the beginning of the growing season. More information on the crop yield forecasting algorithm can be found in Boogaard et al. (2002).

CGMS is part of the MARS (Monitoring Agriculture by Remote Sensing) crop yield forecasting system developed by the AgriFish unit of the Joint Research Centre in Ispra, Italy. The MARS system was developed in the early nineties and consists of several components including crop monitoring with low resolution satellite data and an agrometeorological crop monitoring system currently known as CGMS. Since 1994, CGMS monitors crop growth in Europe, Anatolia and the Maghreb with a spatial resolution of  $50 \times 50$  km and a temporal resolution of one day. Its main purpose is to provide information on weather indicators and crop status during the growing seasons and to provide objective forecasts of crop yield on the level of EU member states early in the crop growth season. Its main user is the European Commission’s Directorate General for Agriculture.

### 3.2.3 Study area

The study area is located in Germany and France (Figure 3.1). The motivations for this choice were that from north to south a clear gradient exists from temperate maritime conditions in Northern Germany to Mediterranean condi-

tions in the south of France. Besides, time-series of yield statistics are available for Germany and France which could be used for yield forecasting purposes. Finally, the study area is small enough to allow reasonable processing times.

### 3.2.4 Soil and weather inputs

Soil inputs for CGMS are derived from the 1:1,000,000 European soil map (King et al., 1995) and from the 1:5,000,000 global soil database developed by the Food and Agriculture Organisation for areas outside Western and Central Europe. The CGMS  $50 \times 50$  km grid was overlayed with the soil data in order to determine which soils were available in each CGMS grid. Soil moisture contents at different pressure heads (saturation, field capacity, wilting point) are estimated from the soil physiological description and together with the estimated rooting depth they determine the water retention capacity and hydraulic conductivity of the soil. This information is used for the water balance calculations that are needed for water-limited production estimates. Besides estimating soil hydraulic properties, the soil map is also used for estimating the suitability of soils for different crops and for weighing the simulation results to grids and administrative units.

The weather information in CGMS is currently derived from about 2500 weather stations over the entire area, the total number of stations varies somewhat over time. For France and Germany 182 weather stations are available. These weather stations provide daily estimates of minimum and maximum temperature, wind speed, vapour pressure and precipitation. Radiation is only available from a limited number of stations and therefore radiation is estimated at station level using relationships with temperature, cloud duration or sunshine hours (Supit and van Kappel, 1998).

Next, an interpolation routine is applied to estimate weather variables for each  $50 \times 50$  km grid cell (Voet et al., 1994). Each cell receives values for temperature, radiation, vapour pressure, evapotranspiration and wind speed as the weighted average from suitable surrounding weather stations using inverse distance weighting. Determination of the most suitable weather stations takes place on the basis of the so-called 'meteorological distance'. This meteorological distance is a virtual distance which is not only based on the true distance between the grid cell and the weather station, but also on factors like altitude, distance to coast and the existence of climate barriers (e.g. mountain ridges, water bodies) between the grid cell and the weather station. In case of rainfall a grid cell receives the value of the weather station with the smallest meteorological distance from the grid cell. This method was chosen in order to avoid the distortion of precipitation sequences caused by averaging precipitation values from multiple weather stations.

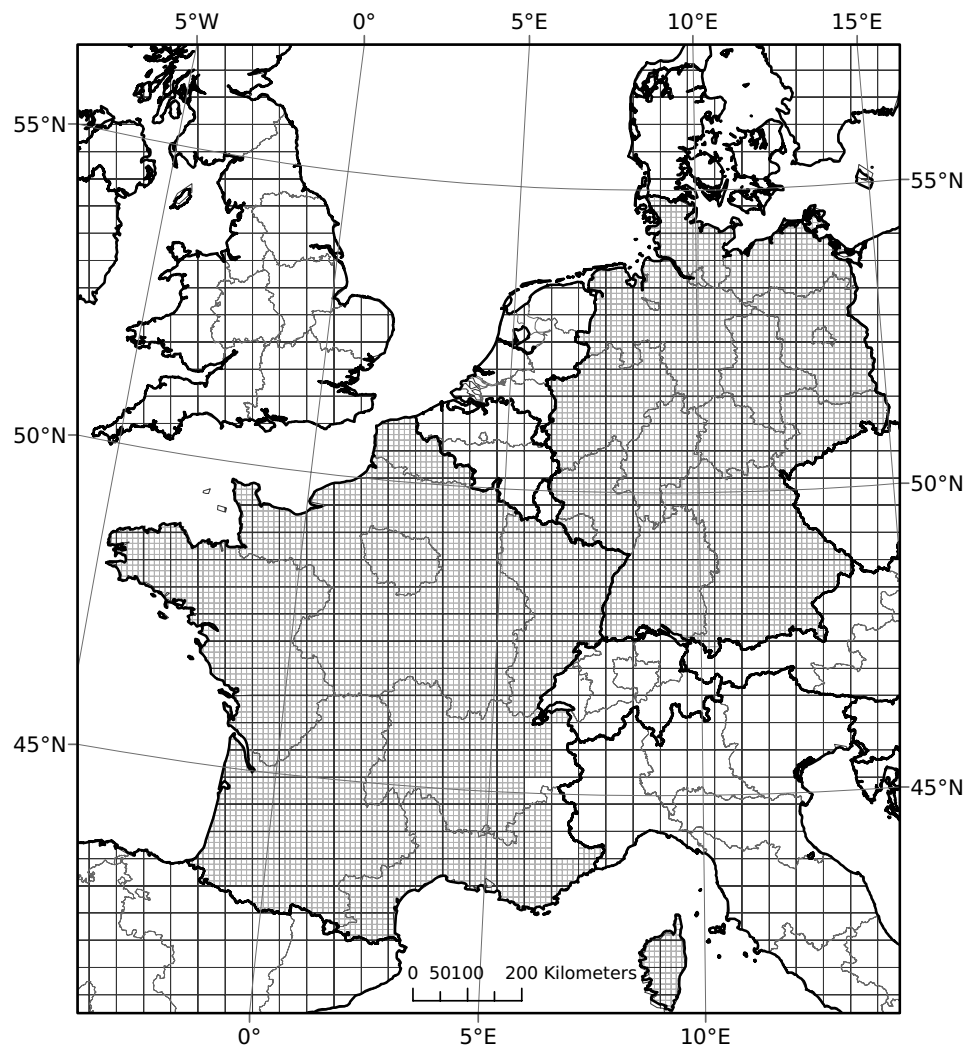


*Figure 3.1:* Overview of the study area showing the NUTS0 regions (thick black country borders), the NUTS1 regions (grey provincial borders), the 50 × 50 km CGMS grid (black square grid) and the 10 × 10 km grid (grey square grid).

### 3.2.5 High resolution precipitation and radiation inputs

The high temporal and spatial resolution databases used in this study were generated in the framework of the ELDAS (European Land Data Assimilation System) project. This EU 5<sup>th</sup> framework project aimed at the development of a data assimilation infrastructure for estimating continental scale soil moisture fields and to validate the use of these fields in numerical weather prediction models.

The ELDAS radiation database is based on the output of a numerical weather forecasting model which was improved by assimilating MeteoSat-derived shortwave radiation and cloud patterns into the model. This system is currently known as the ELDORADO assimilation scheme (Meetschen et al., 2004). The system generated three-hourly estimates of average downwelling longwave and shortwave radiation at approximately 16-km spatial resolution over Europe for the period from 1 October 1999 until 31 December 2000. Validation of the radiation estimates provided by ELDORADO demonstrated that the system provided accurate unbiased estimates of longwave and shortwave radiation. For our purpose, the three-hourly values were aggregated and converted to total daily shortwave radiation in KJ/day.

The ELDAS precipitation database consists of daily precipitation values on a 0.2° grid over Europe for the period from 1 October 1999 until 31 December 2000 (Rubel and Hantel, 2001; Rubel et al., 2004). The precipitation values were interpolated using block kriging based on more than 20,000 bias-corrected rain gauge measurements. Validation has demonstrated that systematic measurement errors for over 90% of the number of stations were within 1 mm/day. Given the sheer volume of rain gauge measurements that were used to generate this database, it will give a far better estimate of the true rainfall patterns compared to the estimates in the CGMS meteorological database.

### 3.2.6 Setup of the experiment

First, an exploratory analysis was carried out to determine the differences between the radiation and precipitation fields of the CGMS and ELDAS databases. The results of this analyses provided necessary background information in order to explain the differences in crop simulation results when using ELDAS precipitation and radiation inputs. We determined the uncertainty in the CGMS radiation and precipitation fields by calculating the average radiation and total precipitation over a period of 10 days for dekads<sup>1</sup> 1, 10, 19 and 28 for both the CGMS and ELDAS databases. The average precipitation

---

<sup>1</sup>The use of the term 'dekad' refers to an FAO convention in order to distinguish 10-year periods (decade) from 10-day periods (dekad).

and radiation values of all ELDAS grid points within a CGMS grid cell were used. We subtracted the ELDAS values from the CGMS values for all grids, calculated mean and standard deviation of the differences and created maps of the differences (maps are not presented).

We carried out three experiments, summarized in Table 3.1. Experiment one (hereafter referred to as ‘CGMS-Standard’) comprised the running of the operational CGMS system for the year 2000 using interpolated weather from about 180 stations over France and Germany. Model simulations were carried out for winter-wheat and grain maize which are good examples of a typical winter and summer crop. No modifications were made to this system and the results therefore served as a baseline for the other two experiments.

In experiment two, we replaced the CGMS interpolated precipitation and radiation values with the average radiation and precipitation values of all ELDAS grid points within a  $50 \times 50$  km CGMS grid box (hereafter referred to as ‘CGMS-ELDAS-50’). This experiment allowed us to estimate the influence of uncertainty in the precipitation and radiation inputs on the crop simulations and its effect on regional aggregated yields and national yield forecasts. All other meteorological input variables and other data were kept to the values that were obtained by the interpolation routine in the CGMS-Standard experiment.

Possible interrelationships between the ELDAS weather variables and the equivalent CGMS interpolated weather variables were not taken into account. For example, consider a situation where the CGMS interpolation routines estimate the maximum temperature for a certain grid on the basis of the surrounding weather stations which were located in areas with clear days. In contrast, at this location the ELDAS database provides a considerable amount of precipitation and also lower radiation values as a result of overcast conditions. Then, one might expect a lower maximum temperature than the interpolated one because the precipitation and lower radiation values were completely ‘missed’ by the interpolation routine. This kind of relationships have not been taken into account and as a result, we assume that the inconsistency between the interpolated and the ELDAS weather variables has little effect on the final simulation results. The CGMS-ELDAS-50 experiment was applied for the year 2000 in order to simulate growth of winter-wheat and grain maize.

In the third experiment, we introduced a major change in the system by increasing the grid density from  $50 \times 50$  km to  $10 \times 10$  km (hereafter referred to as ‘CGMS-ELDAS-10’). This experiment allowed us to estimate the within-grid variability of the crop simulation results in order to infer if averaging weather inputs has a linear impact.

We defined a  $10 \times 10$  km grid that coincides with the  $50 \times 50$  km grid, each  $50 \times 50$  km grid box contained 25  $10 \times 10$  km grids. Each  $10 \times 10$  km

Table 3.1: Summary of experiments and related scales and input data.

<i>Experiment</i>	<i>Scale</i>	<i>Precipitation input</i>	<i>Radiation input</i>
CGMS-standard	50 km	CGMS	CGMS
CGMS-ELDAS-50	50 km	ELDAS 50-km mean	ELDAS 50-km mean
CGMS-ELDAS-10	10 km	ELDAS 0.2°	ELDAS 0.2°

grid received the precipitation and radiation values of the nearest ELDAS grid point, while all other meteorological variables were derived from underlying  $50 \times 50$  km grid based on the CGMS-Standard experiment. Our approach was basically a shortcut in order to avoid redefining and recalibrating the CGMS interpolation procedure on the  $10 \times 10$  km grid. We assume that this shortcut has little influence on the simulation results. The final adaptation we made was to create an overlay between the soil map and the  $10 \times 10$  km grid. This procedure results in a new set of simulation units (unique combinations of climatic grid cell and soil type). The CGMS-ELDAS-10 experiment was applied for the year 2000 in order to simulate growth of winter-wheat and grain maize.

For determining the influence of the weather inputs on the yield forecast at national level we used the EUROSTAT yield statistics (EUROSTAT, 2005) and the output of the operational CGMS system over the period 1990–1999 to develop the forecasting regression equations. We applied those regression equations to the crop simulations results of the CGMS-Standard and CGMS-ELDAS-50 experiments (aggregated to national level) for France and Germany for the year 2000. Note that a true assessment of the influence of the uncertainty in weather inputs on the yield forecast cannot be carried out because this exercise would need 10 years of ELDAS type radiation and precipitation data. Our approach merely determines the influence of the ELDAS results on the forecasting regression equations calibrated on the operational CGMS.

### 3.3 Results

#### 3.3.1 Comparison of CGMS and ELDAS radiation and precipitation fields

In Table 3.2, the differences between the CGMS and ELDAS radiation values demonstrate that CGMS has a tendency to overestimate radiation (positive differences). In general CGMS overestimates radiation values in the southern Mediterranean areas in all four dekads. For all other areas large positive

Table 3.2: Summary statistics of the differences between the CGMS and ELDAS databases (CGMS minus ELDAS) for radiation and precipitation averaged over all CGMS grids.

Dekad	Average radiation [kJ/m <sup>2</sup> ]			Total precipitation [mm]		
	Mean CGMS <sup>a</sup>	Mean diff <sup>b</sup>	St. Dev. diff <sup>c</sup>	Mean CGMS <sup>d</sup>	Mean diff <sup>e</sup>	St. Dev. diff <sup>f</sup>
1	3929	564.6	1137.0	10.6	-5.4	17.7
10	12597	-231.0	1946.6	16.3	-4.8	12.1
19	20202	1182.6	3649.7	18.9	-1.6	14.5
28	9222	539.0	1495.8	17.8	-3.2	16.9

<sup>a</sup> Average dekadal radiation, averaged over all CGMS grids.

<sup>b</sup> Average of the differences in average dekadal radiation of all 50 × 50 km grids.

<sup>c</sup> Standard deviation of the differences in average dekadal radiation of all 50 × 50 km grids.

<sup>d</sup> Total dekadal precipitation, averaged over all CGMS grids.

<sup>e</sup> Average of the differences in total dekadal precipitation of all 50 × 50 km grids.

<sup>f</sup> Standard deviation of the differences in total dekadal precipitation of all 50 × 50 km grids.

and negative differences occur, for example in dekad 10 radiation is underestimated with values of 3000 to 4000 kJ/m<sup>2</sup> in northern Europe, while in dekad 19 radiation is overestimated with 3000 to 5000 kJ/m<sup>2</sup> in large parts of Central and Eastern Europe.

The differences between the CGMS and ELDAS precipitation values (Table 3.2) demonstrate that CGMS has a tendency to underestimate precipitation (negative differences). In general no clear trends can be derived from the spatial distribution of the differences and under or overestimation of precipitation tends to occur rather randomly.

### 3.3.2 Uncertainty of simulated crop yields

The uncertainty in the radiation and precipitation fields as demonstrated in the previous section will have influence on the crop simulation results. We assessed this uncertainty by comparing the results for the simulated potential and water-limited biomass of the storage organs of the CGMS-Standard and CGMS-ELDAS-50 experiments.



Table 3.3: Summary statistics of the crop yield at  $50 \times 50$  km grids obtained by the CGMS-Standard and CGMS-ELDAS-50 experiments.

	<i>Winter-wheat</i>		<i>Grain maize</i>	
	Potential yield	Water-lim. yield	Potential yield	Water-lim. yield
<i>Simulation results [kg/ha]</i>				
A: CGMS-Standard <sup>a</sup>	9217.0	7461.8	8780.2	5782.4
B: CGMS-ELDAS-50 <sup>a</sup>	9195.7	8130.7	8649.7	6203.0
<i>Differences (A-B)</i>				
Mean <sup>b</sup>	21.3	-668.8	130.5	-420.6
St. Deviation <sup>c</sup>	644.4	1164.9	351.5	1479.4
RMSE <sup>d</sup>	644.0	1342.1	374.6	1536.3

<sup>a</sup> Yield storage organs averaged over all  $50 \times 50$  km grids.

<sup>b</sup> Average of the differences in yield storage organs of all  $50 \times 50$  km grids.

<sup>c</sup> Standard deviation of the differences in yield storage organs of all  $50 \times 50$  km grids.

<sup>d</sup> RMSE of the differences in yield storage organs of all  $50 \times 50$  km grids.

For winter-wheat under potential production, the mean of the differences is slightly positive (21.3 kg/ha) which can be explained by the overestimation of radiation by CGMS leading to higher CGMS-Standard yields compared to CGMS-ELDAS-50 yields (Table 3.3). For water-limited production on the other hand, the mean of the differences becomes strongly negative (-668.8 kg/ha) due to the underestimation of precipitation by CGMS; also the standard deviation and root mean squared error (RMSE) become twice as large. This is confirmed by the scatter plot of CGMS-Standard versus CGMS-ELDAS-50 yield which shows a considerable deviation from the 1:1 line and a majority of pixels above the diagonal (Figure 3.2A).

For grain maize under potential production, the mean of the differences is also positive (130.5 kg/ha) which confirms the overestimation of radiation by CGMS-Standard. The effect of uncertainty in the precipitation on grain maize simulation is even larger compared to winter-wheat because the standard deviation and RMSE of the differences are four times larger compared to the potential simulations. These results demonstrate that the effect of uncertainty in precipitation is particularly strong for summer crops which are more influenced by high transpiration rates during the summer. The scatter plot confirms the large uncertainty in the CGMS-Standard simulation results (Figure 3.2B). The plot also shows a clustering of pixels near the origin and the upper right

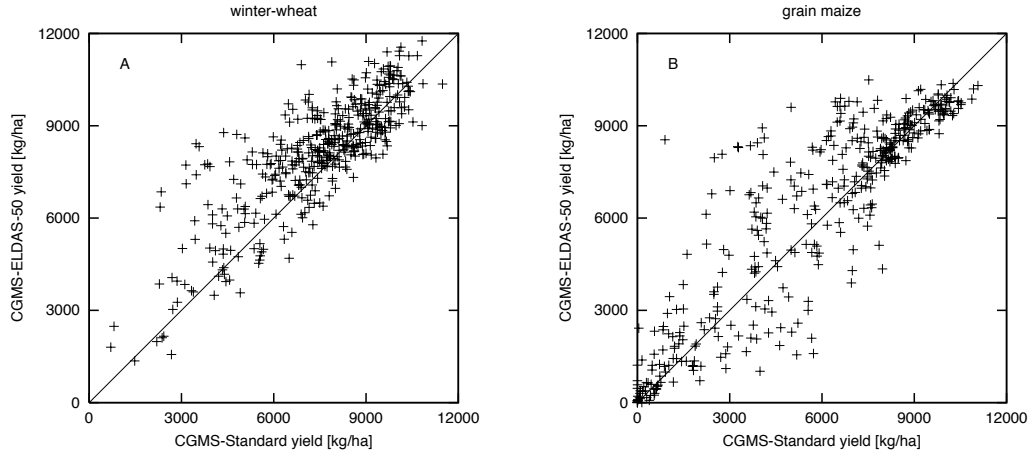


Figure 3.2: Scatter plot between water-limited yield storage organs (yield) at 50-km grid level obtained from the CGMS-Standard and CGMS-ELDAS-50 experiments for winter-wheat (A) and grain maize (B).

part of the chart which indicates that yield is not influenced under wet (potential yield) or dry (no yield) conditions, but instead the marginal zones are sensitive to uncertainty in precipitation.

For yield forecasting it was necessary to aggregate the yield of individual grid cells to larger spatial regions. When the CGMS-Standard and CGMS-ELDAS-50 simulation results at the  $50 \times 50$  km grid level were spatially aggregated to NUTS1 regions the variability between the CGMS-Standard and the CGMS-ELDAS-50 water-limited yield storage organs became much smaller (Figure 3.3A). For winter-wheat an upward bias remains (Table 3.4) and even increases in magnitude from -668.8 kg/ha at  $50 \times 50$  km grid level to -1000.9 kg/ha at NUTS1 level. As a result of this bias, the RMSE between CGMS-Standard and CGMS-ELDAS-50 yields at NUTS1 level is still relatively high (1255.6 kg/ha). However, the standard deviation decreases from 1164.9 kg/ha at  $50 \times 50$  km grid level to 774.3 kg/ha at NUTS1 level indicating a decrease in variability (Table 3.3).

The results for grain maize at NUTS1 level are more evenly distributed along the 1:1 axis (Figure 3.3B). The mean of the differences (Table 3.4) decreases in magnitude from -420.6 kg/ha to -368.8 kg/ha and also the standard deviation and RMSE decrease from 1479.4 and 1536 kg/ha to 651.4 and 736.7 kg/ha indicating a considerable decrease in variability. These results demonstrate the necessity to aggregate CGMS results to larger regions in order to decrease uncertainty on the simulation results.

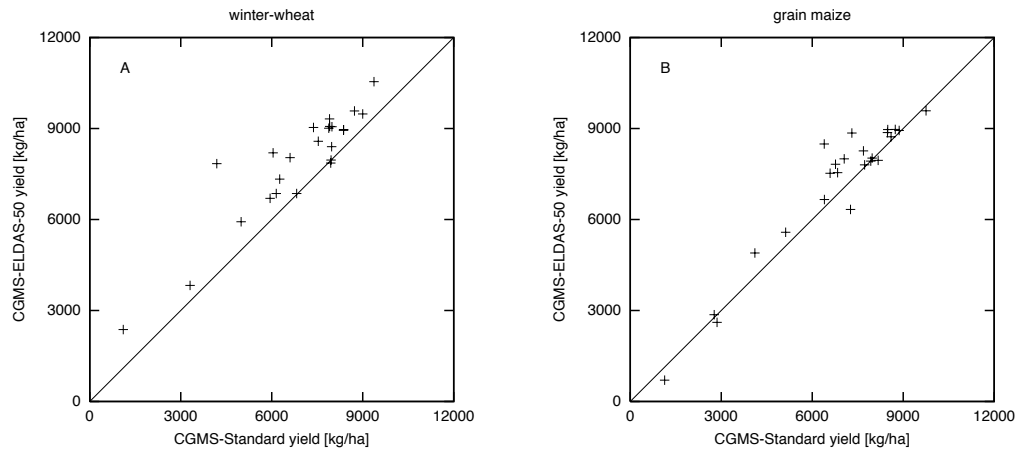


Figure 3.3: Scatter plot between water-limited yield storage organs (yield) at NUTS1 level obtained from the CGMS-Standard and CGMS-ELDAS-50 experiments for winter-wheat (A) and grain maize (B).

### 3.3.3 Scaling of crop yield simulation results

We investigated the spatial scaling of CGMS by comparing the water-limited biomass of the storage organs of the CGMS-ELDAS-50 and CGMS-ELDAS-10 experiments. The mean and standard deviation of the water-limited biomass of the storage organs of the CGMS-ELDAS-10 simulations were calculated for each corresponding  $50 \times 50$  km grid in the CGMS-ELDAS-50 experiment (Figure 3.1). The results demonstrate that for water-limited production considerable subgrid variability exists (Y-error bars), but that the results at 50-km grid resolution are almost linearly related to the average of the  $10 \times 10$  km results (Figure 3.4). The few outliers in the scatter plots could be traced back to fragmented CGMS grids located along an irregular coastline. A linear regression on the relationship between the CGMS-ELDAS-50 results and the 50-km averaged CGMS-ELDAS-10 results shows that for both winter-wheat and grain maize the regression coefficient is nearly one and  $R^2$  reaches values of 0.96 to 0.97 (Table 3.5). The intercept was set to zero in the regression.

### 3.3.4 Results at national level and influence on the crop yield forecast

The simulation results at the end of the growing season aggregated to national level show that the differences between the results of the CGMS-Standard and CGMS-ELDAS-50 experiments for potential production are within 3% (Table 3.6). For water-limited production the differences are larger ranging from -

Table 3.4: Summary statistics of the simulated crop yield at NUTS1 level of the CGMS-Standard and CGMS-ELDAS-50 experiments.

	Winter-wheat		Grain maize	
	Potential yield	Water-lim. yield	Potential yield	Water-lim. yield
<i>Simulation results [kg/ha]</i>				
A: CGMS-Standard <sup>a</sup>	9276.2	6905.2	8619.1	6793.0
B: CGMS-ELDAS-50 <sup>a</sup>	9428.8	7906.2	8605.4	7161.8
<i>Differences (A-B)</i>				
Mean <sup>b</sup>	-152.4	-1000.9	13.7	-368.8
St. Deviation <sup>c</sup>	481.7	774.3	258.7	651.4
RMSE <sup>d</sup>	495.6	1255.6	253.6	736.7

<sup>a</sup> Yield storage organs averaged over all NUTS1 regions.

<sup>b</sup> Average of the differences in yield storage organs of all NUTS1 regions.

<sup>c</sup> Standard deviation of the differences in yield storage organs of all NUTS1 regions.

<sup>d</sup> RMSE of the differences in yield storage organs of all NUTS1 regions.

Table 3.5: Results from a linear regression between water-limited yield storage organs of the CGMS-ELDAS-50 experiment ( $50 \times 50$  km) and the water-limited yield storage organs of the CGMS-ELDAS-10 experiment ( $10 \times 10$  km). CGMS-ELDAS-10 results are averaged over the CGMS-ELDAS-50 grid. The intercept of the regression is assumed to be zero.

	Regression coefficient	$R^2$	RMSE [kg/ha]
Winter-wheat	0.989	0.967	327.8
Grain maize	0.997	0.989	335.0

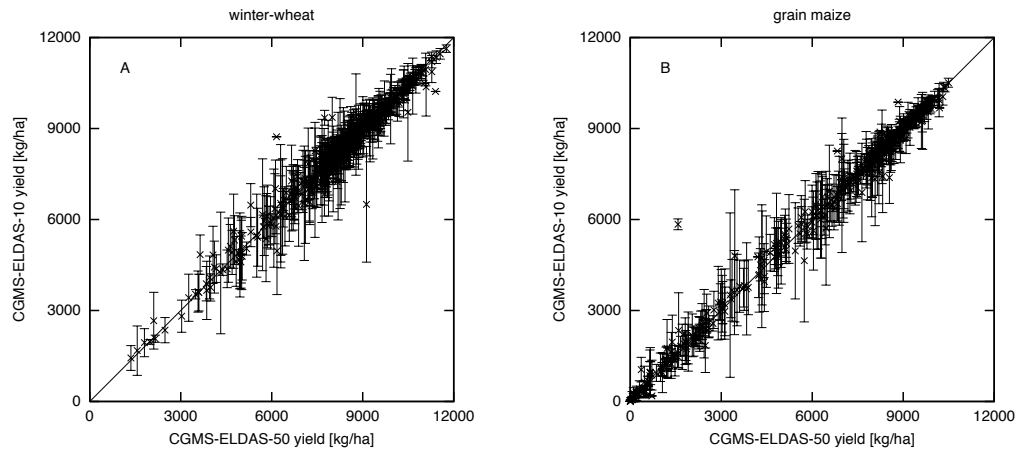


Figure 3.4: Scatter plot between water-limited yield storage organs (yield) obtained from the CGMS-ELDAS-50 experiment and the average water-limited yield storage organs obtained from the CGMS-ELDAS-10 experiment for winter-wheat (A) and grain maize (B). Error bars are plus and minus one standard deviation.

1.10% for water-limited yield biomass of grain maize in Germany to -10.38% for water-limited yield storage organs for winter-wheat in Germany. The fact that all results of the water-limited CGMS-ELDAS-50 experiment are higher compared to the CGMS-Standard experiment confirms the underestimation of rainfall in CGMS.

The influence of these differences in simulated biomass on the yield forecast could only be evaluated for grain-maize. Table 3.7 lists the  $R^2$  values of the regression equations produced by the yield forecasting module. For winter-wheat in Germany and France, the CGMS yield forecasting module rejected all CGMS indicators because a regression based on a combination of the technology trend and one of the CGMS indicators could not improve the yield forecast beyond a yield forecast based on the technology trend only. For grain maize in France and Germany good relationships could be established which improved the  $R^2$  value from 0.731 and 0.745 for the trend only, to 0.895 and 0.912 for the combined trend and CGMS indicators. The system selected the CGMS indicator 'water-limited yield biomass' as the best predictor of grain maize yield in Germany and France.

The time evolution of the yield forecast of grain maize in Germany demonstrates that the influence of uncertainty in radiation and precipitation on the yield forecast is small and the difference between the CGMS-Standard forecast and the CGMS-ELDAS-50 forecast is never larger than 0.53% except for dekad 14 (2.59%), but this is at the beginning of the growing season and

Table 3.6: Simulation results obtained by the CGMS-Standard and CGMS-ELDAS-50 experiments at the end of the growing season aggregated to the national level for France and Germany.

	France		Germany	
	Winter-wheat	Grain maize	Winter-wheat	Grain maize
<i>A: CGMS-Standard [kg/ha]</i>				
Potential yield biomass	19169	24814	18388	22533
Potential yield storage organs	9480	8742	9398	8939
Water-limited yield biomass	17810	16865	15516	21491
Water-limited yield storage organs	8142	3910	6960	8527
<i>B: CGMS-ELDAS-50 [kg/ha]</i>				
Potential yield biomass	19146	24777	18468	22111
Potential yield storage organs	9758	8569	9485	8876
Water-limited yield biomass	18311	18213	16334	21727
Water-limited yield storage organs	8925	4131	7683	8781
<i>(A-B)/A [%]</i>				
Potential yield biomass	0.12%	0.15%	-0.44%	1.87%
Potential yield storage organs	-2.93%	1.98%	-0.93%	0.71%
Water-limited yield biomass	-2.81%	-7.99%	-5.27%	-1.10%
Water-limited yield storage organs	-9.61%	-5.65%	-10.38%	-2.97%

Table 3.7:  $R^2$  values describing the results from the regression between the official yield statistics as reported by the European Statistical Office (EUROSTAT) and the crop yield indicators derived from the Crop Growth Monitoring System (CGMS) over the period 1990–1999.

	France		Germany	
	Winter-wheat	Grain maize	Winter-wheat	Grain maize
Trend only	0.550	0.731	0.756	0.745
Trend + CGMS indicator	-	0.895	-	0.912

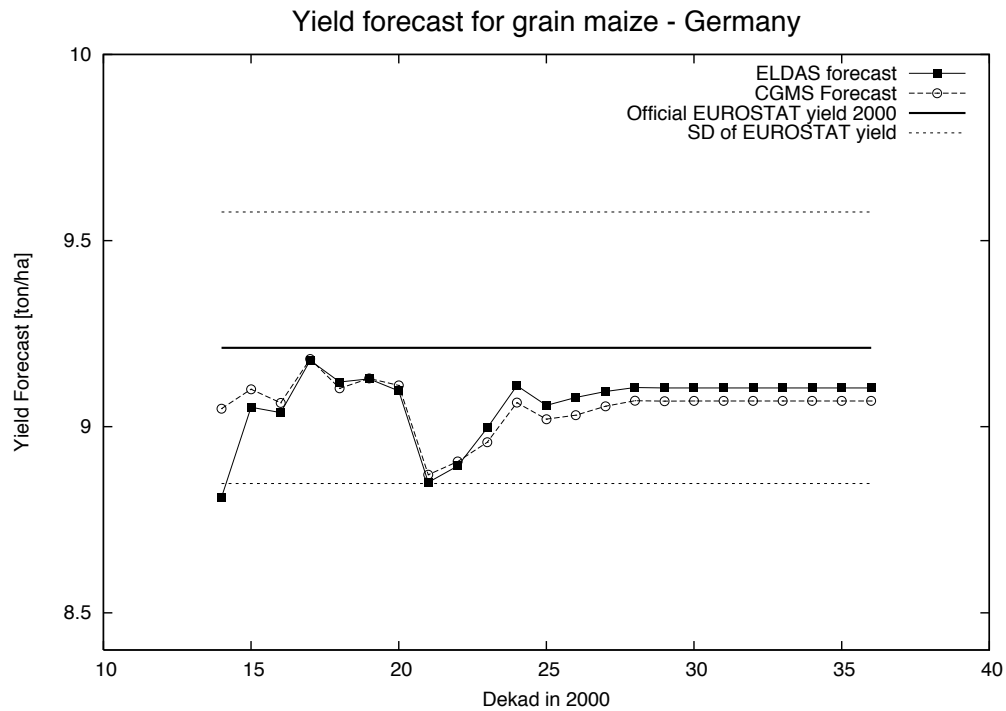


Figure 3.5: Time evolution of the yield forecast for grain maize in Germany for the year 2000. The thick line is the official yield for the year 2000 as reported by the European Statistical Office (EUROSTAT). The dotted lines are plus and minus one standard deviation of the de-trended EUROSTAT yields over the period 1990–1999.

therefore unreliable (Figure 3.5). The progression of the yield forecast during the growing season is similar for the CGMS-Standard forecast and the CGMS-ELDAS-50 forecast. Moreover, the CGMS-ELDAS-50 forecast is closer to the EUROSTAT official yield, but, more importantly, the difference between the CGMS-Standard forecast and the CGMS-ELDAS-50 forecast is much smaller than the standard deviation of the de-trended EUROSTAT yield over the period 1990–1999. This demonstrates that the effect of uncertainty in precipitation and radiation on the forecast is small compared to the dynamic range of the signal we are trying to model.

The time evolution of the yield forecast of grain maize in France demonstrates that the influence of uncertainty in radiation and precipitation on the yield forecast is considerably larger compared to Germany and the difference between CGMS-Standard and CGMS-ELDAS-50 yield forecast is 2.38% at the end of the growing season (Figure 3.6). This is not surprising given the much larger difference in the water-limited yield biomass for France compared to

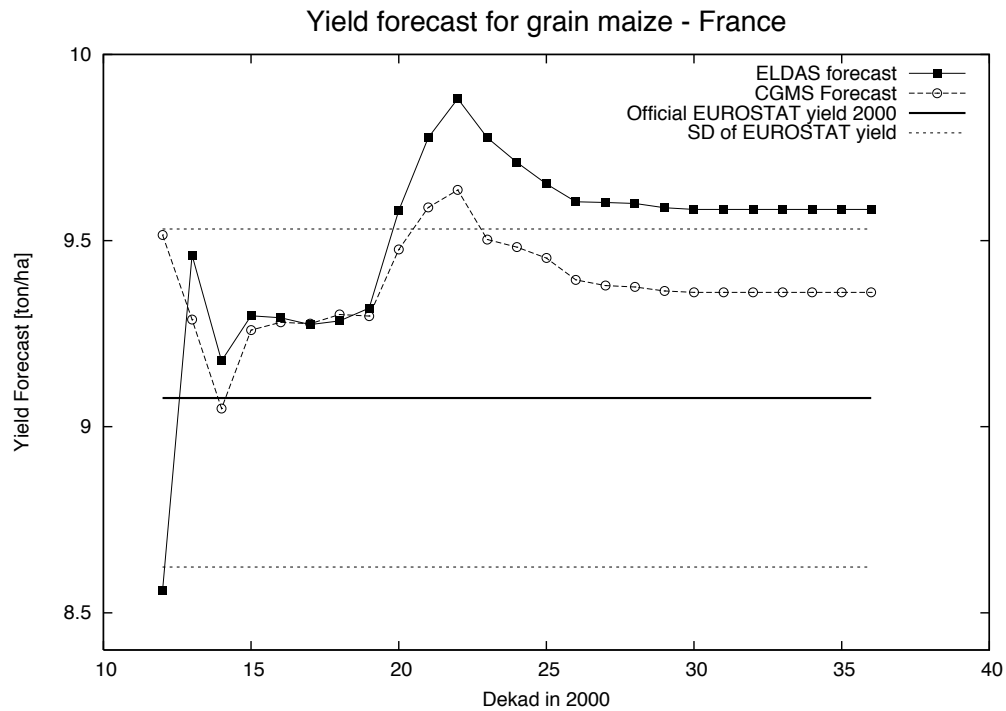


Figure 3.6: Time evolution of the yield forecast for grain maize in France for the year 2000. The thick line is the official yield for the year 2000 as reported by the European Statistical Office (EUROSTAT). The dotted lines are plus and minus one standard deviation of the de-trended EUROSTAT yields over the period 1990–1999.

Germany (Table 3.4). However, the difference between the CGMS-Standard and CGMS-ELDAS-50 forecasts is still considerably smaller than the standard deviation of the de-trended EUROSTAT yield over the period 1990–1999.

### 3.4 Discussion

The results of our study demonstrate that uncertainty in precipitation and radiation estimates obtained by the interpolation from weather stations can produce a considerable uncertainty on the simulation results aggregated to 50-km grid level. When the simulation results were aggregated to NUTS1 regions this uncertainty strongly decreased as a result of averaging. No analyses was carried out on the ability of CGMS to forecast crop yield at NUTS1 level and the influence of uncertainty in weather inputs at this level. On the one hand, the influence of uncertainty in radiation and precipitation inputs on the aggregated yields will be larger at NUTS1 level compared to NUTS0 level. This



may deteriorate CGMS ability to forecast yields on NUTS1 level compared to NUTS0. On the other hand it can be argued that the dynamic range in the official yield statistics at NUTS1 level is also larger compared to the national level (NUTS0). These two effects may compensate each other down to a certain scale level at which the input precipitation and radiation fields have an inadequate spatial resolution and no reliable forecast can be made.

At the national level, we demonstrated that the uncertainty in the crop simulation results has a small effect on the yield forecast of grain maize. For France, uncertainty is larger compared to Germany probably as a result of France being a more marginal climate for maize growth compared to Germany. It is useful to point out that the uncertainty for France is probably even overestimated. The comparison of the ELDAS precipitation database with the precipitation values in the CGMS database demonstrates that rainfall is systematically underestimated by CGMS. As a result, the CGMS-ELDAS-50 water-limited simulation results indicate systematically larger production compared to the CGMS-Standard results. However, the regression equations were developed with the simulation results from the operational CGMS. If those regression equations could have been developed with 10 years of CGMS-ELDAS-50 simulation results then the bias in model output could have been compensated by the forecasting regression.

Based on the results of the simulations at  $10 \times 10$  km grid (CGMS-ELDAS-10) with distributed rainfall and radiation data we conclude that there is little merit in increasing the resolution of the CGMS grid. The average simulation results at  $10 \times 10$  km scale almost linearly with the simulation results at  $50 \times 50$  km using averaged rainfall and radiation. Therefore the operational CGMS is able to make unbiased estimates of crop yield if unbiased average radiation and rainfall would be available at the  $50 \times 50$  km grid. These results support the notion by other authors that some level of spatial partitioning of climate data exists which preserves linear climate-crop model interactions. Easterling et al. (1998) found this level to be  $0.9^\circ \times 0.9^\circ$  and found no improvement between simulated and observed crop yields when increasing the density of weather input to  $0.5^\circ \times 0.5^\circ$ . These results are consistent with the results found in this study, but may not be generally applicable depending on factors such as climate and orography.

An aspect not treated in this study is the influence of uncertainty in soil properties. A number of studies have demonstrated that the uncertainty in soil data has relatively little influence on the aggregated regional simulation results (Easterling et al., 1998; Mathe-Gaspar et al., 2005; Mearns et al., 2001). Since the prime focus of CGMS is to forecast crop yield at national level its investigation is therefore not of prime importance. There are other arguments not mentioned so far why the soil is of minor importance. Crop yield forecast-

ing applications are mainly driven by year-to-year variability in a yield level rather than the yield level itself because a bias in yield level is compensated by the forecasting regression equations. Soil mainly determines the yield level and, although it can moderate the effects of year-to-year variability in weather conditions on yield, it is not a driver of year-to-year variability. Given the difficulties that exist in characterizing soil parameters (Gijssman et al., 2002) it may be worthwhile to investigate how yield forecasting applications perform using a standardized soil.

### 3.5 Conclusions

The results presented in this paper lead us to conclude that uncertainty in radiation and precipitation values in the Crop Growth Monitoring System has little influence on the CGMS yield forecasts at national level. This conclusion was validated for grain maize in Germany and France; but is probably valid for other European countries with similar climates and crops as well. On the level of individual grids and NUTS1 regions the uncertainty is much larger and more research is needed to investigate if CGMS results can be used for decision making at this level. Furthermore, we conclude that the CGMS grid size of  $50 \times 50$  km is an appropriate resolution because the distributed simulation results at  $10 \times 10$  km scale almost linearly with the results at  $50 \times 50$  km using aggregated rainfall and radiation. Improvements of the system should therefore focus on providing average unbiased estimates of weather variables at  $50 \times 50$  resolution, rather than increasing the grid resolution.

## Chapter 4

# Representing uncertainty in continental-scale gridded precipitation fields for agrometeorological modelling\*

### 4.1 Introduction

Process-based mechanistic crop models are an important tool for translating the effect of crop management, weather and soil on crop growth. Although many crop models were originally designed and tested at the plot scale, they are nowadays applied in systems with typical spatial resolutions of 0.5 to 2.5 degrees and their aggregated output is used to predict crop yield and production at regional, national and continental scales. Such information on the outlook of yield and production of crops over large regions is essential for government services dealing with import and export of food crops, for agencies playing a role in food relief, for international organisations with a mandate in monitoring the world food production and trade, and for commodity traders.

Given the scales at which these systems operate, the model simulation results are subject to large uncertainties because the conditions to crop growth are difficult to define due to the large spatial and temporal variability in weather, soil and crop management. It is generally acknowledged that at the spatial scales under consideration, the weather input represents the largest uncertainty (Aggarwal, 1995; Easterling et al., 1998; Mathe-Gaspar

---

\*Chapter based on: Wit, A.J.W. d., Bruin, S. d. and Torfs, P.: 2007, Representing uncertainty in continental-scale gridded precipitation fields for agrometeorological modelling, *Journal of hydrometeorology* **revised version submitted**

et al., 2005; Mearns et al., 2001). The main reason for the dominant effect of uncertainty in weather is that systems aimed at regional yield prediction do not predict crop yield directly, but merely aim to capture the year-to-year pattern of crop response to weather variability. The forecasting of crop yield then takes place by searching for a relationship between the historic time-series of simulated yearly crop yields and the reported crop yield statistics for administrative regions. In such a system, the influence of relatively stable factors like soil and management is secondary to factors that generate the year-to-year variability in simulated crop yield (mainly variability in weather). Although crop management and crop varieties do change (often improve) over the years, this is usually taken care of by de-trending the statistical crop yields before regression models are established.

The currently operational yield forecasting systems are generally deterministic in nature and are not capable of quantifying uncertainties that are inherent in all parts of the system. A shift is therefore necessary towards probabilistic systems which are commonplace nowadays in meteorological and hydrological applications. Of particular interest is the comparison with hydrological land surface models which aim to characterise the hydrologic state of the land surface, but have otherwise large similarity with crop models (both models simulate processes like evapotranspiration, plant growth and soil moisture). Two important insights can be learned from probabilistic applications of land surface models: 1) Rainfall is the key input for modelling the hydrologic state of the land surface (Syed et al., 2004) and 2) ensemble-based approaches are often used to represent uncertainty of an available rainfall product which allows for hydrologic error propagation in a probabilistic way (Carpenter and Georgakakos, 2004; Crow, 2003; Georgakakos et al., 2004; Reichle, McLaughlin and Entekhabi, 2002; Seo et al., 2000). A first step for ensemble-based probabilistic crop modelling is thus to develop a rainfall ensemble product tailored to the temporal and spatial scale required for regional crop modelling.

Nevertheless, there are evident differences between a crop model and a land surface model. From a temporal perspective, land surface models often operate at time steps of an hour or less to take into account the effect of high intensity–short duration rainfall events. This is necessary because the partitioning of energy and water fluxes is dependent on the antecedent conditions (in particular near surface soil moisture) which change in a highly dynamic way. In contrast, crop models simulate root-zone soil moisture in order to estimate the effect of water stress on plant growth and are therefore less sensitive to instantaneous events, but more to the cumulative effect of rainfall events on soil moisture levels. This is illustrated by the fact that most crop models operate at steps of one day or more and by the development of simple indices such as the FAO crop water satisfaction index which is basically an index re-

lating seasonal accumulated evapotranspiration to accumulated precipitation (Frère and Popov, 1986; Verdin and Klaver, 2002).

Another important aspect is the spatial scale at which to generate an ensemble-based rainfall product for regional crop modelling. Defining the appropriate spatial scale is necessary because of the non-linear behaviour of many crop models to weather inputs and the resulting aggregation errors that may occur when aggregating model output to administrative regions (Hansen and Jones, 2000). Existing studies are not entirely consistent on this aspect. Easterling et al. (1998) report maximum correlation between simulated and observed yield for maize in the US Great Plains when weather data at a scale of  $100 \times 100$  km was used as input. Challinor et al. (2003) found maximum correlation between rainfall data and ground nut yield over India at a scale roughly corresponding to  $250 \times 250$  km, while Wit et al. (2005) found linear scaling of crop model simulated biomass when precipitation and radiation inputs were scaled from  $10 \times 10$  km to  $50 \times 50$  km. In contrast, Oleson et al. (2000) found relatively little influence of scale of precipitation inputs to the explanatory power of crop model results for winter-wheat in Denmark. However, the authors notice that the variability in winter-wheat yield in Denmark is dominated by secondary effects (disease, pests, harvest conditions), rather than weather conditions. The above-mentioned results are not conclusive on the spatial scale, however they point to a spatial scale between  $50 \times 50$  km to  $100 \times 100$  km as being relevant for regional crop modelling.

Many ensemble generation approaches for rainfall can be found in the literature. They can be divided into two main categories. In the first category, ensemble techniques are used in weather generator applications which generate synthetic time-series of precipitation on single locations or on multiple locations with or without spatial dependence. The generator is often conditioned on a set of observed rainfall properties (for example monthly totals). The variability in the precipitation ensemble aims to represent the natural variability in the precipitation process. Therefore, an ensemble of precipitation sequences is more informative than a single precipitation sequence, particularly for risk assessment applications. Examples of generating precipitation ensembles on single or multiple point locations were summarised by Wilks and Wilby (1999) and have recently been extended using generalised linear models by Yang et al. (2005). The applications are often limited to weather generation at single stations or otherwise relatively small areas with multiple stations.

In the second category, ensemble techniques are used to characterise the spatio-temporal properties of the rainfall sequence or field that actually occurred in a given area, but which is uncertain as a result of limitations in the observed or forecasted data itself. For example, the ensemble can quantify the uncertainty as a result of limited rain gauge network density or inaccu-

rate precipitation estimates from numerical weather prediction (NWP) models, radar satellites or ground radar. Additionally, ensemble techniques are used to downscale a coarse-resolution precipitation field to equiprobable precipitation fields at a higher spatial and/or temporal resolution.

Examples for ensemble predictions on weather station locations by downscaling NWP forecasts have been provided by Bates et al. (1998) and (Charles et al., 2004). Although their methods do not necessarily preserve spatial correlation between sites in the ensemble, post-processing techniques have been developed for recovering the spatial correlation (Clark et al., 2004). Seo et al. (2000) proposed an ensemble technique method for downscaling coarse resolution daily NWP forecasts ( $64 \times 64$  km) to high-resolution precipitation ensembles ( $4 \times 4$  km), for input into a river stage forecasting model. Similarly, Mackay et al. (2001) use ensembles to downscale GCM precipitation at  $40 \times 40$  km resolution to  $8 \times 8$  km. In the temporal domain, Margulis and Entekhabi (2001) use ensemble techniques for disaggregation of coarse resolution satellite-based monthly precipitation estimates to daily values. Hossain and Anagnostou (2006) developed an ensemble-based framework for characterising the error in satellite radar rainfall estimates.

Examples of ensemble techniques applied to classical interpolation from rain gauge networks have also been described by various authors. Carpenter and Georgakakos (2004) use a simple multiplicative approach for generating ensembles of precipitation inputs at catchment level. With such an approach there is no uncertainty when the input precipitation is zero. More advanced approaches have been proposed by Lanza (2000) who simulated the precipitation fields as Gaussian random fields conditioned on rainfall at station locations and Pardo-Igúzquiza et al. (2006) who used a similar technique for generating ensembles of intermittent rainfall fields, but modelled the processes of rainfall occurrence amounts separately. Finally, Kyriakidis et al. (2004) did not model the rainfall amounts directly but used sequential simulation to generate realisations of the precipitation residuals which were then added to temporal trend models of precipitation at individual grid points.

In the current paper, we propose a relatively simple method for generating ensembles of gridded precipitation fields at a temporal and spatial scale (daily values and  $50 \times 50$  km averages) which is consistent with the requirements for crop model applications that target large area crop yield prediction. The developed methodology does not simulate the precipitation field directly, but it simulates residual error fields that have to be added to the precipitation field in order to obtain the ensemble trace. This procedure has the advantage of simplicity and eliminates the need to account for temporal autocorrelation and seasonality because it assumes that the operational product contains enough information to represent the basic patterns of seasonal, re-

gional and day-to-day variability. Additionally, the use of residuals avoids the problem of climate variability at decadal scales given that the decadal variability should be reflected in the measured data itself rather than in the residuals. This is particularly important for agrometeorological applications, given that often fairly long times-series of data need to be generated ( $\geq 10$  years). The developed method takes into account spatial correlation in the ensemble; it should reproduce the input statistics and presents a pragmatic solution that can be parameterised relatively easily.

For the implementation, we used the weather database of the European Crop Growth Monitoring System (CGMS) as the operational (but uncertain) precipitation product and we calibrated the ensemble generator using a highly accurate rainfall product available for a limited period. Next, we generate an ensemble of precipitation inputs that characterises the uncertainty in the CGMS precipitation product, and validate the statistical properties of the ensemble with the reference dataset. Finally, we illustrate the use of precipitation ensembles in crop yield forecasting by running the precipitation ensemble through a distributed crop growth model for a district in South-France.

## 4.2 Data

### 4.2.1 CGMS meteorological database

An important component of the Crop Growth Monitoring System is the CGMS meteorological database. This database contains daily weather data measured at stations starting in the 1970's and it is continuously updated with weather information. This long time-series of weather data is important for retrospective analyses of crop stress situations and validation of crop yield forecasts. The information in the database is currently derived from about 2500 weather stations over Europe, Turkey and the Maghreb. The total number of stations varies over time as a result of stations being discontinued or new ones established.

CGMS operates at grid cells of  $50 \times 50$  km, therefore an interpolation routine is applied to estimate weather variables for each  $50 \times 50$  km grid cell (Voet et al., 1994). Each cell receives values for temperature, radiation, vapour pressure, evapotranspiration and wind speed using inverse distance weighting, while rainfall is assigned from the nearest most similar station in terms of elevation and distance to the coast. This method was chosen to avoid the misrepresentation of precipitation sequences caused by averaging values from multiple weather stations. In spite of its simplicity, the CGMS interpolation scheme is known to perform well in terms of accuracy and robustness

in comparison with more advanced interpolations schemes (Gozzini and Paniagua, 2000). Uncertainty in the CGMS precipitation fields is thus a combined uncertainty as a result of limited station density and rain gauge sampling error which cannot be separated but which is known to influence the crop model simulation results (Wit et al., 2005).

#### 4.2.2 ELDAS precipitation data

The ELDAS precipitation database consists of daily precipitation values on a  $0.2^\circ$  grid ( $\pm 15$  km) over Europe for the period 1 October 1999 until 31 December 2000 (Rubel and Hantel, 2001; Rubel et al., 2004). The precipitation values were interpolated using block kriging based on more than 20,000 bias-corrected rain gauge measurements. The collection of these rain gauge measurements was a one-off activity and no update is to be expected in the near future. Validation has demonstrated that systematic measurement errors for over 90% of the number of stations are within 1 mm/day.

It is important to notice that the ELDAS precipitation estimates are much smoother than a real precipitation field and should be regarded as spatial averages. Nevertheless, given the sheer volume of rain gauge measurements that were used to generate this database, it will give a far better estimate of the true daily average rainfall field as compared to the estimates in the CGMS meteorological database.

We used the ELDAS database as a reference for modelling the error structure in the CGMS precipitation fields. The ELDAS precipitation database was converted to the  $50 \times 50$  km CGMS grid by taking the average precipitation of ELDAS cells within a CGMS grid cell (on average 7.5 ELDAS nodes in one CGMS grid cell).

#### 4.2.3 Exploratory analyses of ELDAS and CGMS precipitation databases

##### **Spatial distribution of RMSE between ELDAS and CGMS precipitation databases**

We calculated the root mean squared error (RMSE) between the ELDAS and CGMS daily precipitation values at the resolution of the  $0.2^\circ$  ELDAS grid over the entire period 1 October 1999 until 31 December 2000. Each ELDAS grid was combined with the precipitation value of the CGMS grid in which it was located. The results (Figure 4.1) demonstrate that the spatial patterns in the RMSE are dominated by areas of high RMSE values which correspond mainly



to mountainous areas with west-wind driven precipitation patterns. The precipitation values in the CGMS database do not properly represent the strong temporal and spatial variability of precipitation in these areas leading to higher RMSE values.

Based on these results we decided to remove grids with high RMSE due to mountainous terrain because these grids are not relevant for agricultural applications. CGMS grids were removed using the criteria that the average slope was larger than  $3.5^\circ$  over the  $50 \times 50$  km grid. Slope was derived from the USGS HYDRO1K dataset (<http://lpdaac.usgs.gov/gtopo30/hydro/index.asp>) as the average value within a  $50 \times 50$  km CGMS grid cell. Figure 4.1 demonstrates that mainly grids in the Alps, Scandinavia, Spanish and Italian mountain ranges, Greece, Turkey as well as in Rumania were removed from the analysis. Although the number of grids that were removed is considerable, there are no important agricultural areas with annual crops located within these grids.

### Scatter plot of CGMS precipitation versus precipitation residuals

Figure 4.2 shows the scatter plot of CGMS daily precipitation versus the precipitation residuals (ELDAS minus CGMS) over the period 1 October 1999 until 31 December 2000. Some important observations can be made from this figure:

- The vertical banding shows that most CGMS precipitation values are integers, whereas the ELDAS precipitation values are real numbers. Based on this observation we decided to convert all CGMS precipitation values to integer values during further analyses by rounding them to the nearest integer.
- The distributions of the residuals are asymmetric and vary with CGMS precipitation. With low CGMS precipitation, the residuals are mainly clustered near zero, but this tendency vanishes with increasing CGMS precipitation values.

### Comparison of precipitation distribution classes

An overview of the errors in the CGMS precipitation database is provided by an error matrix between precipitation distribution classes in the CGMS and ELDAS databases (Table 4.1, page 84). The average ELDAS precipitation per CGMS grid was used over the period 1 October 1999 until 31 December 2000. The number of counts in the first column corresponds to roughly 60% of the



Figure 4.1: Root Mean Squared Error of daily precipitation values in the CGMS database versus the ELDAS reference dataset for the period 1-October-1999 until 31-December-2000. The black skewed rectangles represent CGMS grids that were removed from the analyses based on a slope criterion.

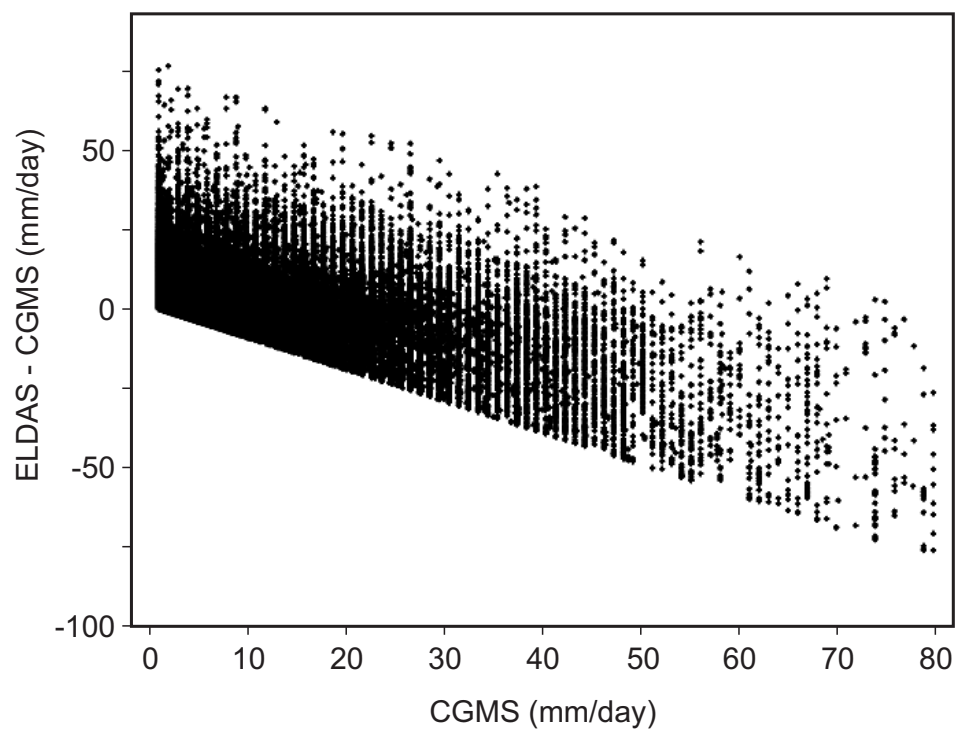


Figure 4.2: Scatter plot of precipitation residuals (ELDAS - CGMS) versus CGMS precipitation amounts.

total grid/day combinations. In order to avoid small fractions, all values are given as a percentage of the column total. Precipitation values larger than 80 mm were removed from the analyses, because these events are rare and not of interest for the application at hand and they would thus needlessly complicate further analysis.

The first observation that can be made from table 4.1 is the large percentage of events (47.3%) where CGMS precipitation equals zero, while ELDAS precipitation is between zero and one. There are probably several reasons for this effect:

- Greater accuracy of the precipitation values in the ELDAS database;
- The interpolation applied for creating the ELDAS database (block kriging) causes a smoothing of precipitation values;
- Averaging of multiple ELDAS grid points within one CGMS grid.

To compensate for this effect we decided to treat ELDAS precipitation values lower than one mm as zero mm for events where CGMS precipitation was zero. This procedure effectively adds the 47.3% to the 39.6% in the upper left cell of the matrix (table 4.1). This decision is justified because the precipitation values lower than one mm are insignificant from an agricultural point of view. The second important observation is that the distribution of ELDAS precipitation classes within one CGMS precipitation class is often not normal and that the standard deviation of the distribution becomes larger with increasing CGMS precipitation.

## 4.3 Method

### 4.3.1 Conceptual modelling

We consider  $Prec(x, t)$  to be the (unknown) true average precipitation at grid cell  $x$  and day  $t$ ,  $Prec_{CGMS}(x, t)$  the precipitation as recorded in the CGMS system, and  $\epsilon(\cdot)$  a random spatially and/or temporally correlated residual. Our spatio-temporal error model for the data concerned is then given by:

$$\epsilon(x, t) = Prec(x, t) - Prec_{CGMS}(x, t) \quad (4.1)$$

Note that no statement is made about  $\epsilon(\cdot)$  having zero mean, as  $Prec_{CGMS}(x, t)$  might be biased.

We assume that a sample or observed realisation of the residual variable can be obtained using the ELDAS precipitation data resampled to the CGMS grid,  $Prec_{ELDAS}(x, t)$ , as a reference:

$$\epsilon_0(x, t) = Prec_{ELDAS}(x, t) - Prec_{CGMS}(x, t) \quad (4.2)$$

Where  $\epsilon_0(x, t)$  denotes an observed residual at location  $x$  and date  $t$ .

Figure 4.2 is a scatter plot of the observed residuals, which obviously do not follow a Gaussian distribution. The basic assumption underlying our method is that the residuals  $\epsilon_0(x, t)$  can be transformed to standard (marginal) normality by some transform function  $f(\cdot)$  and that correlated standard Gaussian fields can be back transformed to residual precipitation fields by the inverse of that function, i.e.  $f^{-1}(\cdot)$ . Note that by design the transformation functions should handle any bias in the CGMS precipitation data. We thus obtain the following model for the random residual precipitation field,  $\epsilon_M(x, t)$ :

$$\epsilon_M(x, t) = f^{-1}(\delta(x, t), args) \quad (4.3)$$

Where  $\delta(\cdot)$  denotes a correlated standard Gaussian random field and  $args$  are any required additional arguments. Section 4.3.2 (below) explains that the residuals in case of zero CGMS precipitation require additional modelling. Once the transformation functions  $f(\cdot)$  and  $f^{-1}(\cdot)$  and the random function generating  $\delta(\cdot)$  are configured using the observed  $\epsilon_0(x, t)$ , we are able to generate multiple realisations of  $\epsilon_M(x, t)$  using a standard Gaussian simulation algorithm. By summing the simulated residuals to observed CGMS precipitation data the required ensemble traces are obtained.

### 4.3.2 Normal score transformation

We tried several mathematical expressions to transform the observed  $\epsilon_0(x, t)$  to a standard Gaussian distribution as a function of  $Prec_{CGMS}(x, t)$ , but with our data set we could not find any useful parametric function. Also, checks for seasonal and spatial trends (the latter as a function of the density of weather stations) in the means of the precipitation residuals were unsuccessful with our time-series.

We thus decided to use quantile based normal score transforms for a series of  $Prec_{CGMS}(\cdot)$  intervals. The dataset for the year 2000 was divided into 13 CGMS precipitation intervals (the same as listed in table 4.1) and for each of these a histogram of the observed residuals  $\epsilon_0(\cdot)$  was produced. These histograms were visually compared with histograms constructed on data from the last 3 month of 1999 as a second check on our assumption of absence of a temporal trend. Next, the normal scores of the observed residuals and 13 transfor-

mation tables were obtained by finding the  $z$  scores of a standard Gaussian distribution corresponding to quantiles of the observed cumulative distributions. The computations were done using the GSLIB2 program `nscore` (Deutsch and Journel, 1998). Note that the random de-spiking algorithm which is part of the original program was disabled as it would cause artefacts that would interfere with subsequent analysis (particularly variogram determination).

The first bin  $Prec_{CGMS}(x, t) = 0$  required additional processing, because the transformation algorithm could not properly transform the large number of zeros (i.e.  $\epsilon_0(x, t) < 1$  mm) in the residuals. Therefore, we introduced a multiplicative —spatially correlated— indicator variable (also: step variable)  $i(x, t)$  to treat the  $\epsilon_0(x, t) < 1$  mm data given  $Prec_{CGMS}(x, t) = 0$  mm separately. Hence, in the first bin only the residuals  $\epsilon_0(x, t) \geq 1$  mm are handled by a normal score transform and Eq. 4.3 was modified into:

$$\epsilon_M(x, t) = \begin{cases} i(x, t) \cdot f^{-1}(\delta(x, t), Prec_{CGMS}(x, t)) & \text{if } Prec_{CGMS}(x, t) = 0 \\ f^{-1}(\delta(x, t), Prec_{CGMS}(x, t)) & \text{if } Prec_{CGMS}(x, t) > 0 \end{cases} \quad (4.4)$$

In the current work, dependence of  $i(x, t)$  on  $Prec_{CGMS}(\cdot) | Prec_{CGMS}(x, t) > 0$  and  $\delta(\cdot)$  is not considered.

### 4.3.3 Variogram modelling

#### Normal score transformed data

Normal score transformed residuals  $\epsilon_0'(x, t)$  were computed for all  $Prec_{CGMS}(x, t) > 0$  mm and for  $Prec_{CGMS}(x, t) = 0$  mm with  $\epsilon_0(x, t) \geq 1$  mm. The thus obtained data was exhaustively sampled in the spatial domain and thrice-monthly, i.e. on the 1<sup>st</sup>, 11<sup>th</sup> and 21<sup>st</sup> of a month in the temporal domain to determine the experimental variogram of the spatially auto-correlated Gaussian variable.

#### Indicator variable

The indicator variable  $i(\cdot)$  (see Eq. 4.4) was considered to be spatially auto-correlated. The indicator variogram was obtained by transforming the precipitation data according to Eq. 4.5.

$$i(x, t) = \begin{cases} null & \text{if } Prec_{CGMS}(x, t) > 0 \text{ mm} \\ 1 & \text{if } \epsilon_0(x, t) \geq 1 \text{ mm} \\ 0 & \text{otherwise} \end{cases} \quad (4.5)$$

The upper option just states that the indicator variable is not used in case  $Prec_{CGMS}(x, t) > 0$  mm.

### Checking two-point normality

The normal score transformed residuals  $\epsilon_0'(x, t)$  are by construction univariate normally distributed, but the `nscore` transform does not impose multivariate normality on  $\epsilon_0'(x, t)$ . Nonetheless, the random function  $\delta(\cdot)$  (Eq. 4.4), which is configured on  $\epsilon_0'(x, t)$  assumes the two-point distribution of any pair of values at different locations to be Gaussian. To check the consequences of this assumption for the intended use of the data, we employed a procedure given in Goovaerts (1997, pages 271–275) and Deutsch and Journel (1998, pages 142–144) which consists in graphically comparing experimental and Gaussian model-induced indicator variograms of the normal score data at different  $p$ -quantiles of the cumulative distribution. The procedure is equivalent to comparing theoretical and empirical proportions of the transformed residuals below selected thresholds for a series of distances.

We used the GSLIB2 program `bigaus` to derive the model-induced indicator variograms from the variogram of  $\epsilon_0'(x, t)$  (see 4.3.2). The experimental indicator variograms were obtained by applying thresholds on the data  $\epsilon_0'(x, t)$  as follows:

$$j(x, t) = \begin{cases} 1 & \text{if } \epsilon_0'(x, t) \geq z(p) \\ 0 & \text{otherwise} \end{cases} \quad (4.6)$$

where  $j(x, t)$  denotes an indicator transformed data point and  $z(p)$  is the  $z$  score of the standard normal distribution for quantile  $p$  ( $p = 0.10, 0.25, 0.5, 0.75, 0.90$ ). Subsequently, date-averaged variogram values were computed from  $j(x, t)$  data that was exhaustively sampled in the spatial domain and three per month in the temporal domain.

#### 4.3.4 Simulation of residual fields

Figure 4.3 shows how we implemented Eq. 4.4 in our simulation method which needs the CGMS precipitation data, the Gaussian random fields, the indicator random fields and a set of transformation tables as input. If  $Prec_{CGMS}(x, t) > 0$  mm, then the right-hand branch of the flow diagram suffices, i.e. unconditional standard Gaussian simulation followed by a back transform. In the other case, unconditional indicator simulation is used to model the event of a positive residual  $\epsilon_M(x, t)$  given  $Prec_{CGMS}(x, t) = 0$  mm.

Note, however, that both branches are always executed and that the conditions  $Prec_{CGMS}(x, t) = 0$  mm or  $Prec_{CGMS}(x, t) > 0$  mm are handled by post processing (lower box in figure 4.3).

The Gaussian and indicator simulations were performed using the public domain sequential simulation programs *sgsim* and *sisim* included in *GSLIB2* (Deutsch and Journel, 1998). Both programs employ sequential stochastic simulation which implies that in random order they simulate the nodes of a recursively refined grid. Previously simulated nodes are used as conditioning data for subsequent simulations within the same realisation if they are within a given search neighbourhood.

The back transforms and post processing were performed by the *LINT2* module in the *TTUTIL* Library (Kraalingen and Rappoldt, 2000) and the Python scripting language. A set of 100 alternative realisations of daily precipitation was generated by adding back transformed simulated residuals to the CGMS precipitation data.

#### 4.3.5 Evaluation of precipitation realisations

We evaluated the realisations of the precipitation fields on four different aspects. Firstly, the reproduction of the histograms of the ELDAS precipitation was checked by quantile-quantile plots of ELDAS and CGMS precipitation against 100 precipitation realisations for selected grids. Secondly, variogram reproduction of the ELDAS precipitation fields was evaluated for two selected days and five realisations. Thirdly, the rainfall temporal intermittency characteristics for both dry and wet periods were compared for 6 representative sites for the CGMS precipitation, ELDAS precipitation and 25 realisations. Finally, an error matrix similar to table 4.1 was generated which shows the distribution of CGMS precipitation classes versus the precipitation realisations over the whole grid and the complete time-series.

#### 4.3.6 Probabilistic crop yield forecasting

In order to illustrate the use of rainfall realisations in agrometeorological applications, we used the *WOFOST* crop growth model (Diepen et al., 1989) implemented in the framework of the Crop Growth Monitoring System (Genovese, 1998; Vossen and Rijks, 1995) to make a probabilistic yield forecast for the year 2000, for grain maize in the region ‘Centre-Est’ in south-east France. First, individual rainfall realisations were used as input for *WOFOST* simulations to obtain an ensemble of simulated biomass values. This procedure was repeated for all  $50 \times 50$  km grids in the region ‘Centre-Est’ and



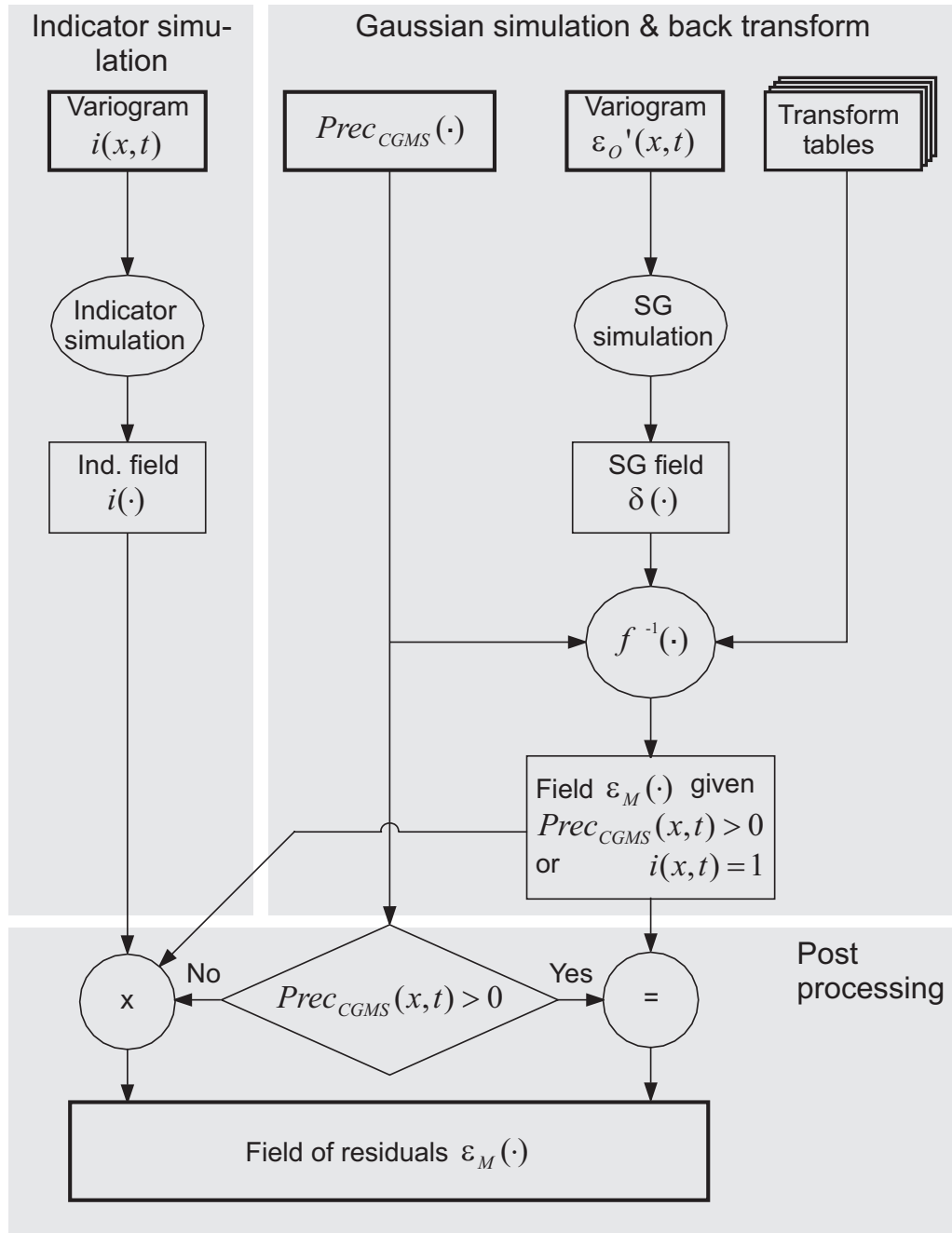


Figure 4.3: Flow diagram of the ensemble simulation approach.

the resulting time-series of simulated biomass values for individual grids were spatially aggregated. The final result of this procedure was an ensemble of space-averaged simulated biomass values that was representative for the region.

In a second step, we used the deterministic version of CGMS for the same crop and region to simulate grain maize biomass values over the period 1992–1999. The time-series of official reported grain maize yields (EUROSTAT, 2005) for this region were used as dependent variable in a regression model with a time-trend and the simulated biomass results as independent variables (Supit, 1997). The coefficients of this regression model were determined for each dekadal<sup>1</sup> time step during the growing season. Finally, the regression models explaining the relationship between reported yield and simulation results over the years 1992–1999 were applied in prognostic mode in order to make a forecast using both the deterministic output for 2000 as well as the output from all ensemble members for the year 2000.

## 4.4 Results

### 4.4.1 Distribution of precipitation residuals for selected CGMS precipitation classes

Figure 4.4 shows four selected histograms of the precipitation residuals (CGMS-ELDAS) for a given CGMS precipitation value or interval. The distribution of precipitation residuals per CGMS precipitation interval were used to model the residuals as a function of the CGMS precipitation itself. Histograms were calculated separately for the year 2000 and the three remaining months in 1999 in order to check if the histograms were stable over time.

At CGMS precipitation zero, the precipitation residuals were zero for nearly 50% of the data while a relatively large percentage of precipitation residuals had values between zero and one (Figure 4.4A). At CGMS precipitation of 4 mm the width of the whole histogram becomes wider demonstrating larger errors in the CGMS precipitation values (Figure 4.4B). A small peak is present at residual of -4 mm, indicating a relative overrepresentation of cases where ELDAS predicts no precipitation at all. Note that there is a good match between the precipitation residuals obtained with the ELDAS data from 1999 and 2000, although the overrepresentation is not present in the 1999 histogram. At CGMS precipitation values between 10 and 12 mm and between

<sup>1</sup>The use of the term ‘dekad’ refers to an FAO convention in order to distinguish 10-year periods (decade) from 10-day periods (dekad).

15 and 30 mm (Figures 4.4C & 4.4D) the shape of the histogram remains a more or less truncated normal distribution which becomes progressively wider. This confirms that the magnitude of the errors is related to the precipitation amount itself. A small shift seems to be present between the histograms of 1999 and 2000 where the distribution of the 2000 data is shifted to more negative residuals. Although the effect is small, this could indicate an effect of seasonal differences in precipitation residuals.

#### 4.4.2 Variogram modelling

##### Transformed precipitation residuals

Figure 4.5 shows the variograms of normal score transformed precipitation residuals, for  $Prec_{CGMS}(x, t) > 0$  mm. The black dotted lines correspond to variograms of individual dates while the grey continuous line represents the average variogram over all sampled dates. There is considerable spread among the variograms of the individual dates; however, they all indicate that the transformed residuals are spatially correlated with similar range. The average variogram was modelled by the sum of two exponential components (Goovaerts, 1997); one with a partial sill of 0.802 and a practical range of 315 km and another with 0.198 and 6000 km for partial sill and practical range respectively. This variogram model was used in the Gaussian simulations. Likewise, the indicator variogram for the data transformed by Equation 4.5 (not shown here) was modelled by two exponential components with partial sills and ranges of (0.0372, 180 km) and (0.0828, 1500 km) respectively.

The level of temporal auto-correlation in was assessed by computing temporal variograms for 6 CGMS grid cells that were selected to represent climatic variability over the region (southern Spain, northern Spain, southern France, northern France, central Germany and Denmark). The temporal variography for 6 selected CGMS grid cells, shown in Figure 4.6, did not point at significant temporal correlation of the transformed residuals. Therefore, our model did not account for such correlation.

##### Two point normality

Based on graphical comparisons of the experimental and Gaussian model-induced indicator variograms of the normal score data, shown in Figure 4.7, we decided to accept the assumption of two-point normality in space for the purpose of our study. Nonetheless, the experimental indicator values for the first decile ( $p = 0.1$ ) deviate substantially from the model induced variogram. This indicates that observed small transformed residuals were more connected

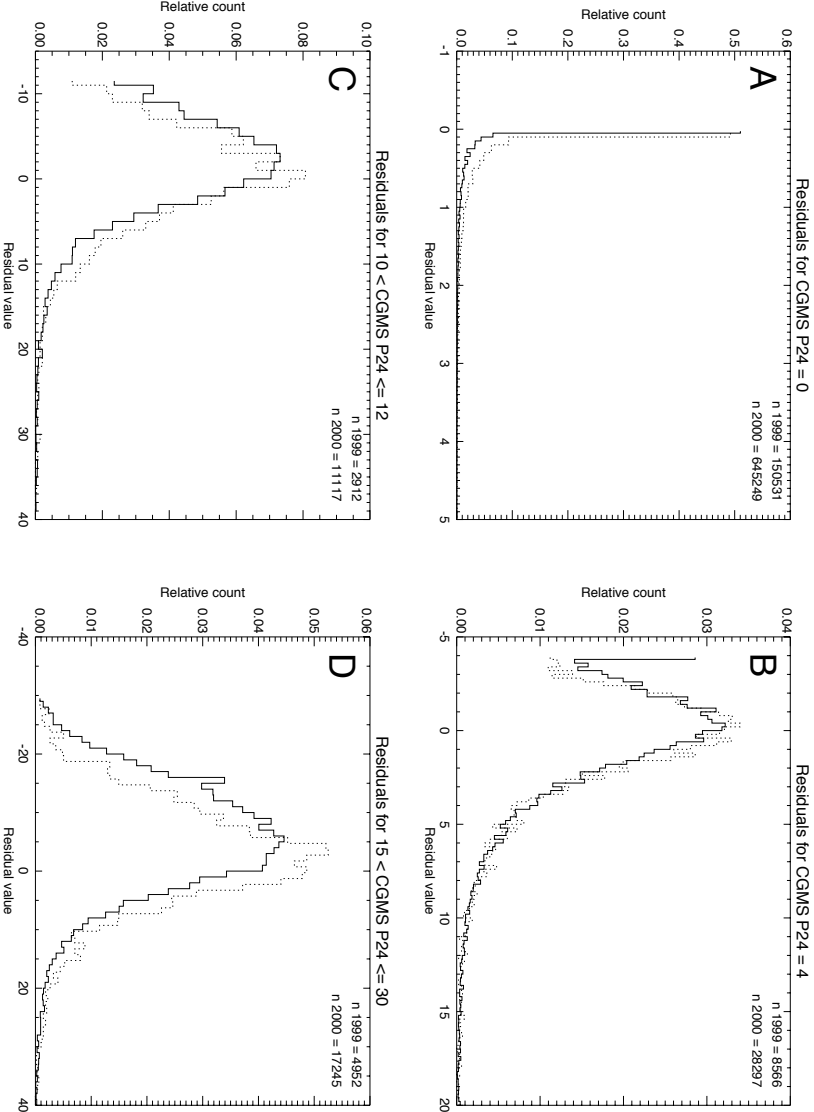


Figure 4.4: Histograms of precipitation residuals for selected CGMS precipitation intervals. Continuous lines represent the normalised histogram for the period 1-January-2000 until 31-December-2000. Dashed lines represent the normalised histogram for the period 1-October-1999 until 31-December-1999.

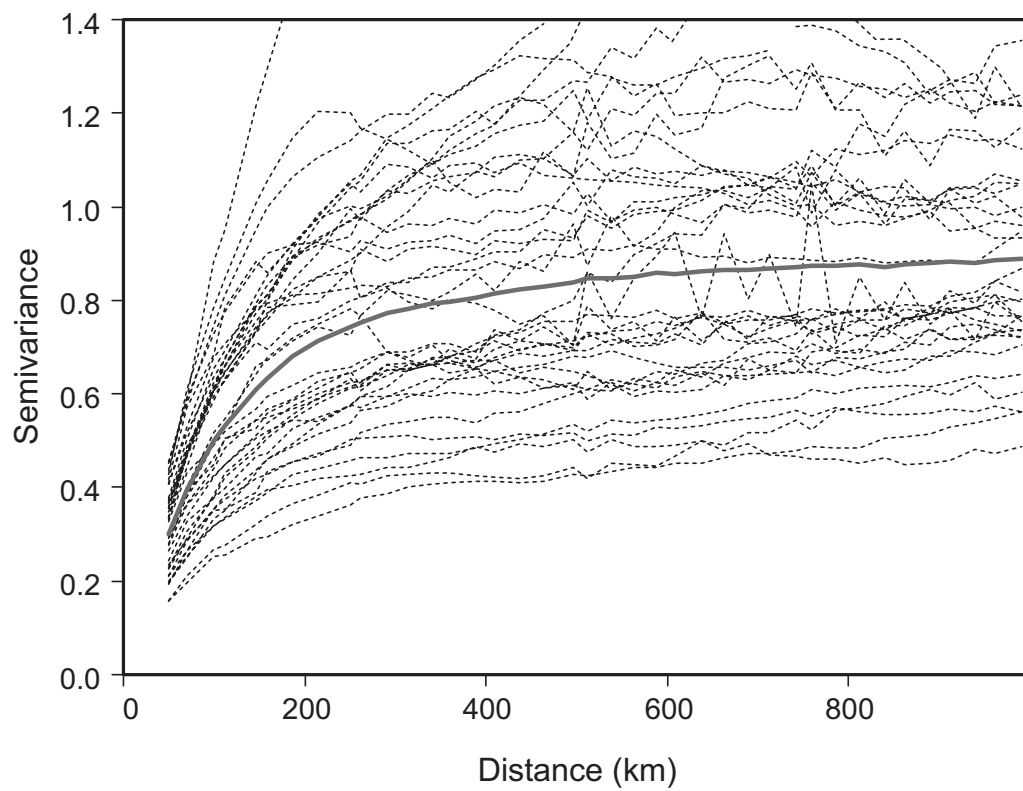


Figure 4.5: Spatial variograms of the normal score transformed residuals for selected dates (dashed lines; 1<sup>st</sup>, 11<sup>th</sup>, 21<sup>st</sup> of each month) and weighted average variogram of all selected dates (thick continuous line).

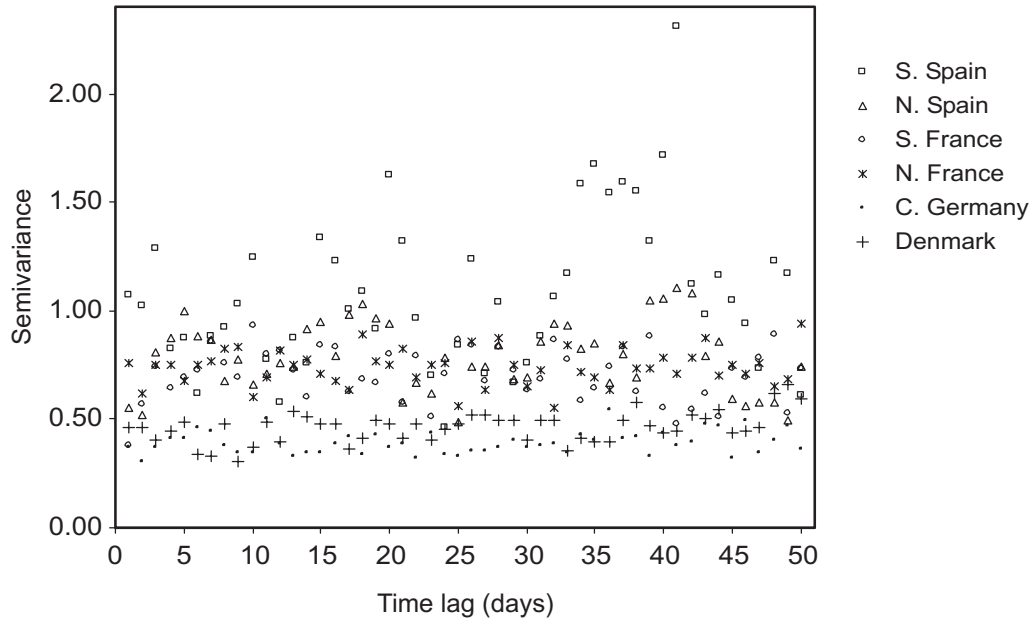


Figure 4.6: Temporal variograms of the normal score transformed residuals for selected CGMS grids.

in space than under the Gaussian model. However, for the other quantiles (and the vast majority of the data) the fits of the two models are remarkably good. Also in the temporal domain, the density plot of normal score data on subsequent days (not shown) demonstrated that the normal score data are approximately bivariate normally distributed.

#### 4.4.3 Precipitation realisations

The reproduction of the histograms of the ELDAS precipitation for the entire year at grid locations in South-Spain (30032), South-France (43044) and Central-Germany (59061) is shown in the quantile-quantile (Q-Q) plots of Figures 4.8A–4.8F. Both the Q-Q plots of ELDAS vs. CGMS and ELDAS vs. 100 realisations to allow comparisons between the original CGMS precipitation data and the realisations of the error model.

For the grid in South-Spain (30032) the distributions of ELDAS and CGMS are nearly identical showing a clustering of points along the 1:1 line (Figure 4.8A). Also in the Q-Q plot of ELDAS vs. 100 realisations, most points are clustered near the 1:1 line except for the 100th percentile which is located near the top of the chart (Figure 4.8B). The grid in South-France shows a similar pattern with a slight underestimation of precipitation values by CGMS up to 15 mm and an overestimation of values larger than 20 mm (Figure 4.8C).

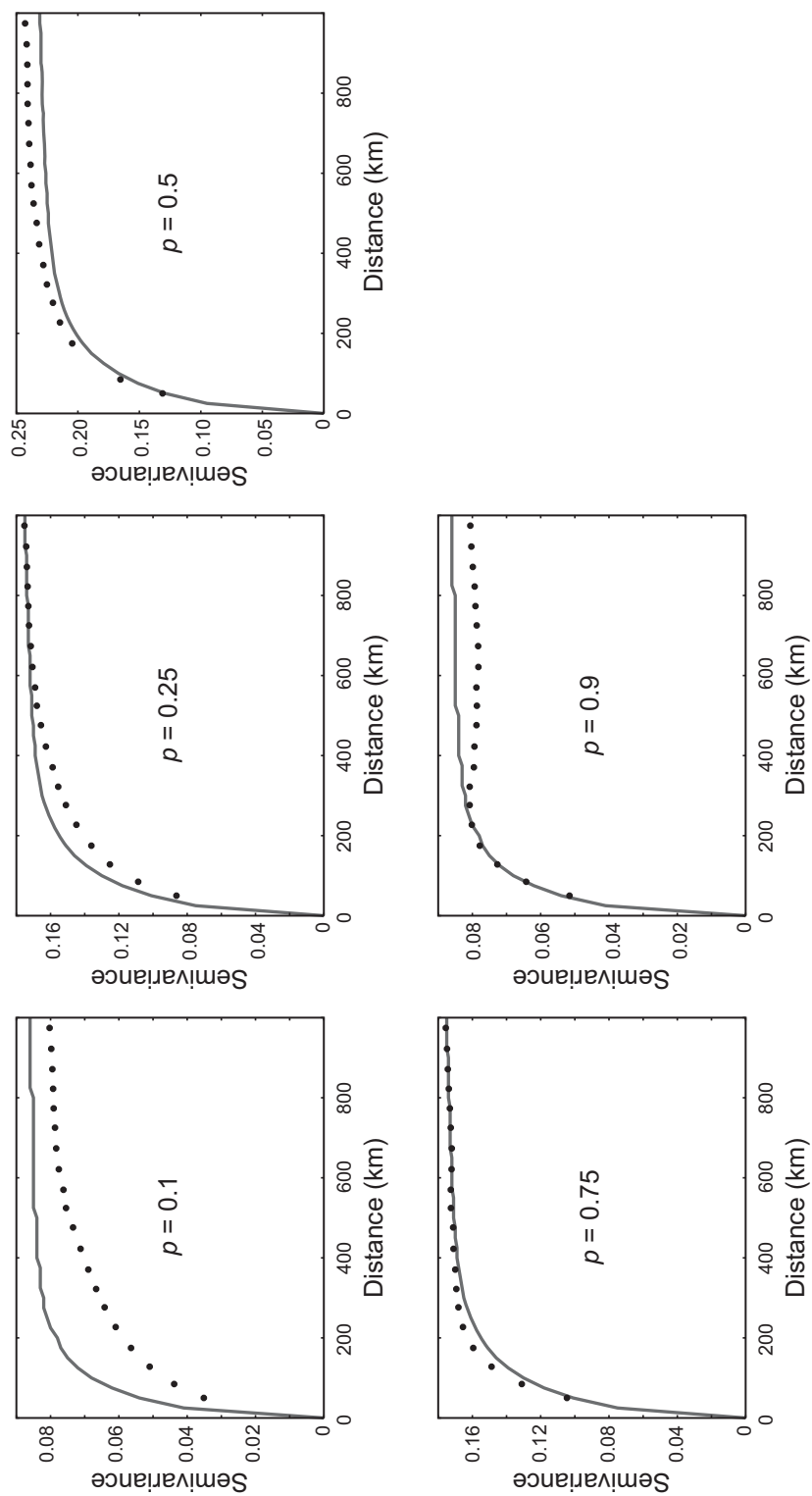


Figure 4.7: Comparison of model-induced indicator variograms (continuous line) and observed indicator variograms for different quantiles ( $p$ ) of the normal score transformed residuals.

The underestimation is corrected for in the realisations but the overestimation cannot be corrected and could even be slightly amplified (Figure 4.8D). Also in this case, the 100th percentile in the realisations is strongly shifted towards the upper part of the chart. Finally, the grid located in Central Germany shows a similar pattern, except for a slight overestimation of precipitation values greater than 10 mm and again a shifting of the 100th percentile to higher precipitation values (Figure 4.8E–F).

These results demonstrate that the method reproduced the histograms for the selected sites fairly well, but generated too large precipitation values when compared to the largest values present in the original precipitation sequence. This result is caused by the random character of the procedure which will inevitably sample the tails of the distribution in some realisations thereby producing large precipitation values.

The variograms of the 5 realisations at 21 November 2000 and 11 July 2000 are shown in figure 4.9A and 4.9B. The figures demonstrate that the overall variance (the sill) of the realisations can be both smaller and larger than the ELDAS variance (grey line), but that the range of the spatial correlation was similar to the ELDAS reference dataset. However, at small ranges all realisations had larger semi-variance compared to the target variance, indicating larger variability in precipitation values at small ranges compared to ELDAS.

The intermittency characteristics of the dry periods were determined for six representative sites located in areas with major agricultural production (Figure 4.10). The results for South-Spain (Andalusia) demonstrate that the proposed simulation approach was not able to reproduce the dry period statistics well. The characteristic long dry summer in Andalusia with dry periods as long as 130 days is not reproduced in the realisations. This is a result of the fact that the simulation approach can generate a precipitation residual for zero CGMS precipitation, depending on the outcome of the independent indicator simulation, which was configured on averages rather than on site and season specific data. This property of the simulation approach may break the very long dry periods typical of the Andalusian summer. Similar effects can be observed in the results for Northern Spain and Southern France albeit less pronounced (Figures 4.10 B & C).

The results for the sites located in more temperate climate regions (Northern-France, Central-Germany, Denmark) demonstrated that the simulation approach performed better in reproducing the dry period statistics. For these three sites, there are realisations which reproduce the maximum, or even larger, dry period length, although the dry period lengths in the realisations are, on average, still shorter.

The intermittency characteristics of the wet periods were determined for



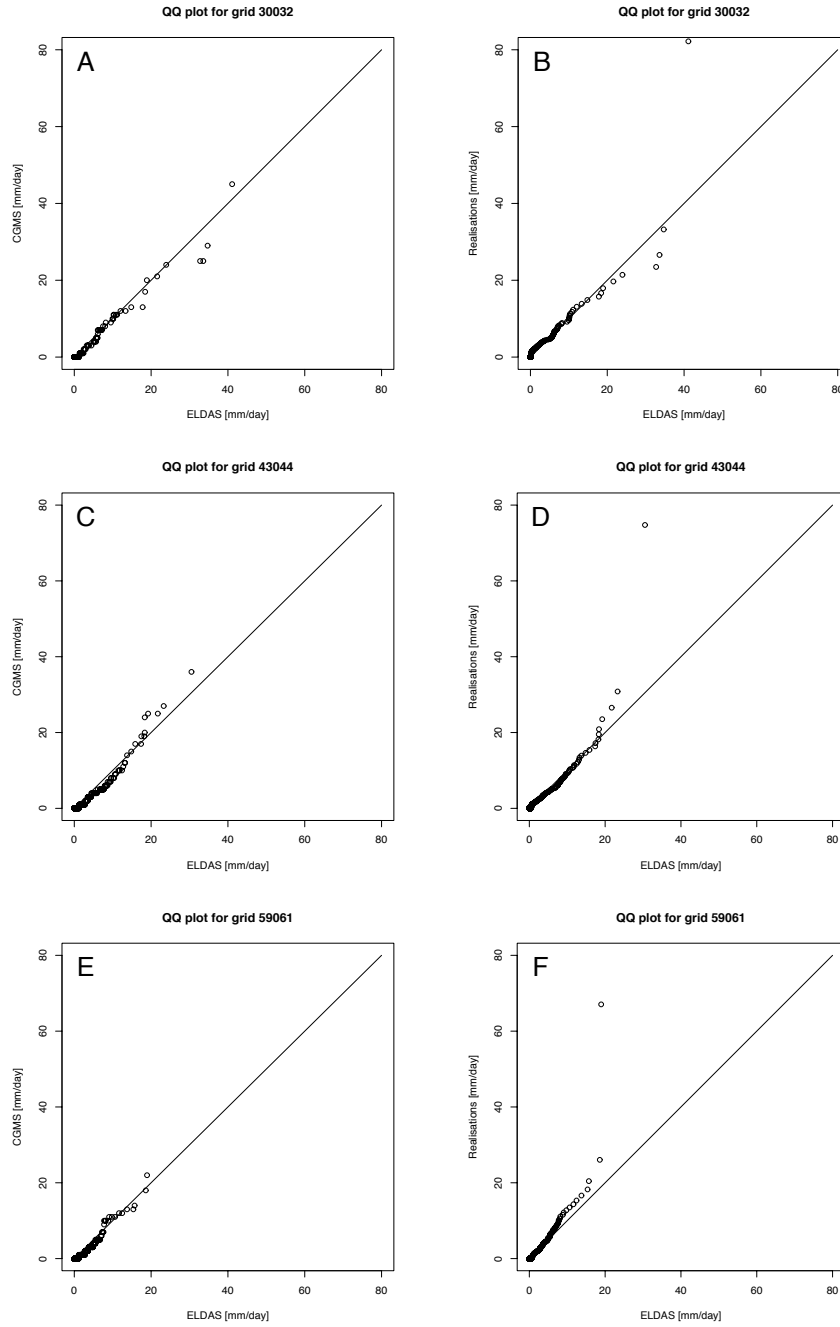


Figure 4.8: Quantile-Quantile plots of precipitation quantiles for precipitation time-series of three selected grids in South-Spain (30032), South-France (43044) and C-Germany (59051): ELDAS precipitation sequence vs. CGMS precipitation sequence (figure A, C & E) and ELDAS precipitation sequence vs. 100 realised precipitation sequences (figure B, D & F).

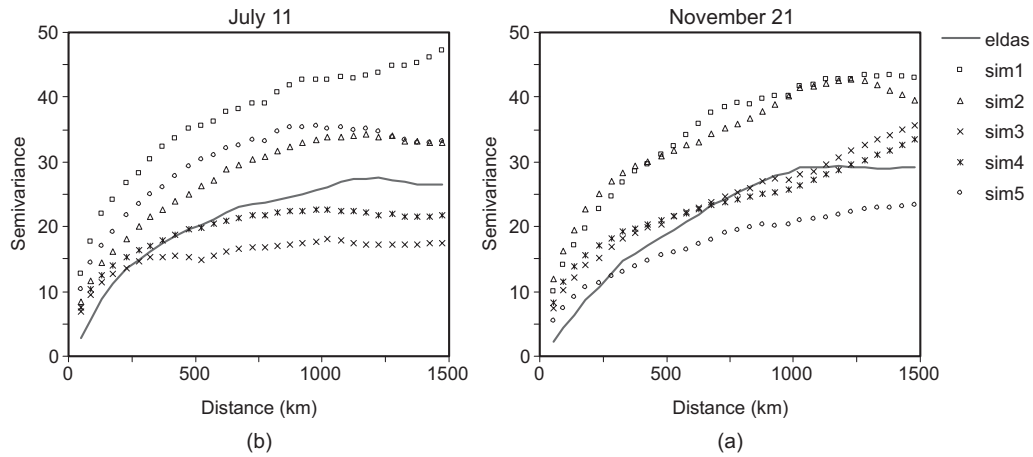


Figure 4.9: Variograms of the ELDAS precipitation data (continuous line) and simulated precipitation fields (symbols; five realisations).

the same six sites (Figure 4.11). It can be observed that, compared to the dry period length, the simulation approach performs much better in reproducing the wet period intermittency characteristics. Nevertheless an increase in the number of wet day sequences greater or equal to one day can be observed for nearly all sites.

Figure 4.12 (page 79) shows precipitation maps for 11 July 2000 according to the CGMS, ELDAS and the first of a series of realisations of our model (marked with 'sim1' in figure 4.9A). The map of the precipitation realisations shows that large precipitation amounts were drawn from the error distribution for locations in Western Germany and Belgium as well as in the Eastern part of the Alps. This is consistent with figure 4.9A showing that precipitation realisation 1 has a larger variance compared to the ELDAS precipitation field. In Northern Finland, small rainfall amounts were generated on locations where no precipitation is present in the CGMS gridded precipitation, demonstrating the effect of the indicator kriging which creates occurrences of precipitation in dry areas.

A final check on the validity of our methodology was carried out by determining the distribution of CGMS precipitation classes versus the precipitation realisations over the whole grid and the year 2000, averaged over 100 realisations (Table 4.2, page 85). Tables 4.1 and 4.2 can be compared directly and demonstrate that our method reproduces the target distributions (ELDAS) well. The only exception is that for CGMS precipitation classes larger than 15 mm, there was an increase in the number of zero precipitation occurrences in the ensembles. Due to the large width of the precipitation intervals used in the back transform, negative precipitation values can be produced. For example,

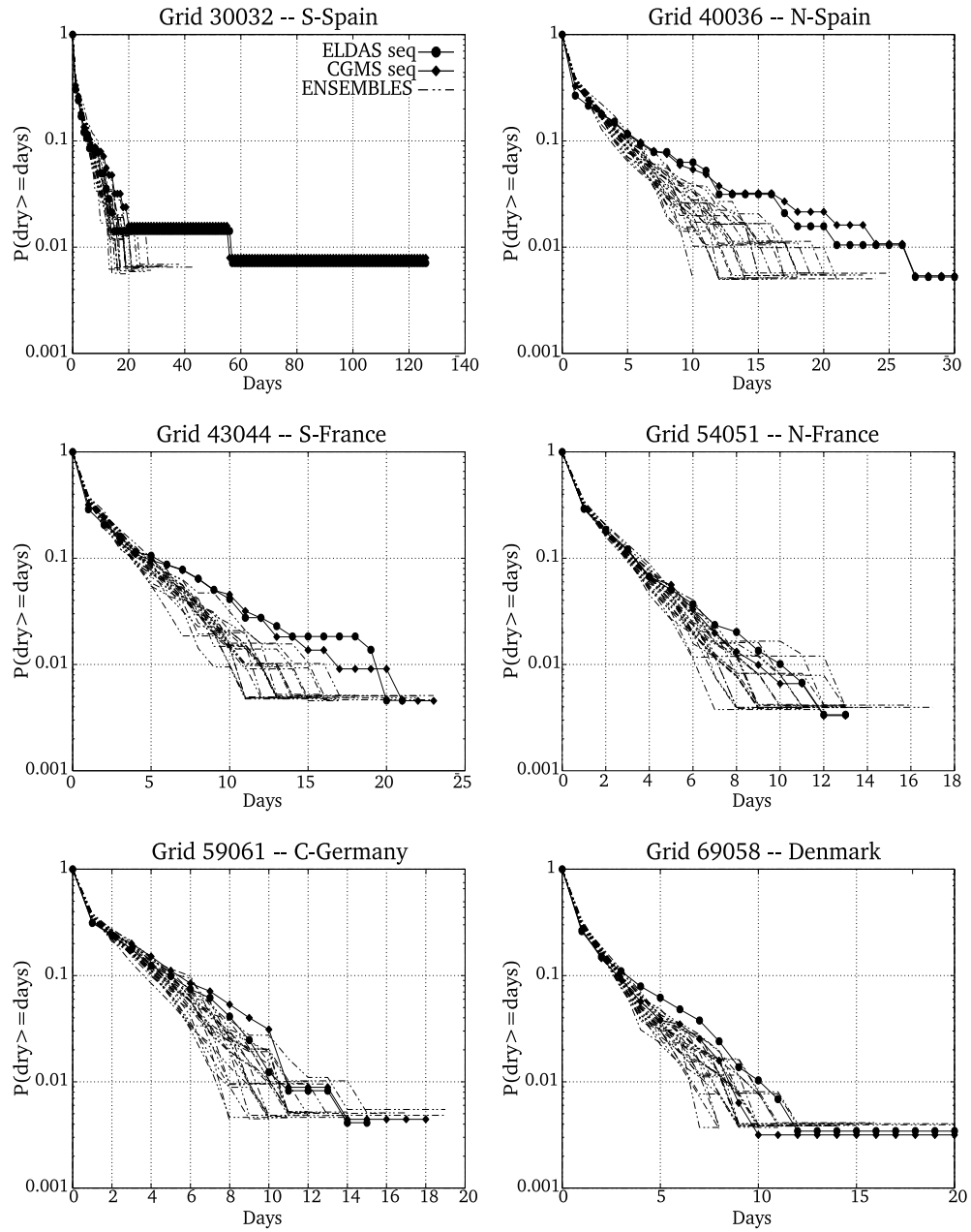


Figure 4.10: Dry-spell lengths from the CGMS and ELDAS precipitation datasets and dry-spell lengths for 25 precipitation simulations, for six representative sites.

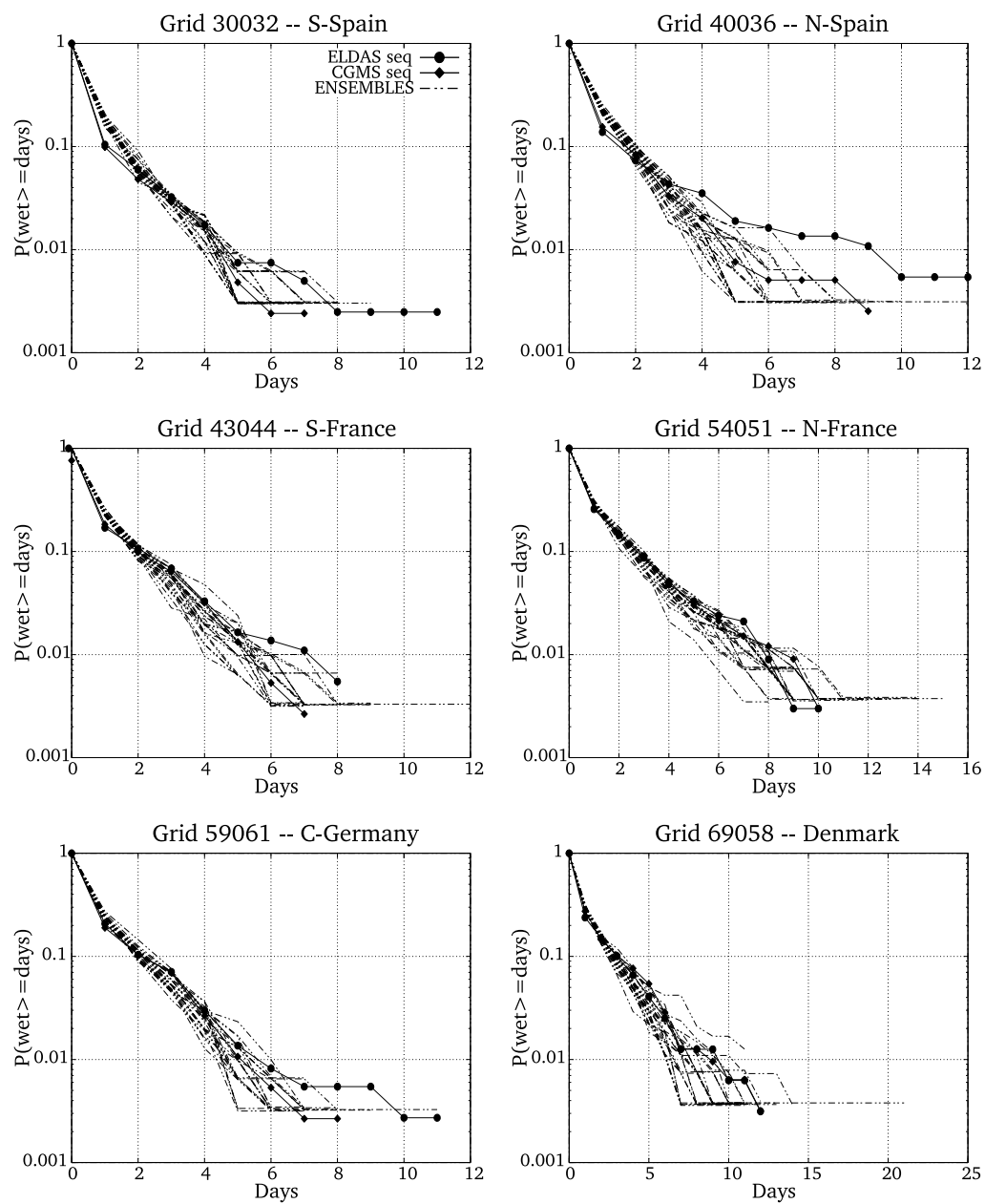


Figure 4.11: Wet-spell lengths from the CGMS and ELDAS precipitation datasets and wet-spell lengths for 25 precipitation simulations, for six representative sites.

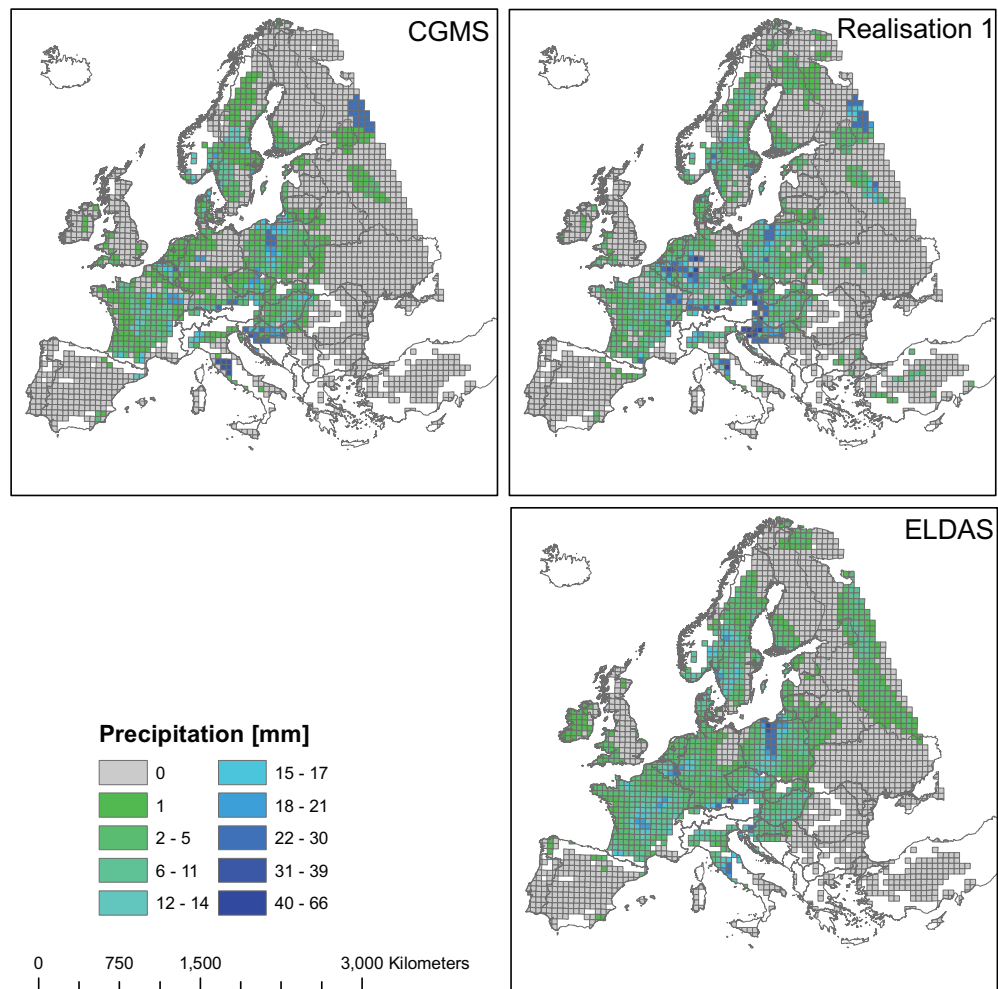


Figure 4.12: Comparison of a single precipitation realization, the CGMS input precipitation field and the ELDAS reference precipitation field.

for a CGMS precipitation amount of 16 mm, a residual of up to -30 mm can be generated. In our current implementation, negative precipitation amounts are set to zero.

#### 4.4.4 Probabilistic crop yield forecasting

The regression models that were established between historic EUROSTAT reported yields and the simulated biomass values, could explain a considerable percentage of variance in the yield statistics with  $R^2$  values starting at 0.57 in dekad 16, then gradually increasing up to 0.83 in dekad 26 and finally slightly decreasing to 0.78 in dekad 30. The regression was significant starting at dekad 21 (significance level = 0.05) up to dekad 30. The probabilistic yield forecast (Figure 4.13, page 83) based on the regression models demonstrates that the uncertainty in precipitation has a profound influence on the value of the yield forecast during the growing season. Compared to the deterministic yield forecast (blue line), the probabilistic yield forecast shows a diverging ensemble of yield forecasts which keeps diverging almost up to end of growing season with maximum spread in the yield forecast of around 0.65 ton/ha. Given that EUROSTAT uses a tolerance of 0.2 ton/ha as an acceptable accuracy for yield forecasts (G. Genovese, pers. comm.), this is a significant deviation. The average ensemble yield forecast is clearly higher than the deterministic forecast. However, this is probably due to underestimation of precipitation in the CGMS data set (Wit et al., 2005). This bias is corrected in the precipitation ensemble, but not in the forecast regression. Finally, the density plots demonstrate that the shape of the yield forecast ensemble is non-Gaussian and propagates in a non-linear way.

### 4.5 Discussion

This paper presents a methodology for generating precipitation ensembles tailored to the temporal and spatial scale required for regional crop modelling. Given that crop models are relatively insensitive to intermittency of precipitation, we used an additive approach to create ensembles of daily precipitation values. For applications where intermittency characteristics at small time scales (hourly values) are of prime importance, our approach is probably not suitable and other methods should be applied which are more tailored to such requirements (Hossain and Anagnostou, 2006).

Our method uses a histogram-based approach for transforming heterogeneously distributed precipitation residuals into a Gaussian random variable. The thus transformed precipitation residuals appeared to be approximately

multivariate Gaussian. Similar to results obtained by Kyriakidis et al. (2004), they exhibited strong spatial correlation, while temporal correlation was very weak. The virtually absent temporal correlation in the residuals indicates that the daily CGMS records captured temporal precipitation patterns relatively well in our time series. We therefore decided to disregard the temporal correlation component.

The possibility of having precipitation at locations where CGMS predicted a dry day was handled by an independent indicator simulation which generates rain storms in areas where no precipitation was recorded. The precipitation amount is then obtained through the Gaussian simulation. Currently, the indicator simulation is assumed to be temporally uncorrelated and stationary in space and time.

A potential drawback of our approach is that the Gaussian simulation and the indicator simulation are implemented as independent processes. Therefore, it is not guaranteed to produce small precipitation amounts near dry sites and new precipitation events along the fringes of existing wet areas. Dependency between these processes will be difficult to implement within the current framework given that the precipitation amounts are not simulated directly but are only retrieved by post-processing of the results of the Gaussian simulation. Yang et al. (2005) also signalled this problem but they pointed out that currently available simulation methods addressing this problem also suffer from drawbacks, because these typically assume the same spatial correlation structure for occurrence and amount of rainfall. The extent to which this problem propagates through applications is not clear yet.

Currently, our approach assumes stationary processes in space and time for both the Gaussian simulation and the indicator simulation which use one variogram model each and a single set of back-transforms. Consequently, it reproduces the histogram of the entire dataset, but it does not necessarily reproduce the histogram or other statistical properties of any particular location or time-instant. Many of the deviations from the target properties (ELDAS) that we found during our evaluation of the precipitation realisations can be related to this design choice.

One example is that the approach does not reproduce dry-spell lengths in Spain because too many precipitation events are generated during summer. Although this is an unfavourable characteristic of the proposed simulation approach, its effect should not be overestimated. The results in figure 10 are based on binary sequences of rain/no-rain events which do not take into account the amount of precipitation. When the wet day threshold was raised to 2.5 mm/day, the situation greatly improves. Another example is the consistent shifting of the 100<sup>th</sup> percentile in the distribution of precipitation realisations (Figure 4.8) to large precipitation values. Similar effects on monthly total pre-

cipitation have been described by Margulis and Entekhabi (2001) who suggested resampling of the realisations in order to select only those realisations with the desired characteristics.

Finally, an important aspect in ensemble generation is the performance of the system in terms of computation time. Our system is build around parts of the TTUTIL library, the `sgsim` and `sisim` tools from the GSLIB2 library and the MySQL database. These components are glued together using the Python scripting language. Currently it takes 7.5 minutes to generate 100 realisations for one day over the full CGMS grid (11330 nodes) on a 2.6 GHz PC running GNU/Linux. For operational use, realisations would only need to be generated incrementally and this performance would be sufficient. However, generating a full year of data (100 realisations) for retrospective analyses takes nearly 46 hours.

Profiling of the application showed that of the different steps within the simulation, 61% was used for generating the Gaussian and indicator simulations with `sgsim` and `sisim`, 31% was used for post-processing the Gaussian and indicator simulations using Python and only 8% was used for database communication and miscellaneous tasks. Performance could thus be greatly increased when more efficient methods would be used for simulation of random fields such as a Modified Turning Bands algorithm (Mellor et al., 2000).

## 4.6 Conclusions

This paper presents a methodology for characterising and quantifying uncertainty in gridded precipitation fields through an ensemble of precipitation realisations with a specific application as target: regional agrometeorological modelling for crop yield prediction. We defined the temporal and spatial scales which are relevant for this application and developed a relatively simple histogram-based approach which generates residual error fields that are added to the input precipitation field in order to obtain the ensemble traces.

We calibrated our method using a highly accurate precipitation database and applied it to the precipitation database of the European Crop Growth Monitoring System. Histograms, intermittency characteristics and spatial structure of the rainfall field were reproduced reasonably well in the realisations and the deviations that were found (shifting of 100<sup>th</sup> percentile, failure to produce prolonged dry spells) are of minor importance for the application at hand.

Finally, we demonstrated that the uncertainty in input precipitation fields and the resulting variability in crop model simulation results considerably influence the yield forecast for a region in South-France. These results demonstrate that there is considerable potential benefit from a probabilistic approach



in agrometeorological modelling and crop yield forecasting. Such an approach could be an important support to quantitative risk analysis in a decision making process.

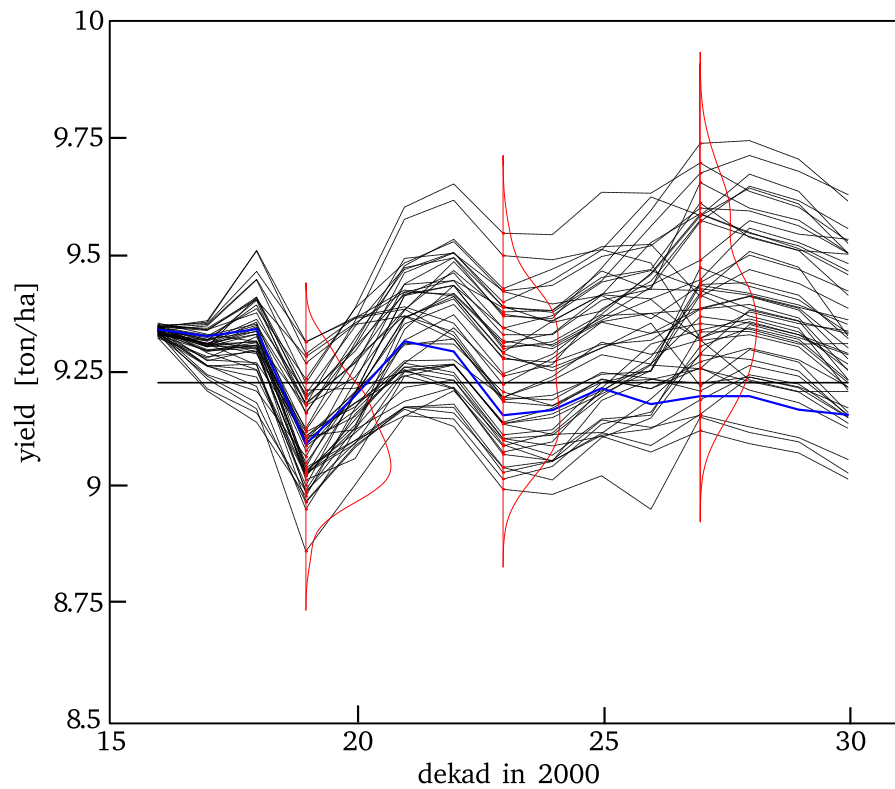


*Figure 4.13:* Crop yield forecast during the growing season in 2000. Thick black line is the official reported yield by EUROSTAT, the blue line represents the deterministic yield forecast and the dotted lines represent the influence of uncertainty in precipitation on the yield forecast. Density plots indicate the shape of the yield forecast ensemble at three moments during the growing season.



CGMS Precipitation

[illegible]



# Chapter 5

## Crop model data assimilation with the ensemble Kalman filter for improving regional crop yield forecasts\*

### 5.1 Introduction

Crop yield forecasting applications applied over large areas and relying on a spatially distributed crop growth model are typically confronted with large uncertainty in the spatial distribution of soil properties and initial soil conditions, crop parameters and meteorological forcings (Hansen and Jones, 2000). Within the crop growth model, this uncertainty influences the simulation of two important physiological processes: 1) the simulation of the crop canopy development which determines light interception and the potential for photosynthesis; 2) the simulation of moisture content in the soil which determines the actual evapotranspiration and reduction of photosynthesis as a result of drought stress. Improving the simulation of these two processes by using remotely sensed observations has been a field of active research and an overview will be given in relation to the impact on operational application in yield forecasting systems.

Research on improving the simulation of crop canopy development has mostly focused on the use of sequences of high-resolution satellite imagery (20-30 m) to either recalibrate crop model parameters such as the emer-

---

\*Chapter based on: Wit, A.J.W d. and Diepen, C.A. v.: 2007, Crop model data assimilation with the ensemble Kalman filter for improving regional crop yield forecasts, *Agricultural and Forest Meteorology* **in press**

gence date, or to integrate the observations into the model using a forcing or updating approach (Bach and Mauser, 2003; Boegh et al., 2004; Bouman, 1995; Guérif and Duke, 2000; Maas, 1988; Moulin et al., 1998; Prevot et al., 2003; Schneider, 2003). Although results demonstrated that many crop model states (simulated biomass, LAI, yield) could be improved using satellite observations, such methods have proven difficult to apply in crop yield forecasting applications at regional to continental scales.

The main reason for this slow adoption is the disparity in scales between the process (crop growth on fields often as small as 1 hectare) and the type of observing system that can be used operationally and economically over large areas with high temporal frequency (satellite sensor observations with a spatial resolution ranging from 250 m to 1 km). Given the relatively coarse spatial resolution of such satellite sensors, in many parts of the world the observations consist of a mixture of various land cover types, making it difficult to estimate the value of crop states (LAI, biomass) for specific crops. Some studies have attempted to cope with the sub-pixel heterogeneity directly (De Wit, 1999; Fischer, 1994; Moulin et al., 1995), while others attempted to unmix a coarse resolution signal into its underlying spectral components (Cherchali et al., 2000; Faivre and Fischer, 1997). The general drawback of these approaches is that they rely on the availability of ancillary data (e.g. land cover/crop maps) which are usually not available over large areas for the current growing season.

A few studies describe yield forecasting results obtained from directly integrating coarse resolution satellite observations in crop simulation models at regional scales (Doraiswamy et al., 2005; Mo et al., 2005). Although, these results show the benefit of using such an approach, the application is limited to regions with homogeneous land cover and a limited number of crop types. These studies also recognise that the results deteriorate in areas with complex land cover patterns where the satellite sensor signal consists of a mixture of many crop types.

Considerable work has also been carried out on the estimation of vegetation evapotranspiration or soil moisture by satellite thermal infrared observations with the aim of improving estimates of drought stress or water use, see an overview by Courault et al. (2005) and the work of Oliso et al. (2005). Although promising semi-operational results have been obtained by some studies (Bastiaanssen and Ali, 2003; Roebeling et al., 2004), the use of these kind of observations in crop models is very limited (Oliso et al., 2005). Besides the scale issues outlined before, other factors which limit operational application play a role, such as that no generally accepted operational systems have been available to routinely estimate evapotranspiration over large areas using satellite observations.

Besides the limitations on the observation side, it is justified to say that crop models have not evolved in a way that would make it easy to assimilate satellite observations into the model. Crop models are still generally deterministic in contrast to models within the fields of oceanography, meteorology and (more recently) land surface hydrology, where probabilistic approaches are generally accepted and advanced algorithms for sequential data assimilation such as nudging, variational methods and (Ensemble) Kalman filtering have been developed. As a result, crop models provide no information on uncertainties of the model states during simulation which is crucial for a successful application of most sequential data assimilation algorithms.

In principle, probabilistic methods and data assimilation can be applied to crop growth models as well. Particularly the use of the Ensemble Kalman filter (EnKF) is interesting for crop models because it combines a probabilistic approach with sequential data assimilation. Moreover, the structure of many crop models lends itself well for implementation in the EnKF and the state vector in crop models is relatively small (Dorigo et al., 2006). An example of such an approach has been provided by Pellenq and Boulet (2004), who applied an ensemble Kalman filter to assimilate field-scale satellite observations of NDVI and land surface temperature in a crop growth model.

Within this paper we present results obtained from a spatially distributed probabilistic crop growth model coupled to an ensemble Kalman filter, applied to selected European countries over the period 1992–2000. Currently, there are no databases available of remote sensing derived crop-specific variables (e.g. LAI, actual evapotranspiration) that span large time series and are available over the whole study area. Our system currently uses coarse resolution satellite microwave sensor derived soil moisture estimates for correcting errors in the water balance of the model during the crop simulation caused by uncertainty in rainfall or model initialisation. We assume that soil moisture estimates on this scale are still relevant for crop modelling because spatial patterns in soil moisture are not only driven by local crop - soil interactions, but also by atmosphere related patterns (rainfall) acting on a much larger scale (Vinnikov et al., 1996; Vinnikov et al., 1999). Some evidence on the suitability of coarse resolution soil moisture patterns for correcting models with grids of much smaller resolution has been provided previously by Crow and Wood (2003).

The main objective of this work is to determine if the assimilation of satellite observations of soil moisture into the crop yield forecasting system results in improved relationships between model output and crop yield statistics for administrative regions. Additionally, the innovations of the ensemble Kalman filter can provide some diagnostics that can help to trace deficiencies in the model. With the development of this probabilistic crop modelling and data

assimilation system, we anticipate on the near real-time availability of satellite soil moisture estimates as can be expected from the sensors aboard the METOP satellites (Hasenauer et al., 2006), as well as the SMOS mission (Kerr et al., 2001). Furthermore, when satellite sensors are available with sufficient spatial resolution and temporal frequency to provide crop specific variables operationally over large areas, they can be assimilated within the same framework relatively easily.

## **5.2 Spatially distributed probabilistic crop growth model**

### **5.2.1 The crop growth model**

We used the WOFOST (WOrld FOod STudies) crop simulation model as a basis for our work (Diepen et al., 1989; van Ittersum et al., 2003). WOFOST is a mechanistic crop growth model that describes plant growth by using light interception and CO<sub>2</sub> assimilation as growth driving processes and by using crop phenological development as growth controlling process. The model can be applied in two different ways: 1) a potential mode, where crop growth is purely driven by temperature and solar radiation and no growth limiting factors are taken into account; 2) a water-limited mode, where crop growth is limited by the availability of water. The difference in yield between the potential and water-limited mode can be interpreted as the effect of drought. Currently, no other yield-limiting factors (nutrients, pests, weeds, farm management) are taken into account.

The WOFOST model was cast into a probabilistic framework using an ensemble approach which means that an ensemble of models is used to represent the probability distribution of model results at each time step during model execution. Model uncertainty can be assessed by sampling from probability distributions of crop parameter values and by providing ensembles of meteorological forcings that characterise the uncertainty in the forcing data. Finally, an Ensemble Kalman filter was integrated into the probabilistic framework, see section 5.2.3 for details.

### **5.2.2 Spatial implementation of crop growth simulations**

Our crop simulation model was implemented spatially by building on the framework provided by the Crop Growth Monitoring System (CGMS). CGMS allows regional application of WOFOST by providing a database framework



which handles model input (weather, soil, crop parameters), model output (crop indicators such as total biomass and leaf area index), aggregation to statistical regions and yield forecasting (Boogaard et al., 2002; Diepen et al., 1998; Genovese, 1998; Vossen and Rijks, 1995). CGMS is part of the MARS (Monitoring Agriculture by Remote Sensing) crop yield forecasting system developed by the AgriFish unit of the Joint Research Centre in Ispra, Italy. Since 1994, CGMS monitors crop growth in Europe, Anatolia and the Maghreb with a spatial resolution of  $50 \times 50$  km and a temporal resolution of one day. Its main purpose is to provide information on weather indicators and crop status during the growing seasons and to provide objective forecasts of crop yield on the level of EU member states early in the crop growth season. Its main user is the European Commission's Directorate General for Agriculture.

Modifications to the CGMS framework were made in order to store ensemble meteorological forcings and to (temporarily) store the ensemble output from the WOFOST model ensemble.

### 5.2.3 The ensemble Kalman filter

For the implementation of the ensemble Kalman filter (EnKF) we based ourselves on the work of Evensen (2003) who describes the theoretical framework and practical implementation for the EnKF. The basic analyses step in an EnKF for each ensemble member can be defined as:

$$A^a = A + P_e H (H P_e H^T + R_e)^{-1} (D - H A) \quad (5.1)$$

where  $A$  and  $A^a$  are the forecasted and analysed matrices of ensemble states,  $P_e$  and  $R_e$  are the ensemble and observation covariance matrices,  $H$  is the measurement operator and  $(D - H A)$  are the innovation vectors.

In our current setup the model soil moisture is the only variable which is used for the assimilation process. The WOFOST model has a root-zone soil water balance consisting of only one layer and the observations that we assimilate are direct observations of the root zone soil moisture in this layer. In this setting  $A^a$  and  $A$  are vectors,  $P_e$  and  $R_e$  are variances and the measurement operator  $H$  is an identity matrix because the model state is observed directly. Equation 5.1 then reduces to:

$$A_i^a = A_i + P_e (P_e + R_e)^{-1} (D_i - A_i) \quad (5.2)$$

where  $A_i^a$  and  $A_i$  are the analysed and forecasted soil moisture state for ensemble member  $i$ ,  $P_e$  and  $R_e$  are the variances on the modelled soil moisture and the observed soil moisture and  $D_i$  is the perturbed soil moisture observation which is used to update ensemble member  $i$  (Burgers et al., 1998). Note that

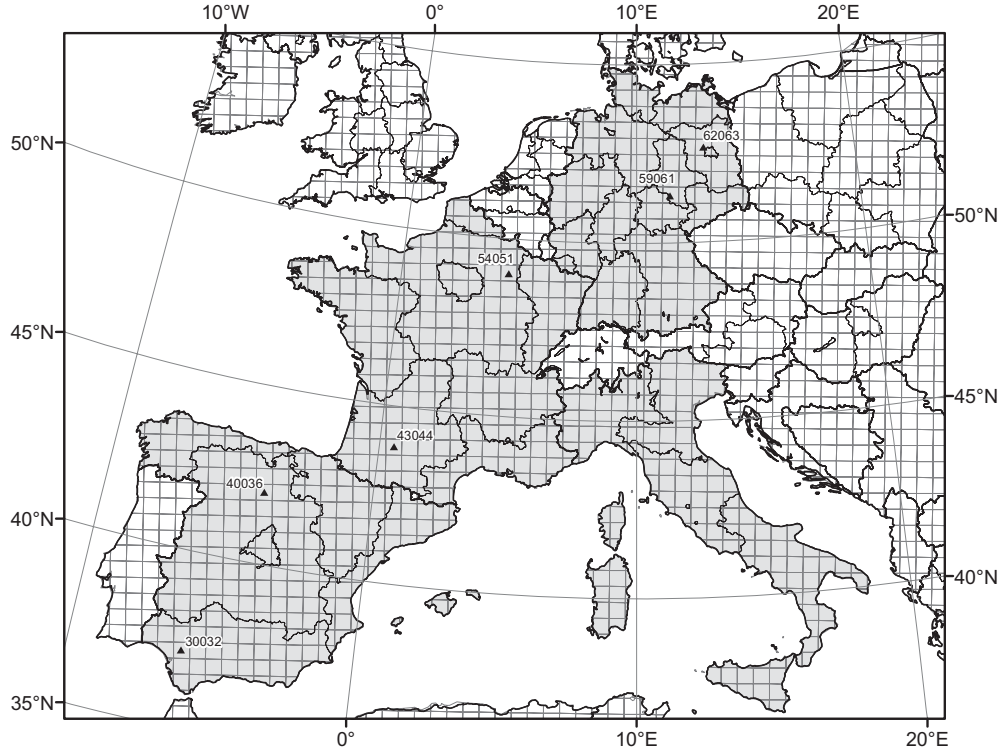


Figure 5.1: Overview of the study area (greyed area) including country borders, provincial borders (NUTS1) and  $50 \times 50$  km CGMS grid.

for simultaneous assimilation of more observations (e.g. soil moisture and Leaf Area Index) equation 5.2 cannot be used and equation 5.1 will need to be used. However, because our state vector is small, the matrix  $(HP_e H^T + R_e)^{-1}$  can be inverted directly.

### 5.3 Study area

Our study area consists of Germany, France, Spain and Italy (Figure 5.1). The motivation for this choice is based on the fact that from north to south a clear gradient exists from temperate maritime conditions in northern Germany to semi-arid Mediterranean conditions in the south of Italy and Spain. Moreover, crop yield statistics at various administrative levels were available that could be used for assessing the relationship with crop yield statistics.

## 5.4 Data and methods

### 5.4.1 Deterministic crop, soil and weather inputs

Soil inputs for the study area were derived from the 1:1,000,000 European soil map (King et al., 1995). The CGMS  $50 \times 50$  km grid was combined with the soil data in order to determine which soils were available in each CGMS grid. Soil moisture contents at different pressure heads (saturation - TWC, field capacity - FC, wilting level - WL) are estimated from the soil physiological description and together with the estimated rooting depth they determine the water retention capacity and hydraulic conductivity of the soil (King, 1990). In order to reduce the number of simulations that had to be carried out, we selected the soil type with the largest area coverage (majority) for each CGMS grid. In case of two soil types having exactly the same majority area fraction, we selected the soil type with the largest water holding capacity, assuming that it was more suitable for agricultural production.

Deterministic weather inputs were derived from the operational CGMS which currently derives its weather information from about 2500 weather stations over Europe. These weather stations provide daily estimates of minimum and maximum temperature, wind speed, vapour pressure and precipitation. Radiation is only available from a limited number of stations and therefore radiation is estimated at station level using relationships with temperature, cloud duration or sunshine hours (Supit and van Kappel, 1998).

An interpolation routine is applied to estimate weather variables for each  $50 \times 50$  km grid cell. Each cell receives values for temperature, radiation, vapour pressure, evapotranspiration and wind speed as the weighted average from suitable surrounding weather stations using inverse distance weighting. Determination of the most suitable weather stations takes place on the basis of the so-called 'meteorological distance'. This meteorological distance is a virtual distance which is not only based on the true distance between the grid cell and the weather station, but also on factors like altitude, distance to coast and the existence of climate barriers (e.g. mountain ridges, water bodies) between the grid cell and the weather station. In case of rainfall a grid cell receives the value of the weather station with the smallest meteorological distance from the grid cell (Voet et al., 1994).

Finally, crop parameter values and crop calendars were derived from the operational CGMS.

### 5.4.2 Probabilistic weather inputs

According to many studies on land surface hydrology, precipitation is regarded to be one of the prime sources of uncertainty in land surface hydrological models (Chaubey et al., 1999; Crow, 2003; Margulis et al., 2006; Syed et al., 2004). In WOFOST, soil moisture is the only factor during crop growth simulation which limits the potential production and its proper estimation is therefore of high importance. Wit et al. (2005) demonstrated that the influence of uncertainty in precipitation inputs on the outcome of WOFOST simulations can be large, particularly in areas with climates that are marginal for crop growth. Moreover, several studies (Easterling et al., 1998; Mearns et al., 2001) demonstrate that when aggregating model output to regional scales, uncertainty in the input forcings becomes dominant over uncertainty in soil parameters. Pellenq and Boulet (2004) state that parameter uncertainty represents the largest source of uncertainty in crop modelling. This is indeed likely for point application of a crop model, where meteorological conditions are relatively well known. However, for regional applications we decided that precipitation was a prime candidate for specifying input uncertainty in the water balance of our probabilistic WOFOST simulations.

In order to generate precipitation ensembles, we used an error model fitted to a highly accurate precipitation dataset which was available for the year 2000. Our error model consisted of two components. The first is an additive component generating precipitation residues over the entire spatial domain. The residues are generated by quantile-based back transformation of standard Gaussian fields using a set of histograms for different CGMS precipitation bins. The second component is multiplicative and generates binary rain/no-rain events on locations where the CGMS precipitation records report zero precipitation. The error model was used to generate an ensemble of 50 realisations for daily precipitation over the period 1990–2005 and 250 realisations for the year 2000 only. This last set of realisations was used to determine the influence of the size of the ensemble on the estimation of ensemble mean and variance. More information about the precipitation ensemble generation method can be found in Wit and Bruin (2006).

### 5.4.3 Satellite derived soil water index (SWI)

The Soil Water Index (SWI) dataset was provided by the Institute of Photogrammetry and Remote Sensing (IPF) of the Vienna University of Technology and is derived from coarse resolution surface (upper few centimetre) soil moisture measurements from the Scatterometer instrument aboard the ERS1/2 satellites (Ceballos et al., 2005; Wagner et al., 1999; Wagner

et al., 2003). The SWI data are provided on a  $0.25^\circ$  grid in regular intervals of 10 days. The dataset covers the period 1992–2000, but the availability of SWI values varies over years and regions as a result of satellite programming conflicts between the scatterometer and SAR instruments aboard ERS1/2. Over Europe the quality of the SWI product is therefore relatively poor. End of 2007 scatterometer derived soil moisture products will be processed operationally in near real time by EUMETSAT using data from the METOP Satellites (Hasenauer et al., 2006).

The SWI is a trend indicator for the root-zone soil moisture (upper 1 meter) ranging from 0 to 1. For converting this trend indicator in an estimate of volumetric soil moisture content, auxiliary data about soil physical properties is necessary. We used information about soil physical properties provided by the CGMS database (wilting level, field capacity, porosity) to estimate the volumetric soil moisture content with a relationship provided by (Wagner et al., 1999):

$$D = SWI \left( \frac{FC + TWC}{2} - WL \right) + WL \quad (5.3)$$

Where  $D$  is the observed volumetric soil moisture content,  $FC$  and  $TWC$  are field capacity and porosity and  $WL$  is the wilting level.

Information about the variance of the  $SWI$  is necessary in order to parametrise  $R_e$  and to generate an ensemble of perturbed observations  $D_i$  in equation 5.2. The variance information was supplied by IPF for each SWI value and was based on strict error propagation of measurement noise through the retrieval model. Consequently the calculation of the variance only accounts for the effects of noise, but not for deficiencies in the model itself, i.e.  $SWI$  can still deviate from the true soil moisture value if for example vegetation is poorly estimated.

#### 5.4.4 Influence of ensemble size

The EnKF presents a solution to the optimal state estimation problem which uses an ensemble of model states to approximate the mean state and covariance. Given this approximation, the question then rises how large the ensemble needs to be in order to make an acceptable estimate of mean and covariance. Several studies (Crow and Wood, 2003; Reichle, McLaughlin and Entekhabi, 2002; Reichle, Walker, Koster and Houser, 2002) have evaluated the influence of the ensemble size with reference to the true (measured) states. In our case, such measurements are not available and therefore we compare the influence of varying ensemble size with reference to the simulation with the largest ensemble size. We assume that this simulation presents the best estimate of state mean and variance. We carried out simulations for grain maize

for the year 2000 without data assimilation but with ensemble sizes of 10, 25, 50, 100 and 250 members. These simulation were carried out for 5 grids located in different climatic zones and in areas with major agricultural production in southern Spain, northern Spain, southern France, northern France and central Germany.

#### 5.4.5 Crop yield forecasting experiment setup and initialisation

We carried out two experiments in order to determine the influence of assimilating SWI on the yield forecasting performance of the system. The first experiment used a single WOFOST run using only deterministic inputs to generate biomass values per grid (further to be called ‘classic experiment’). The water balance for these simulation was started 30 days before crop emergence or sowing and the initial soil moisture value was set to field capacity.

In the second experiment, we used the probabilistic WOFOST model fed with probabilistic precipitation inputs and we used the EnKF to assimilate SWI soil moisture estimates into the system (further to be called ‘EnKF experiment’). The water balance of each ensemble member was started 30 days before crop emergence or sowing and uncertainty in the initial soil moisture value was reflected by drawing the initial value for each ensemble member from a Gaussian random variable with a mean equal to  $(FC + WL)/2$  and standard deviation equal to  $0.2 \times (FC - WL)$ . Choosing these settings ensures that the initial soil moisture distribution in the ensembles is Gaussian and that more than 95% of the drawn values are between wilting point and field capacity. Values beyond this range were truncated on these limits. Although the EnKF experiment provides an ensemble of simulated crop biomass, we only stored the ensemble average biomass for further analyses.

Both experiments were applied for all grids in Spain, Italy, France and Germany over the period 1992–2000 for winter-wheat and grain maize. The simulation results of both experiments were spatially aggregated to national (NUTS0) and regional level (NUTS1/2).

#### 5.4.6 Spatial aggregation of simulation results

The simulated crop biomass values on individual grids have to be aggregated to regions in order to establish relationships with yield statistics available from European Statistical Office. Ideally, the cultivated area of each crop should be known per CGMS grid cell in order to aggregate simulated yield to regions. However, crop area estimates are not available at the level of individual CGMS

grids and quite often not on administrative regions. Therefore, we decided to substitute crop area with the area arable land within a grid cell. The area of arable land was derived from the PELCOM land cover database (Mücher et al., 2000). Aggregation of simulation results to the European NUTS2/1/0 levels was thus performed by weighting on the area of arable land within each CGMS grid cell within a NUTS region.

#### 5.4.7 Evaluation of model performance

Evaluation of the model performance was carried out by searching for a relationship between the time-series of WOFOST simulated biomass values aggregated to administrative regions, and the historically known crop yield from the European Statistical Office (EUROSTAT, 2005). Within this paper, we assume that these statistical values represent the true crop yield for a region, although uncertainties in the EUROSTAT statistics are probably large, particularly for the lower administrative regions (NUTS2). For example, it has been observed that for some regions the same crop yield value has been reported for a series of years in a row, which is unlikely. Nevertheless, the period 1992–2000 is favourable from a political perspective given that a major reform of the European Agricultural Policy (CAP) was carried out in 1992 and no major political changes were made in the years to follow. Therefore there is no breach of trend in the yield statistics for this period.

We assumed that the time-series of crop yield for a region is composed of three factors: mean yield, multi-annual trend (or technology trend) and residual variation around the trend (Supit, 1997; Vossen, 1992). We used the time-series of yield statistics over the period 1992–2000 to determine a linear technology trend assuming that the trend is stable over this period. The time-series of WOFOST simulation results at each dekad<sup>1</sup> during the growing season were then used to explain the residual deviation from the trend; thus a separate regression model was established for each dekad. Yield forecasting can be carried out by extrapolating the trend for the following year and by feeding the WOFOST simulation results for the following year into the regression models to predict the deviation from the trend for each dekad in the following year.

In the ideal situation, model performance is evaluated using the so-called one-year-ahead prediction, because this mimics the operational conditions. However, in our case the period 1992–2000 is too short to evaluate on the one-year-ahead prediction, given that nine years are already necessary to establish

---

<sup>1</sup>The use of the term ‘dekad’ refers to an FAO convention in order to distinguish 10 year periods (decade) from 10 day periods (dekad).

the regression models. We therefore decided to measure the yield forecasting performance by using the residual error of the regression model employing both the trend and the WOFOST simulation results, relative to the residual error of the regression model employing the technology trend only.

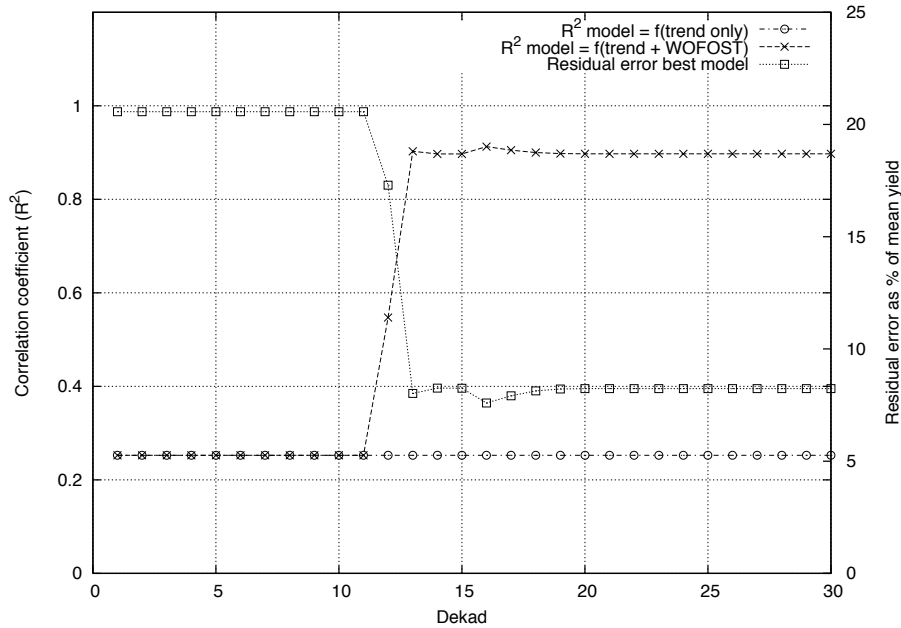


Figure 5.2:  $R^2$  values of a series of regression models (one per dekad) between reported EUROSTAT yield of winter-wheat for Spain and WOFOST simulated total crop biomass of winter-wheat over the period 1992–2000. One series is based on the trend in the statistics only (marked as ‘f(trend only)’) and the second series using both the trend and the WOFOST simulation results (marked as ‘f(trend + WOFOST)’). The residual error of the regression model with the lowest error is plotted as a percentage of mean crop yield.

An example of the output from the crop yield forecasting system is provided in figure 5.2 where the WOFOST simulated total crop biomass of winter-wheat is used to explain the variations in the reported EUROSTAT yield of winter-wheat for Spain over the period 1992–2000. At each dekad the  $R^2$  of two models is plotted, one model applying the trend in the crop yield statistics only (marked as ‘f(trend only)’) and the second model using both the trend and the WOFOST simulation results (marked as ‘f(trend + WOFOST)’). Moreover, the residual error of the regression model with the lowest error is plotted as a percentage of mean crop yield.

Up till dekad 12 there is no skill in the WOFOST simulation results in



explaining the EUROSTAT yield statistics. The  $R^2$  of both regressions models is 0.253 and the residual model error shown is the residual error of the trend-only model (20.57%). In dekad 12, the WOFOST simulation results show some skill in explaining the yield variations (lower residual error). The  $R^2$  of model 'f(trend+WOFOST)' is higher than the  $R^2$  of the model 'f(trend-only)'. In the following dekads, the model residual error decreases (7.59%) and the  $R^2$  increases (0.912) until dekad 16 and then increases slightly until a final regression model is obtained in dekad 20. For dekads 20 to 30 the results do not change any more because the growing season for winter-wheat in Spain is finished.

For evaluating the results of the classic and EnKF experiments, we used the following constraints: 1) A valid regression model must be established up till the end of the growing season. For example, regions for which a model could be established for dekads 16 and 17, but not for later dekads were rejected; 2) The final residual error that was used for benchmarking was defined as the average residual error over dekads 25–30. For winter-wheat the residual error for dekads 25 to 30 is always the same value because the growing season is finished for all regions in the study area. For grain maize, small variability in the residual error is often observed for these dekads because the aggregated simulated biomass results are still changing slightly because of differences in growing season length; 3) Two indicators were used in the regression analysis: the water-limited total crop biomass and the water-limited biomass of the crop storage organs (harvestable product). The best system was selected on the basis of the indicator with the lowest residual error in the regression model.

## 5.5 Results

### 5.5.1 Impact of ensemble size

The influence of the ensemble size on estimate mean and variance of the soil moisture is shown in table 5.1 as the root mean squared error (RMSE) between the reference mean and variance (daily ensemble mean and variance for ensemble size 250), and the calculated mean and variance for one randomly selected ensemble of that size. For the ensemble mean, the RMSE increases when the ensemble size increases from 10 to 25 members, then the RMSE strongly decreases when the ensemble size increases to 50 members and finally a small decrease when the ensemble size increases to 100 members (except for grid 59061). Results for ensemble variance show a different pattern. RMSE on the estimated variance decreases with ensemble size increasing from 10 to 50 members, but then increases again for ensemble size

100. We found that this behaviour is a result of the limited sample size and it disappears when the results of repeated samples of a certain ensemble size are averaged. Nevertheless, the results in table 5.1 are more representative of the results that can be obtained in practice when only one ensemble is available.

Our results indicate that the soil moisture ensemble mean can be estimated well with an ensemble size of 50 and improvements are small when the ensemble size is increased to 100. However, for estimates of variance a larger ensemble size is necessary because the estimated variance is not yet stable for ensembles up to size 100. Our results with regard to estimates of mean and variance in relation to ensemble size are consistent with results from Reichle, McLaughlin and Entekhabi (2002) who showed that error on soil moisture estimates could be reduced considerable with relatively small ensemble sizes (30), but that an ensemble size of at least 500 is necessary for stable variance estimation. Also, Crow and Wood (2003) found little improvement in model prediction performance with ensemble sizes larger than 50. Given constraints on data storage and computational capabilities, we decided that an ensemble size of 50 was a reasonable trade off between ensemble size and accuracy of estimated mean and variance.

The temporal patterns in the soil moisture ensemble mean and variance for different ensemble sizes are shown in figure 5.3 (page 102) for two grids, one in southern Spain (30032) and one in northern France (54041). For southern Spain the simulation starts half February and the ensemble means demonstrate similar patterns of increasing soil moisture content due to spring rainfall events during the first 60 days and a large rainfall event at day 62. Soil moisture levels are relatively stable during days 60–90 and then a gradual dry down of the soil is simulated due to increased water use by the crop and a lack of rainfall during the summer period. The temporal patterns in the variance (Figure 5.3B) show large differences between various ensembles up to day 63 when many ensemble members receive a large amount of rainfall, causing a sharp decrease in the variance. After day 100, variance decreases further as the soils of all ensemble members are gradually drying out until the soil of many ensemble members reaches wilting level at which the variance for all ensemble sizes becomes nearly zero.

For northern France (Figure 5.3C), the figure shows an increase in soil moisture levels due to Spring rainfall and after day 70 a drying trend due to crop water use, which is often interrupted by isolated large Summer rainfall events. After day 175, soil moisture increases again due to a decrease in crop water use in combination with rainfall in Autumn. The ensemble mean can be estimated well with all ensemble sizes except for ensemble size 10, which shows a consistent underestimate of the ensemble mean. The ensemble variance (Figure 5.3D) remains relatively high during most of the growing season,

*Table 5.1:* Estimates of RMSE on ensemble average and ensemble variance of volumetric soil moisture estimates throughout the growing season. Simulations were carried out for grain maize for five grids located in southern Spain (30032), northern Spain (40036), southern France (43044), northern France (54041) and central Germany (59061).

Grid	Ensemble size	RMSE of average	RMSE of variance
30032	10	0.004908	$0.6086 \cdot 10^{-3}$
30032	25	0.009709	$0.1794 \cdot 10^{-3}$
30032	50	0.001994	$0.0332 \cdot 10^{-3}$
30032	100	0.001509	$0.3202 \cdot 10^{-3}$
40036	10	0.007141	$0.7125 \cdot 10^{-3}$
40036	25	0.008705	$0.1145 \cdot 10^{-3}$
40036	50	0.002017	$0.0346 \cdot 10^{-3}$
40036	100	0.000876	$0.3496 \cdot 10^{-3}$
43044	10	0.008075	$0.4954 \cdot 10^{-3}$
43044	25	0.008657	$0.3305 \cdot 10^{-3}$
43044	50	0.001891	$0.1559 \cdot 10^{-3}$
43044	100	0.001736	$0.3063 \cdot 10^{-3}$
54041	10	0.007507	$0.8462 \cdot 10^{-3}$
54041	25	0.011076	$0.2813 \cdot 10^{-3}$
54041	50	0.002380	$0.1772 \cdot 10^{-3}$
54041	100	0.001193	$0.4139 \cdot 10^{-3}$
59061	10	0.009604	$0.9358 \cdot 10^{-3}$
59061	25	0.010587	$0.3326 \cdot 10^{-3}$
59061	50	0.001462	$0.0800 \cdot 10^{-3}$
59061	100	0.002028	$0.5202 \cdot 10^{-3}$

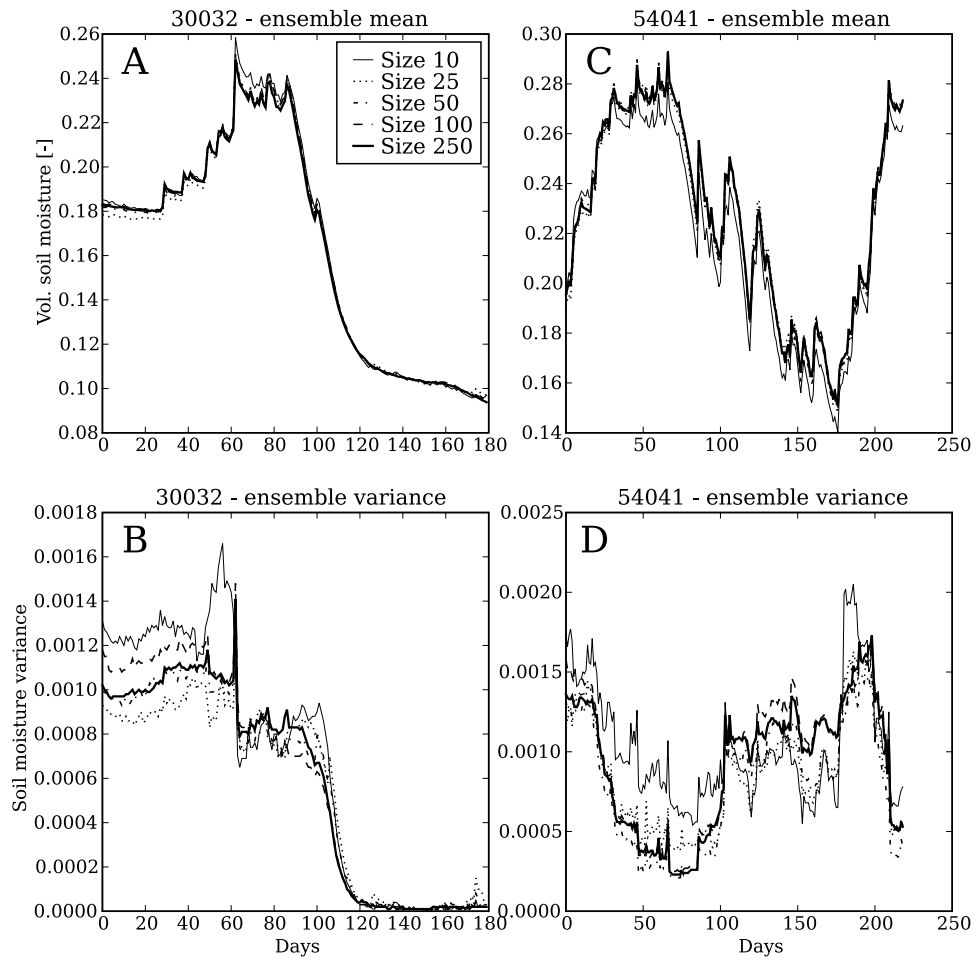


Figure 5.3: Temporal evolution of ensemble mean and variance for grids 30032 and 54041.

this demonstrates that the frequent rainfall events, whose uncertainty is modelled in the ensemble rainfall inputs, continuously can sustain the ensemble spread. Ensemble variance is decreasing during periods of soil water replenishment (days 25–100 and days 190–225) during which the soil moisture content of many ensemble members is near or at field capacity.

### 5.5.2 Analyses of filter innovations

Analyses of the innovations of the EnKF can provide information about systematic deficiencies in the water balance of our model due to for example poorly estimated soil depth, rainfall input or crop model parameters. We present the results of this analyses in three ways: 1) maps of yearly summed soil moisture innovations showing where soil moisture was added or removed; 2) temporal patterns for selected grids of individual soil moisture innovations to the water balance and; 3) a histogram of normalised innovations that characterises the statistical properties of the filter and that can be used for assessing filter performance.

#### Maps of yearly sums of soil moisture innovations

Figure 5.4 (page 105) shows the yearly total soil moisture innovations for grain maize simulations for the campaigns 1993 and 1999. These campaigns were chosen because they present two contrasting years, but the map of 1993 is more representative of the overall pattern in other years. A negative sum of innovations indicates that the soil was too wet and that water was systematically removed from the soil. A positive sum of innovations indicates that the soil was too dry and water was systematically added to the soil.

The map of 1993 shows an overall tendency of negative innovations demonstrating that the modelled amount of soil moisture was too high for large parts of the test area. Large negative innovations are particularly visible in northern France and central Germany, to a lesser extent in Spain while the sum of innovations is only slightly negative for most grids in Italy. Some isolated grids with positive innovations are visible in southern France. The map of 1999 shows large areas with positive innovations, particularly northern Germany, central and southern France. Grids in the western part of Spain and northern Italy also have dominantly positive innovations, but less pronounced.

For winter-wheat (Figure 5.5, page 106), the overall patterns are fairly similar: large negative innovations for northern France (-20 to -60 mm) and large positive innovations for north-eastern Germany (20 to 60 mm) in most of the years. For Spain the overall innovations are slightly negative (-20 to 10

mm) with the exception of 1993 and 1998 where clusters of grids with large negative and positive innovations are present.

### Temporal patterns of soil moisture innovations

Figure 5.6 (page 107) shows the temporal patterns of the soil moisture innovations for grain-maize simulations for four selected grids of the period 1992-2000. The plots for the grids in southern Spain (30032), southern France (43044) and central Germany (59061) demonstrate that there is a temporal correlation in the innovations: mainly negative innovations during the first part of the growing season, mainly positive innovations during the second part of the growing season. The sum of the innovations is dominantly negative, corresponding with the findings in the previous section. Grid 62063 (Figure 5.6) is located in north-eastern Germany which was characterised by mainly positive sums of innovations. The temporal pattern of innovations is also different for this grid showing near-zero innovations during the first part of the growing season, and slightly positive innovations during the second half of the growing season.

Results for winter-wheat are different. Grid 30032 (southern Spain) still shows a pattern of negative innovations during the first part of the growing season and positive innovations during the second part (Figure 5.7, page 108), which is similar to the results for grain-maize. Results for grids 43044 (southern France) and 59061 (central Germany) demonstrate a different pattern which is characterised by a series of near zero innovations during the beginning of the growing season, then the innovations become negative, while at the end of the growing season the innovations are near zero or slightly positive again. Good examples of this pattern are the year 1999 for grid 43044 and 1998 for grid 59061 (Figure 5.7).

### Normalised filter innovations

The consistency of the EnKF results with regard to the assumptions that underlie the Kalman filter (Gaussian forecast error, temporally and spatially uncorrelated innovations) can be evaluated by looking at the distribution of the normalised innovations  $(D - A) / \sqrt{P_e + R_e}$ . If all assumptions are met then this distribution should be Gaussian with mean zero and standard deviation one. We calculated the normalised filter innovations for all years for both winter-wheat and grain maize simulations (Figure 5.8, page 109). It is obvious that the normalised filter innovations do not follow a normal distribution (plotted for reference). The mean of the distribution is -0.4026 indicating that on average the innovations were negative (soil moisture was over predicted), while

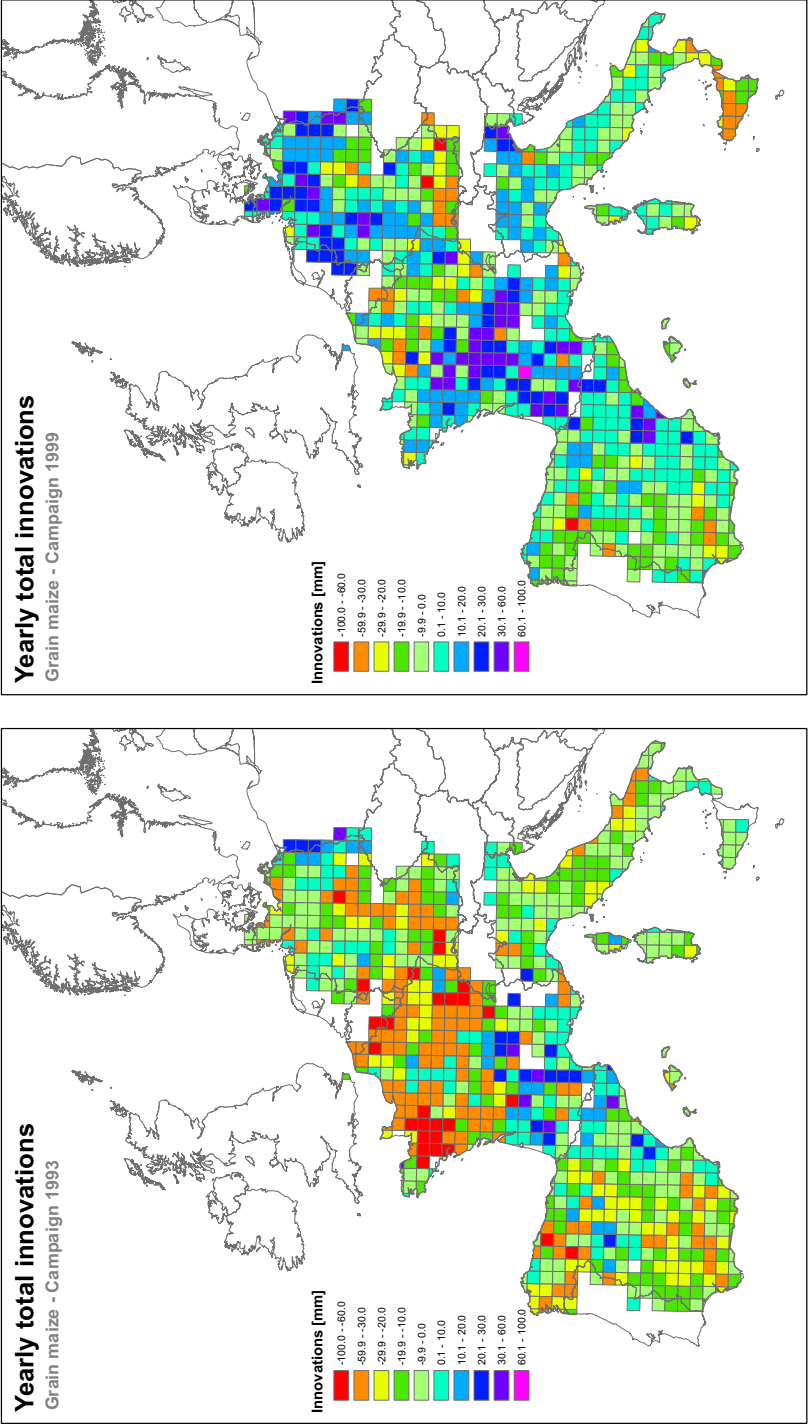


Figure 5.4: Maps of yearly total soil moisture innovations for grain maize simulations for the campaigns 1993 and 1999.

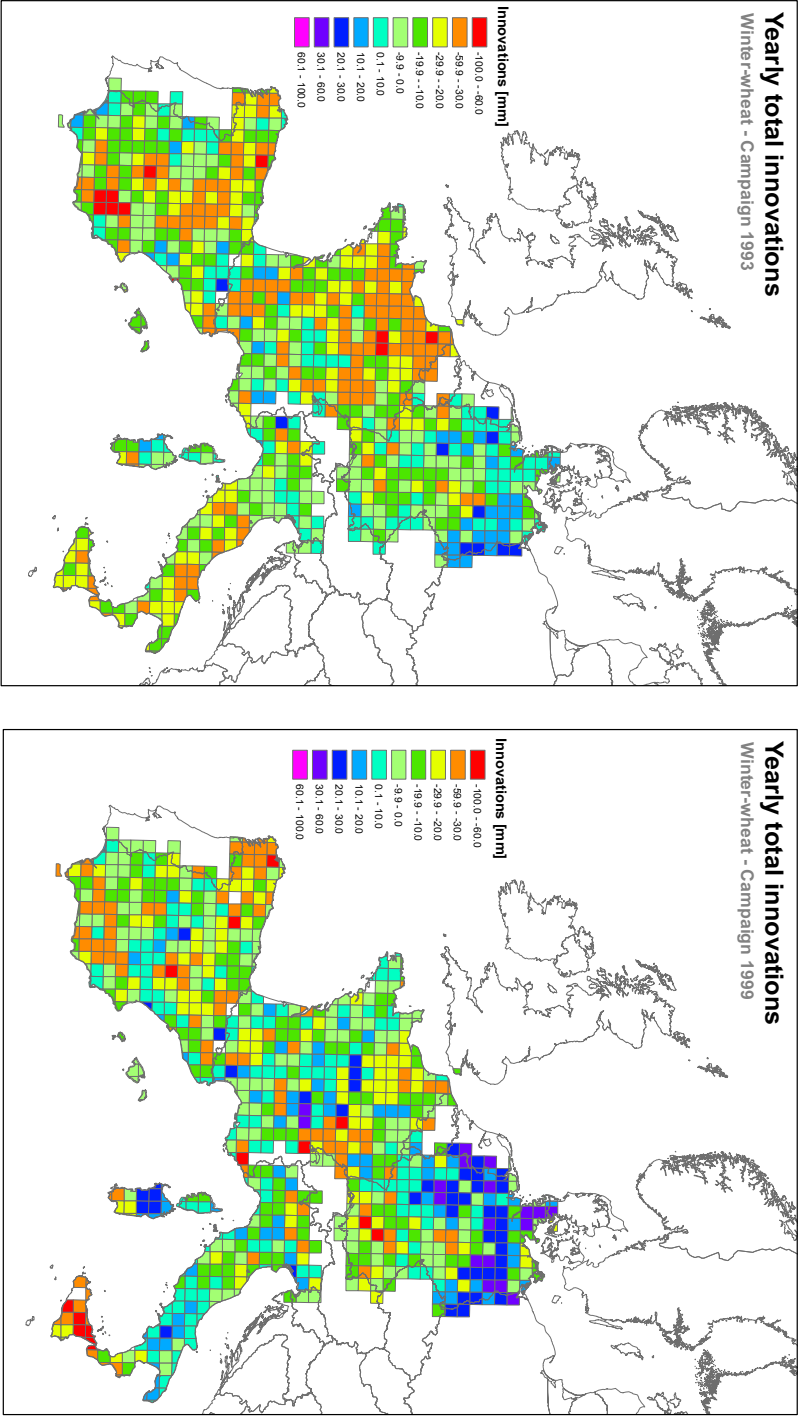


Figure 5.5: Maps of yearly total soil moisture innovations for winter-wheat simulations for the campaigns 1993 and 1999.



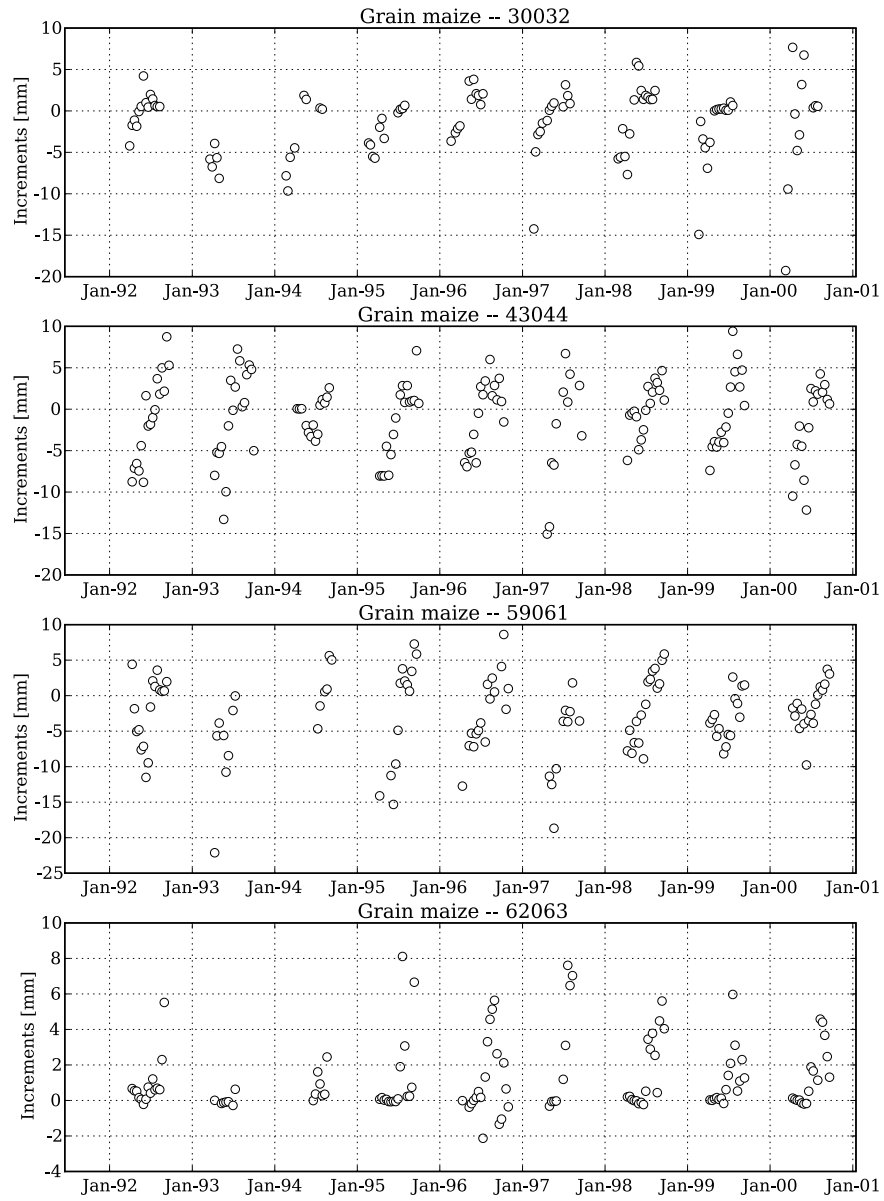


Figure 5.6: Temporal patterns of the soil moisture innovations for grain-maize simulations for four selected grids over the period 1992–2000.

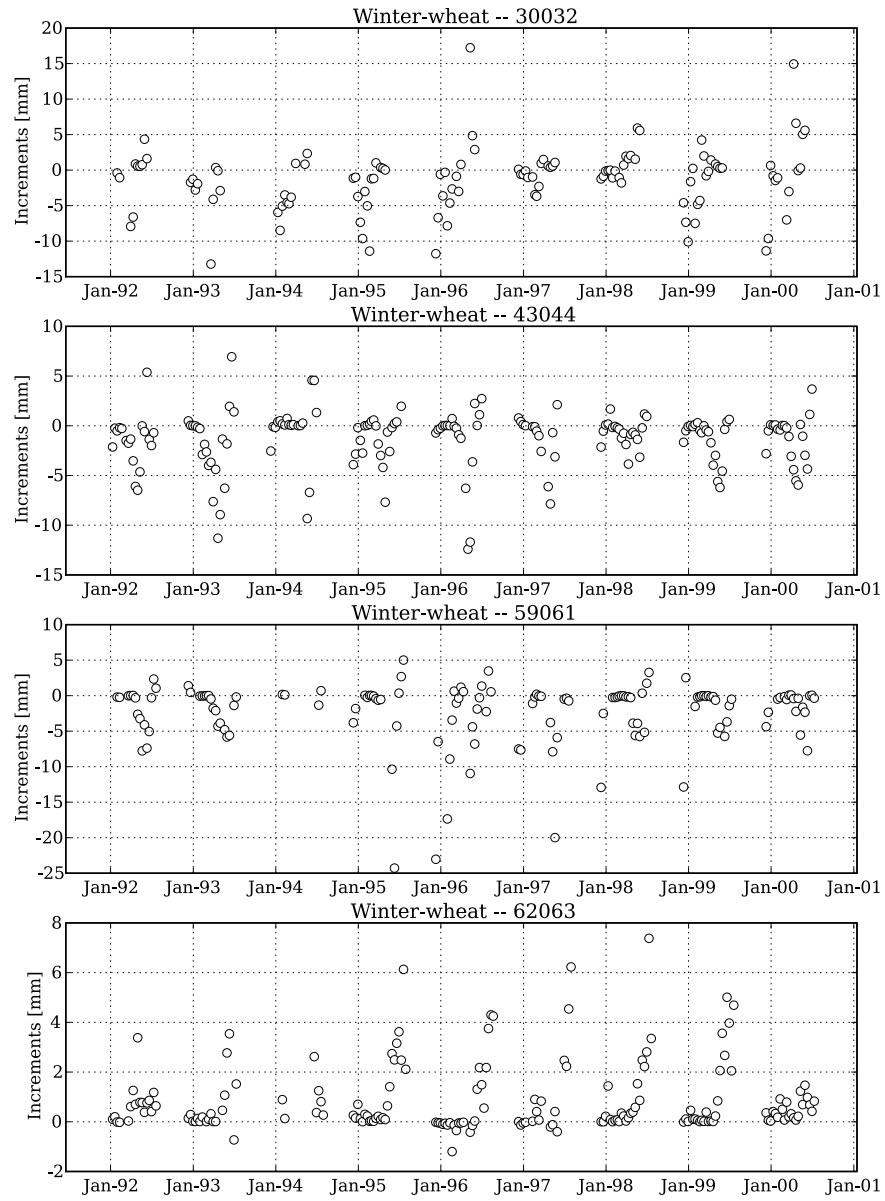


Figure 5.7: Temporal patterns of the soil moisture innovations for winter-wheat simulations for four selected grids over the period 1992–2000.

the standard deviation (2.22) indicates that the assumed error covariances ( $P_e + R_e$ ) are underestimated. The large negative tail indicates too many large negative innovations associated with over prediction of soil moisture levels, while the positive tail indicates too many positive innovations associated with under prediction of soil moisture levels. The distribution of the normalised innovations did not improve when grids were selected that were dominated by winter-wheat demonstrating that the performance of the filter is not depending on the dominant land use within a CGMS grid.

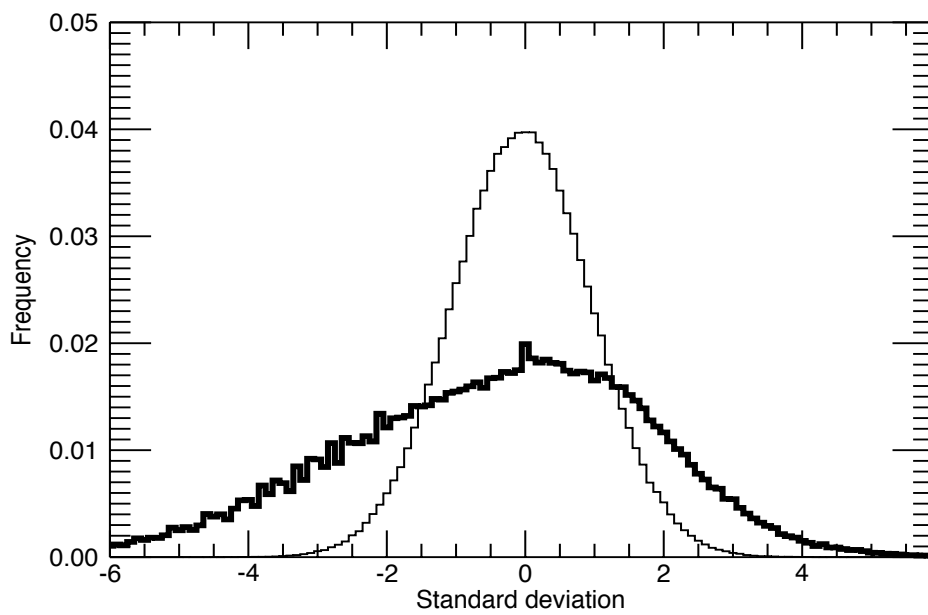


Figure 5.8: Distribution of normalised filter innovations (thick line) and a standard normal distribution (thin line).

A small case study was carried out to analyse and explain the behaviour of the normalised filter innovations in terms of mean and standard deviation. First of all, the negative mean of the normalised filter innovations can be explained by differences in the mean of the climatology of model forecasts and SWI (Reichle and Koster, 2005). Therefore, the climatology of the WOFOST simulated soil moisture for winter-wheat (no assimilation) and the SWI predicted soil moisture over the period 1992-2000 was analysed for a block of  $3 \times 3$  CGMS grids with grid 43044 as the centre grid.

Figure 5.9 (page 110) shows the distribution of soil moisture for the days that SWI derived soil moisture could be compared with the WOFOST results.

The distribution of WOFOST soil moisture has a peak around 0.25 which corresponds to field capacity. This is a result of WOFOST simulating (nearly) bare soil conditions for a considerable part of the season during which no water is extracted by plant roots. The mean of the distributions is 0.229 and 0.207 for the WOFOST and SWI soil moisture estimates. This result proves that at least part of the negative mean in the distribution of normalized innovations can be explained from the differences in the mean of the climatology of the two sources of soil moisture.

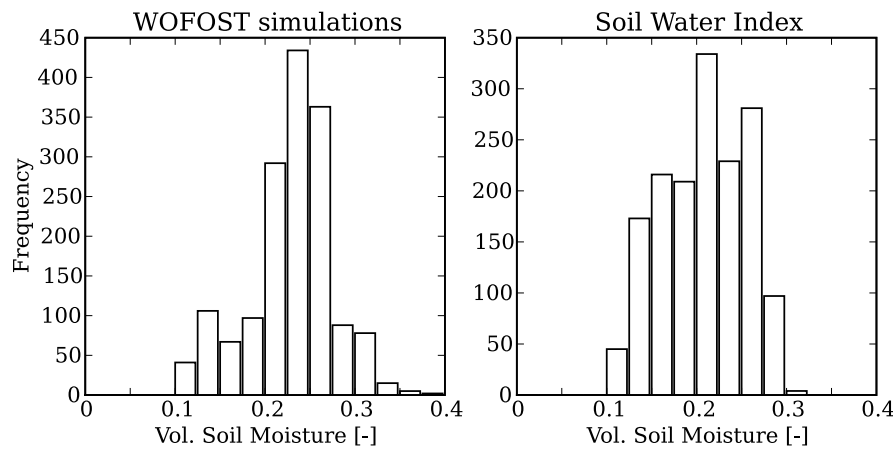


Figure 5.9: Soil moisture climatology for WOFOST simulations (mean 0.229, SD 0.047) and Soil Water Index (mean 0.207, SD 0.045).

Secondly, the excessive spread in the distribution of normalised innovations indicates that the assumed error variances ( $P_e + R_e$ ) are underestimated. Although both  $P_e$  and  $R_e$  are probably to blame, the correct variances cannot be easily inferred because both  $P_e$  and  $R_e$  are variable in space and time. Nevertheless, the effect of increased variance on the distribution of normalised innovations can be easily demonstrated by artificially inflating the observation variance ( $R_e$ ). The WOFOST model coupled to the EnKF was applied for the same test grids, period and crop, but the observation variance ( $R_e$ ) was inflated by a factor 4 (double standard deviation). Figure 5.10 (page 111) compares the distributions of normalised innovations for the normal and inflated observation variance. The figure demonstrates that the excessive spread in the distribution is strongly reduced as the standard deviation decreases from 1.97 to 1.17, while the mean becomes closer to zero (from -0.61 to -0.34).

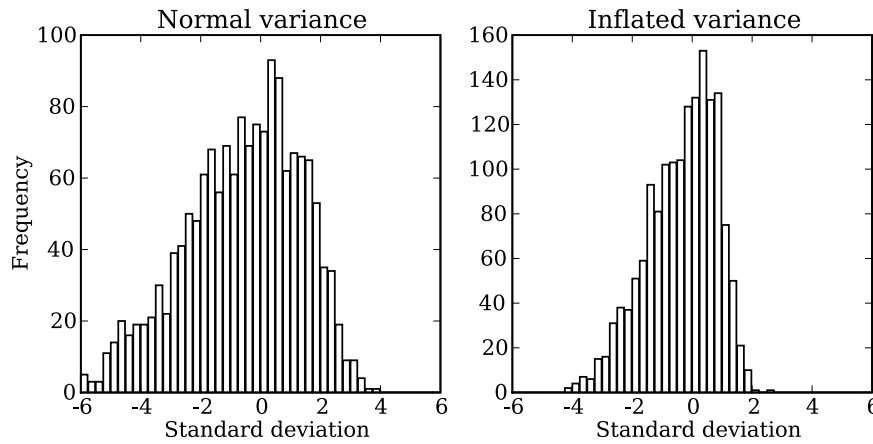


Figure 5.10: Distribution of normalised innovations for normal observation variance (left) and inflated observation variance (right).

### 5.5.3 Yield forecasting performance

Regression results for winter-wheat (Table 5.2, page 118) demonstrate that the assimilation of SWI values has a positive effect on the crop yield prediction. A relationship could be established for 33 regions based on the results from both experiments, for the EnKF experiment in 31 regions and for the classic experiment in 24 regions. Out of these 33 regions, in 22 cases the residual error on the regression model was lower for the EnKF experiment compared to the classic experiment.

Nevertheless, table 5.2 also demonstrates that there are clear limitations for predictability of winter-wheat yield. A relationship could only be established for 33 regions out of 88 regions, a score of only 38%. At national level (NUTS0) a relationship could be established for Germany (DE) and Spain (ES), but not for Italy (IT) and France (FR). In case of Germany, the residual error from classic experiment (2.46%) outperforms the results from the EnKF experiment (2.93%) but both are better than the trend-only (3.43%). In Spain, the opposite is true where the residual error of the trend-only (20.57%) can be reduced to 6.66% using the results from the EnKF experiment, while the residual error of the classic experiment is 8.23%.

We defined the normalised regression performance as the residual error of the EnKF experiment minus the residual error of the classic experiment, divided by the residual error of the trend-only. This measure shows the performance of the EnKF results over the classic results, relative to the error on the trend. Negative values indicate that the residual error of the EnKF results is larger than the residual error of the classic results. The results for winter-

wheat clearly show the improvement in the regression results as the majority of regions is in the right hand (positive) side of the diagram (Figure 5.11, page 112). Most of the improvements in the regression results are between 0 and 10% (13 regions), and between 10% and 25% (7 regions). Nevertheless, the diagram also shows that for two regions, the results strongly deteriorate with values between -75% and -50%.

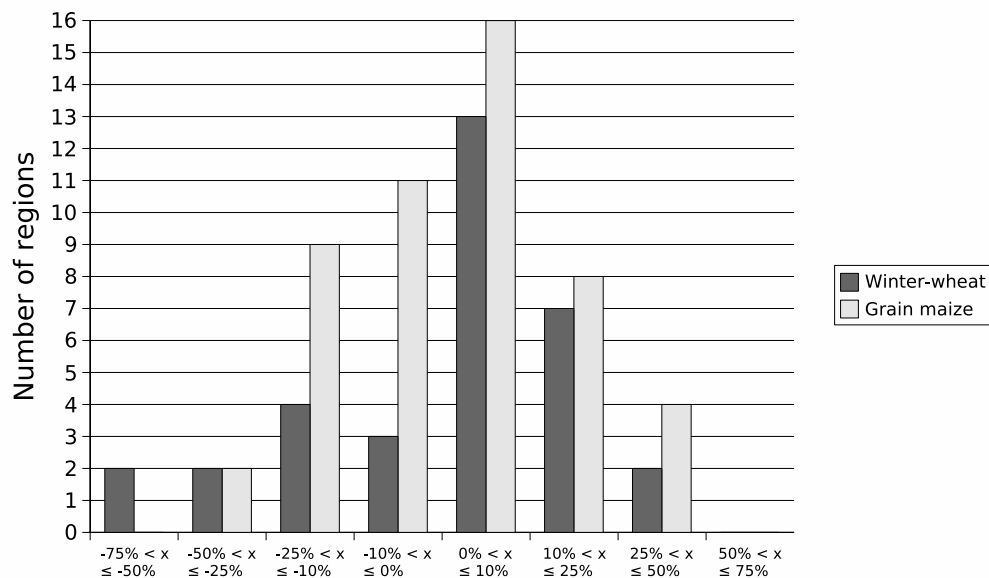


Figure 5.11: Normalised regression performance for winter-wheat and grain maize.

When the regression results at NUTS1 level are plotted as maps (figure 5.12A, page 113), it is clear that predictability of winter-wheat yield is limited mainly to regions in Spain and north-eastern Germany. The majority of regions shows an lower residual error in the regression with EUROSTAT yields for the EnKF experiment, but for some regions the residual error increases compared to the classic experiment. Notably for the large central region in Spain the error increases. At NUTS2 level (Figure 5.12B), results are similar for Spain while no statistical data for Germany exists at NUTS2 level. Furthermore, a relationship could be established at NUTS2 level for some regions in southern Italy, southern France as well as Sardinia and Corsica.

The overall ability of the system to predict yield of grain maize is considerably better compared to winter-wheat (Table 5.3, page 120). A relationship could be established for 50 regions out of 84 regions, a score of 60%. Improvement in performance by the results of the EnKF experiment is however

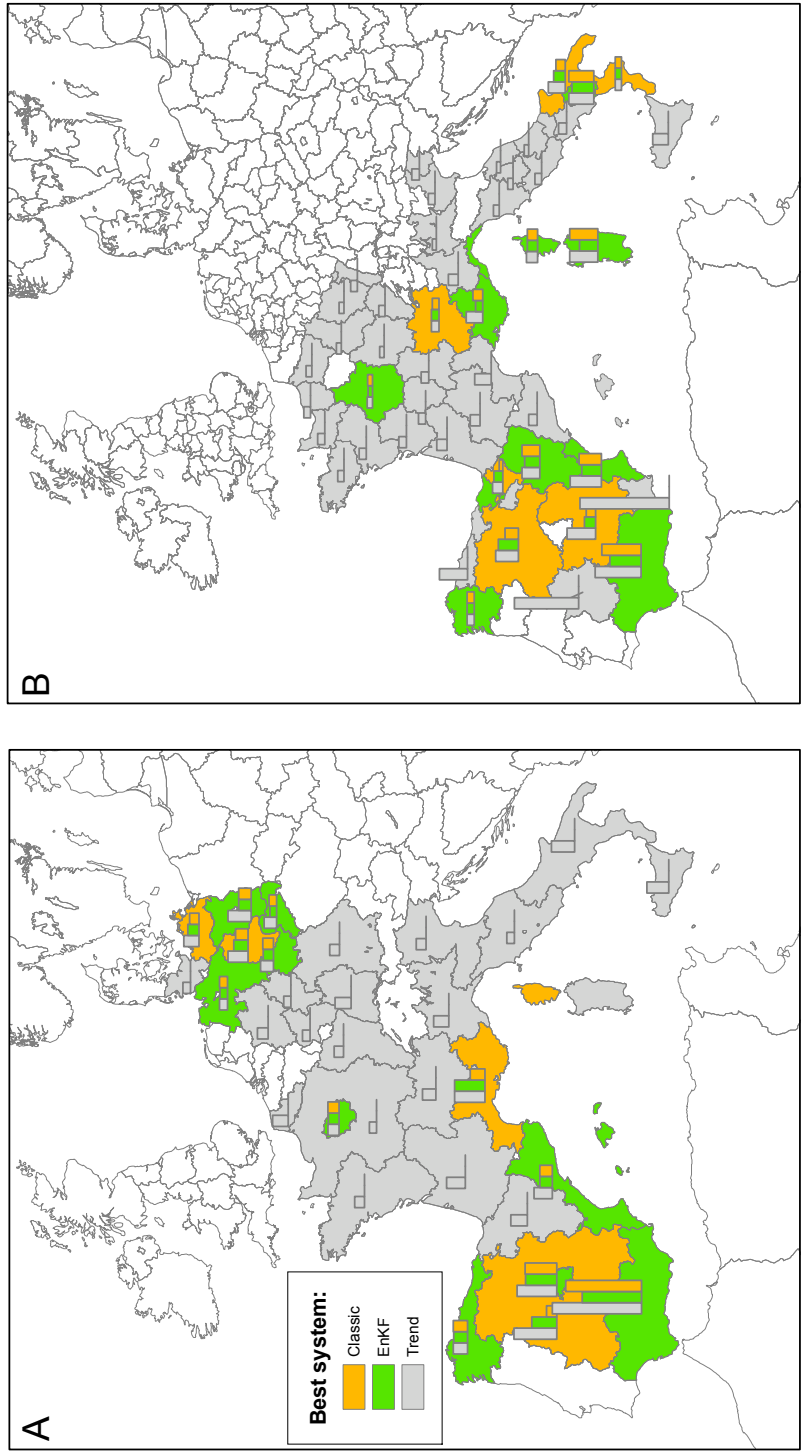


Figure 5.12: Spatial distribution of regression results for NUTS1 (A) and NUTS2 (B) regions for winter-wheat. Bar charts in the maps give a relative indication of the residual error on the regression between EUROSTAT statistics for the trend-only, the EnKF experiment and the classic experiment. Regions are coloured according to the best performing system.

less evident: A relationship could be established for 42 regions based on the results from the EnKF experiment and in 44 regions for the classic experiment. Out of the 50 regions, in 28 regions the residual error on the regression model was lower for the EnKF experiment compared to the classic experiment.

At national level, relationships could be found for Germany (DE), France (FR) and Spain (ES) but only in the case of Spain was the residual error from the EnKF experiment smaller than the residual error from the classic experiment. The normalised yield forecasting performance (Figure 5.11) confirms that the improvement in yield forecasting performance is small.

The spatial distribution of the results for NUTS1 regions (Figure 5.13A, page 115) shows that results improve in north-eastern Germany as well as for some regions in Spain, although the overall predictability of yield in Spain is limited to a few regions. France, Italy and the rest of Germany show no clear patterns and regions with lower or higher residual error seem randomly distributed over the study area. At NUTS2 level (Figure 5.13B), the results for France indicate that for most regions the residual error using results from the classic experiment were lower than the EnKF experiment. For Italy and Spain the predictability is limited to a few regions although these regions generally show lower residual error for the EnKF experiment.

## 5.6 Discussion and conclusions

Uncertainty in spatial and temporal distribution of rainfall in regional crop yield simulations comprises a major fraction of the error on crop model simulation results. This is particularly the case for climates marginal to crop growth where uncertainty in rainfall estimates can have large effect on the simulation of the final biomass production. In this paper, we present the application of an ensemble Kalman filter for assimilating coarse resolution soil moisture estimates in a distributed crop growth model in order to compensate the effect of uncertainty in the rainfall. We evaluated our results with regard to the EnKF filter innovations and the relationship with yield statistics on administrative regions.

Our results demonstrate that the assumptions underlying the EnKF are not entirely fulfilled, given that the normalised innovations are not Gaussian and that the resulting spatial and temporal patterns show a clear correlation structure. This indicates that the innovations made to the model water balance are not the result of random noise, but are the result of systematic deviations in the model dynamics and/or a poorly known error structure in the satellite-derived SWI. A small cases study showed that differences in the mean of the climatology of the forecasted (WOFOST) and observed (SWI) soil moisture



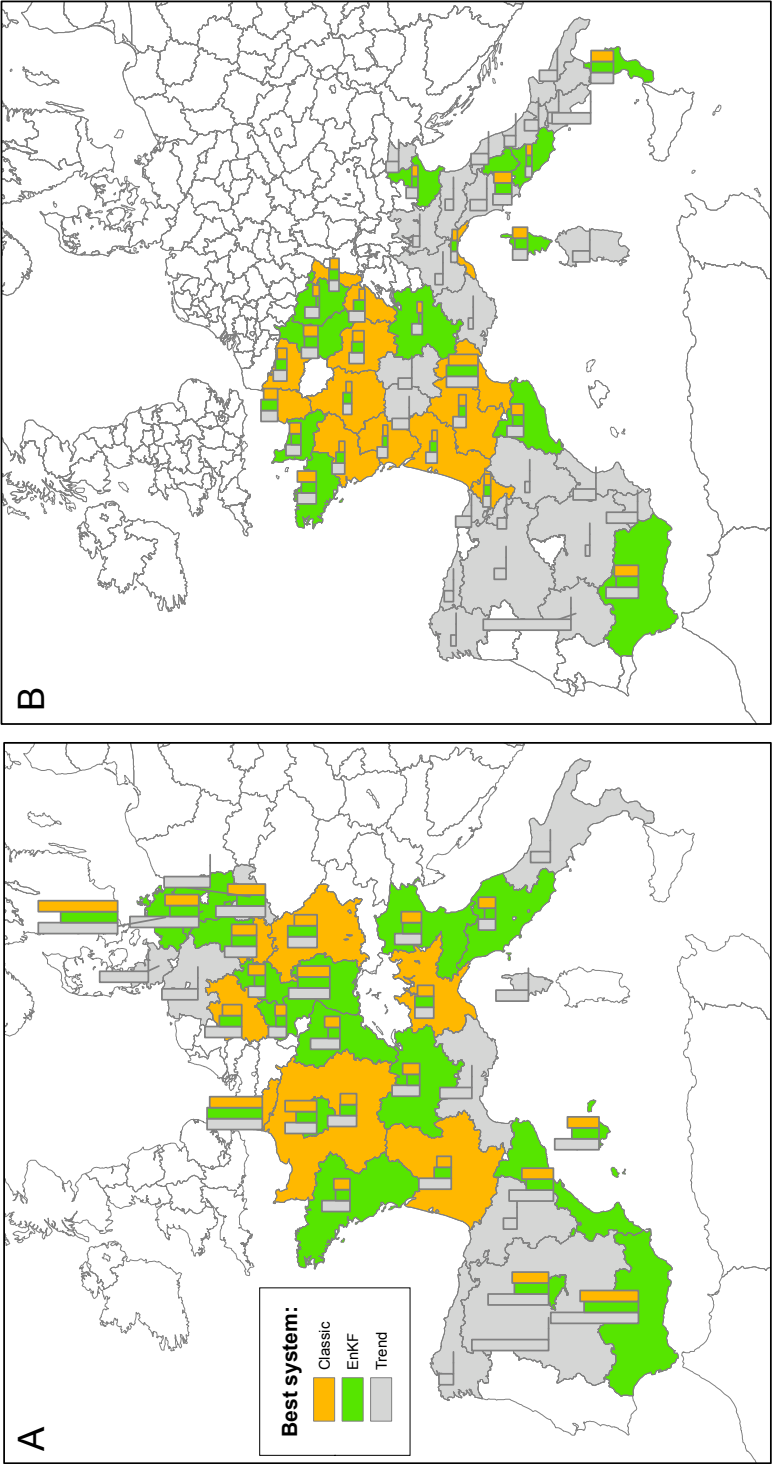


Figure 5.13: Spatial distribution of regression results for NUTS1 (A) and NUTS2 (B) regions for grain maize. Bar charts in the maps give a relative indication of the residual error on the regression between EUROSTAT statistics for the trend-only, the EnKF experiment and the classic experiment. Regions are coloured according to the best performing system.

can (at least partly) explain the non-zero mean in the distribution of the normalised innovations. The excessive spread in the distribution of normalised innovations indicates that the sum of the variances on observations and forecasts ( $P_e + R_e$ ) is underestimated. In hindsight, this is not surprising, since model error is assumed to be due to only precipitation forcing and observation error is assumed to be due to only instrument noise. It is therefore likely that both  $P_e$  and  $R_e$  are to blame and these results clearly indicate that additional sources of error need to be included in the simulations and observations.

The temporal patterns in the innovations for winter-wheat simulations show that the innovations in the beginning of the growing season are close to zero for most grids (Figure 5.7, page 108) indicating that the soil moisture levels compare well with SWI estimates. In contrast, for grain maize simulations innovations in the beginning of the growing season are strongly negative (Figure 5.6, page 107). Given that both simulations have the same point of departure with regard to initial soil moisture (sampled from a random variable with mean half way wilting point and field capacity) this could well be an initialisation problem which points out that the initial conditions are representative for winter-wheat simulations which are already starting in Winter, but not for the grain maize simulations starting several months later. The EnKF is thus correcting the too wet conditions for the grain maize simulations, but needs several assimilation steps to do so. A solution to this problem can be to increase the initialisation period for the water balance for summer crops.

In the second part of the growing season, filter innovations for grain maize simulations are generally positive, while filter innovations for winter-wheat simulations are first negative and then become positive. Filter innovations thus tend to get positive during the warm and relatively dry Summer months when the soil moisture level during crop simulation becomes too low and the EnKF starts to correct for it. An explanation for the effect might be that the crop types in the current system are too drought tolerant and are able to draw water from the soil up to very low soil moisture levels. This hypothesis is supported by earlier work by Nieuwenhuis et al. (1998) who compared satellite estimates of crop evapotranspiration with WOFOST simulated crop evapotranspiration in southern Spain. The WOFOST simulations sustained high evapotranspiration levels up to the point where soil moisture became limiting which resulted in a strong decrease in crop evapotranspiration. In contrast, the satellite estimates showed a much more gradual decline in crop evapotranspiration. This model behaviour could be altered by changing model parameters to make the crop simulations less drought tolerant. The EnKF could then be re-run to see if filter innovations improve.

With regard to the relationship with crop yield statistics, our results demonstrate that the assimilation of SWI has clearly improved the relationship

with crop yield statistics for winter-wheat for the majority of regions (66%) where a relationship could be established. For grain maize the improvement is less evident because improved relationships could only be found for 56% of the regions. At national level, the results of the regression only improved for Spain, but not for Germany, France and Italy. Although the results at national level are somewhat disappointing, it is encouraging that the results do improve for Spain where crop production is most affected by water limitations and thus the potential for improvement using SWI is greatest.

A possible explanation for the relatively poor results of the EnKF experiment for prediction of grain maize is that grain maize is often partially irrigated in southern areas, which is not included in the model. For example, the average yield of grain maize in Spain over the period 1992–2000 is 8.12 ton/ha compared to 2.38 ton/ha for wheat, clearly showing the effect of irrigation of grain maize. Nevertheless, for many areas relationships can be established between EUROSTAT yield statistics and WOFOST water-limited biomass, showing that grain maize is not irrigated to an extent where yield becomes totally independent of rainfall. However, the effect of irrigation is probably not reflected in SWI given the difference in size between the scatterometer footprint and the size of most irrigation systems and this might explain why the results from the EnKF experiment cannot ‘add’ much information compared to the results of the classic experiment.

The overall conclusion that can be drawn from this study is that the assimilation of SWI in the water balance of the crop growth model has a beneficial effect on the overall performance of the yield forecasting system. Although the present results are too limited in scope to claim generality, they are encouraging given that the quality of the SWI data is relatively poor over Europe. Further analyses of the current results will need to focus on the prediction of total crop production (area  $\times$  yield) as the current analyses does not take this into account. Moreover, the precocity of the forecasts needs to be analysed in order to see if the timeliness of the forecast can be improved. Finally, the experiment needs to be repeated for other crop types and regions to determine if similar results can be obtained.

Table 5.2: Residual error (% of mean yield) on the relationship between regional simulated biomass values and the EUROSTAT regional crop yield statistics for winter-wheat.

NUTS code	Trend-only	ENKF		CLASSIC	
		Biomass	Storage	Biomass	Storage
DE	3.43	2.93	.	2.46	.
DE1	.	.	.	.	.
DE2	.	.	.	.	.
DE4	12.62	6.86	9.92	6.89	12.62
DE5	.	.	.	.	.
DE6	.	.	.	.	.
DE7	.	.	.	.	.
DE8	8.16	5.92	7.22	4.85	.
DE9	4.23	3.92	.	.	.
DEA	.	.	.	.	.
DEB	.	.	.	.	.
DED	6.8	4.18	3.77	4.19	4.4
DEE	10.82	7.68	.	6.75	.
DEF	.	.	.	.	.
DEG	6.9	5.54	.	5.78	6.54
ES	20.57	6.66	8.58	8.23	9.08
ES1	7.7	7.32	.	7.52	.
ES11	7.58	7.47	.	7.55	.
ES12	.	.	.	.	.
ES13	.	.	.	.	.
ES2	.	.	.	.	.
ES21	13.31	9.86	10.8	.	.
ES22	11.06	9.72	9.58	3.96	4.41
ES23	.	.	.	.	.
ES24	18.79	.	16.09	.	.
ES3	21.46	.	16.93	.	17.2
ES4	23.08	14.28	13.59	5.66	5.51
ES41	24.22	21.4	21.81	14.08	14.41
ES42	30.62	16	12	10.23	12.56
ES43	.	.	.	.	.
ES5	9.81	6.73	8.14	6.89	6.78
ES51	.	.	.	.	.
ES52	33.08	20.99	24.11	24.04	23.48

*Continued on next page*

Table 5.2 – continued from previous page

	ES53	.	.	.	.	.
	ES6	48.12	31.89	34.61	42.43	40.86
	ES61	48.72	33.2	35.91	43.13	41.89
	ES62	.	.	.	.	.
FR		.	.	.	.	.
	FR1	5.84	.	5.66	.	.
	FR2	.	.	.	.	.
	FR21	.	.	.	.	.
	FR22	.	.	.	.	.
	FR23	.	.	.	.	.
	FR24	5.46	.	4.96	.	5.01
	FR25	.	.	.	.	.
	FR26	.	.	.	.	.
	FR3	.	.	.	.	.
	FR4	.	.	.	.	.
	FR41	.	.	.	.	.
	FR42	.	.	.	.	.
	FR43	.	.	.	.	.
	FR5	.	.	.	.	.
	FR51	.	.	.	.	.
	FR52	.	.	.	.	.
	FR53	.	.	.	.	.
	FR6	.	.	.	.	.
	FR61	.	.	.	.	.
	FR62	.	.	.	.	.
	FR63	.	.	.	.	.
	FR7	.	.	.	.	.
	FR71	7.91	.	.	.	6.76
	FR72	.	.	.	.	.
	FR8	16.29	.	.	7.99	.
	FR81	.	.	.	.	.
	FR82	17.18	7.59	9.35	10.38	10.31
	FR83	11.41	.	10.64	10.64	.
IT		.	.	.	.	.
	ITC	.	.	.	.	.
	ITC1	.	.	.	.	.
	ITC3	21.9	.	19.21	.	.

Continued on next page

Table 5.2 – continued from previous page

	ITC4	.	.	.	.	.
ITD		.	.	.	.	.
	ITD3	.	.	.	.	.
	ITD4	.	.	.	.	.
	ITD5	.	.	4.37	.	.
ITE		.	.	.	.	.
	ITE1	.	.	.	.	.
	ITE2	.	.	.	.	.
	ITE3	.	.	.	.	.
	ITE4	.	.	.	.	.
ITF		.	.	.	.	.
	ITF1	.	.	.	.	.
	ITF2	.	.	.	.	.
	ITF3	.	.	.	.	.
	ITF4	18.01	.	12.37	9.89	13.8
	ITF5	26.24	22.78	.	.	.
	ITF6	6.65	6.69	.	.	.
ITG		.	.	.	.	.
	ITG1	.	.	.	.	.
	ITG2	29.81	19.19	.	.	.

Table 5.3: Residual error (% of mean yield) on the relationship between regional simulated biomass values and the EUROSTAT regional crop yield statistics for grain maize.

NUTS code	Trend-only	ENKF		CLASSIC	
		Biomass	Storage	Biomass	Storage
DE	5.35	3.89	.	2.95	4.67
DE1	7.58	5.9	7.07	5.95	.
DE2	5.43	.	.	4.23	.
DE4	12.72	5.37	9.69	6.22	.
DE7	3.15	.	2.08	.	.
DE8	14.56	10.48	.	.	.
DE9	.	.	.	.	.
DEA	6.82	4.15	4.92	3.6	3.62

Continued on next page

Table 5.3 – continued from previous page

ES	DEB	3.26	1.91	2.59	.	2.03
	DED	.	.	.	.	.
	DEE	9.16	5.24	.	6.98	.
	DEF	.	.	.	.	.
	DEG	5.89	.	4.63	.	4.57
	ES1	7.11	6.02	.	6.23	.
	ES11	.	.	.	.	.
	ES12	.	.	.	.	.
	ES2	.	.	.	.	.
	ES21	.	.	.	.	.
	ES22	4.09	.	3.55	3.4	3.42
	ES23	.	.	.	.	.
	ES24	.	.	.	.	.
	ES3	11.16	6.33	6.35	9.56	6.73
	ES4	.	.	.	.	.
	ES41	.	.	.	.	.
	ES42	.	.	.	.	.
	ES43	.	.	.	.	.
	ES5	8.14	6.05	5.04	5.81	.
	ES51	8.6	.	5.53	6.31	6.97
	ES52	.	.	.	.	.
	ES6	16.16	10.04	14.36	10.76	14.76
	ES61	16.74	11.4	14.45	12.4	15.15
	ES62	.	.	.	.	.
FR	FR	3.9	2.92	3.69	2.03	3.14
	FR1	5.79	3.84	.	.	.
	FR2	5.38	3.1	5.07	3.06	.
	FR21	8.75	7.06	.	7.55	.
	FR22	7	5.7	.	4.91	.
	FR23	8.64	.	.	7.36	7.23
	FR24	4.4	.	.	2.89	.
	FR25	7.65	.	4.82	.	5.82
	FR26	7.52	6.23	.	5.77	.
	FR3	10.16	.	.	9.74	.
	FR4	5.37	2.19	4.68	2.84	4.45
	FR41	7.62	1.75	4.81	3.36	4.85

Continued on next page

Table 5.3 – continued from previous page

IT	FR42	5.15	.	.	4.79	.
	FR43	8.5	5.88	.	2.99	7.22
	FR5	5.21	.	2.65	2.97	3.52
	FR51	.	.	4.54	4.41	3.12
	FR52	9.65	7.75	.	.	.
	FR53	5.43	.	2.89	2.48	3.25
	FR6	6.04	4.41	3.16	3.12	2.73
	FR61	5.87	4.31	3.84	2.73	2.89
	FR62	6.82	5.06	3.95	3.93	3.94
	FR63	.	.	.	.	.
	FR7	5.04	2.37	.	3.1	4.01
	FR71	5.52	.	1.76	.	2.81
	FR72	.	.	.	.	.
	FR8	.	.	.	.	.
	FR81	16.34	.	.	15.29	.
	FR82	.	.	.	.	.
	FR83	7.58	6.59	.	.	.
	ITC	3.48	.	.	2.96	.
	ITC1	.	.	.	.	.
	ITC3	3.31	.	.	2.75	.
	ITC4	.	.	.	.	.
	ITD	4.97	3.47	.	3.72	.
	ITD3	6.15	3.17	5.3	3.33	5.87
	ITD4	.	.	.	.	.
	ITD5	.	.	.	.	.
	ITE	3.12	.	2.03	.	.
	ITE1	.	.	.	.	.
	ITE2	9.59	8.65	.	9.18	.
	ITE3	.	.	.	.	.
	ITE4	3.26	.	2.98	.	2.99
	ITF	.	.	.	.	.
	ITF1	.	.	.	.	.
	ITF2	.	.	.	.	.
	ITF3	.	.	.	.	.
	ITF4	.	.	.	.	.
	ITF5	.	.	.	.	.

Continued on next page



---

*Table 5.3 – continued from previous page*

---

ITG	ITF6	11.71	.	11.4	.	11.51
		.	.	.	.	.
	ITG1	.	.	.	.	.
	ITG2	.	.	.	.	.

---



# Chapter 6

## Conclusions

### 6.1 Introduction

The main objective of this thesis was to establish a basis for probabilistic crop growth modelling and remote sensing data assimilation for improved regional crop yield forecasting. Within this overall objective, the following specific research topics were identified that structure the approach:

- Exploring the uncertainties related to the spatial and temporal variability of the main meteorological forcings necessary for running a crop growth model namely temperature, radiation and precipitation. This research topic was elaborated in chapters 2 and 3;
- Modelling the uncertainty of precipitation input using a stochastic approach on a spatial and temporal scale consistent with the needs of regional crop growth modelling. This research topic was elaborated in chapter 4;
- Developing a probabilistic framework for crop growth modelling coupled to an ensemble Kalman filter for assimilation of remote sensing derived observations. This research topic was elaborated in chapter 5;
- Applying the developed probabilistic framework in a case study and demonstrating the improvements in the relationships between model output and crop yield statistics through the assimilation of soil moisture estimates. This research topic was elaborated in chapter 5.

This chapter will synthesise the main findings of the above and will reflect on related issues such as operational applicability, continuity requirements for satellite missions, computational efficiency and enhanced land cover data. Finally, suggestions for further research will be given.

## 6.2 Synthesis

In chapter 2 it was demonstrated that AVHRR-derived surface temperature can be applied as input into a spatially distributed crop growth model. Nevertheless, in hindsight it was gradually realised that the use of AVHRR derived temperature in an operational crop growth monitoring system is probably not a viable choice. First of all, its use poses a couple of operational difficulties such as incomplete time-series due to persistent cloud cover, necessary corrections for differences between air and surface temperature, systematic effects caused by orbital drift and the processing capacity and data volumes involved.

Secondly, it is unlikely that uncertainty in temperature is an important component in a distributed crop growth model, although the work described in chapter 2 is not conclusive on this aspect. The main reason is that temperature is measured at many locations and it can be interpolated fairly well because it has a long spatial correlation length and known relationships with altitude. Moreover, numerical weather prediction (NWP) models nowadays can provide accurate estimates of near-surface air temperature and have the advantage that long and consistent time-series are available.

Despite the negative outlook of the applicability of the work carried out in chapter 2, it was an important iteration step in updating the research approach. As a result, in chapter 3 the effect of uncertainty in radiation and precipitation on the crop growth model output was explored. In this chapter, the results obtained with the operational CGMS (which derives input from weather stations) is compared with results obtained from CGMS by using highly accurate precipitation and radiation inputs derived from ELDAS. The first conclusion that could be drawn from this work is that uncertainty in radiation and precipitation inputs do have a considerable influence on the simulation results at the level of individual  $50 \times 50$  km grids but that the influence gradually decreases when results are spatially aggregated to provincial and national level.

The second conclusion is related to the influence of sub-grid variability of precipitation and radiation. It was demonstrated that the spatially distributed simulation results at  $10 \times 10$  km scale almost linearly with the results at  $50 \times 50$  km using averaged rainfall and radiation. This means that the precipitation and radiation forcings can be averaged over the  $50 \times 50$  grid box and used as input in the crop growth model without running into aggregation problems related to non-linearity. This is a particularly important finding in relation to the use of the scatterometer derived SWI, because the scatterometer measurements will also average over the footprint of the sensor.

Finally, it was concluded that uncertainty in the precipitation and radiation fields in CGMS had limited influence on the crop yield forecasts at national

level for France and Germany, indicating that the CGMS forecasts at this level of aggregation are fairly robust.

The results presented in chapter 3 prove that the uncertainty in radiation and precipitation forcings is an important aspect which needs to be taken into account when interpreting results of CGMS simulations, particularly for individual  $50 \times 50$  grid boxes or lower administrative regions. However, chapter 3 did not provide a handle on how to operationally quantify and visualise this uncertainty due to input forcings. This aspect is treated in chapter 4 where a method was developed and applied to create ensembles of precipitation inputs.

The priority for precipitation instead of radiation was made in analogy with results from the land surface modelling community where precipitation forcing is generally acknowledged to be the key variable (section 4.1, page 53). Moreover, the effect of uncertainty in precipitation forcings was found to be dominant over radiation forcings (table 3.3 on page 43 and table 3.4 on page 46). Finally, from an operational aspect it can be expected that radiation inputs in CGMS can be readily improved by using output from NWP models (Meetschen et al., 2004), while this it is unclear whether NWP derived precipitation estimates are an improvement over the estimates currently derived by CGMS.

In chapter 4 a method is presented to create ensembles of equiprobable realisations of precipitation fields at a temporal and spatial scale which is consistent with the requirements for crop model applications that target large area crop yield prediction. First of all, it is argued based on theoretical and practical grounds that the current spatial and temporal resolution of CGMS is sufficient for large area crop yield prediction. Secondly, an approach is developed where the CGMS precipitation input field is treated as a first guess of the underlying true precipitation field (assumed to be the ELDAS precipitation dataset). The error model was built by calculating the residuals between the CGMS precipitation fields and the ELDAS precipitation fields for specific intervals of CGMS precipitation and by converting the resulting distributions to standard normality. A second, independent model took care of generating precipitation events in case CGMS predicted zero precipitation. Realisations of the error model were generated by adding back transformed simulated residuals to the CGMS precipitation data and the characteristics were compared with the reference precipitation fields.

The main conclusion that can be drawn is that the precipitation realisations that were generated have favourable characteristics for regional crop growth modelling given that the deviations from the target characteristics (shifting of 100<sup>th</sup> percentile, failure to reproduce prolonged dry spells) are of minor importance for this particular application. Nevertheless, improvements in the en-

semble generator might be achieved by calibrating the system for different seasons and regions separately. For example, the failure to reproduce prolonged dry spells in Spain is a clear indication that the probability of precipitation when CGMS predicts no precipitation is overestimated for South-Spain. This could be improved if calibrations were carried out per climatic zone and/or season (Metzger et al., 2005).

An important characteristic of the approach is that the ensemble generator was calibrated on the mean ELDAS precipitation per grid cell. Besides correcting any biases in the CGMS precipitation, the ensemble generator therefore also takes care of the translation from CGMS precipitation to grid cell mean precipitation which should be reflected in the ensemble mean. In chapter 3 it was shown that the output of WOFOST scales linearly when averaging precipitation and radiation inputs. Therefore, the ensemble mean should present an unbiased estimate of the average rainfall per CGMS grid cell.

The impact of the precipitation realisations on the crop yield forecast was demonstrated for a NUTS1 region in France and caused a total spread in the yield forecast of around 0.65 ton/ha. Moreover, density plots of the yield forecast ensemble showed that the shape of the yield forecast ensemble was non-Gaussian and propagated in a non-linear way through the growing season. This last aspect indicates that the uncertainty on the yield forecast is a result of complex non-linear processes and thus cannot be captured easily through other methods such as for example through the uncertainty on the forecasting regression model.

Finally, in chapter 5 the WOFOST crop growth model was cast into a probabilistic framework and coupled to an ensemble Kalman filter for sequential assimilation of satellite observations. This system was applied for four countries in Europe (Germany, France, Spain and Italy) over the period 1992–2000 and coarse resolution satellite microwave sensor derived soil moisture estimates were assimilated for correcting errors in the water balance of the model during the crop simulation caused by uncertainty in rainfall or model initialisation. The ultimate goal of this work was to demonstrate that assimilation of remote sensing derived soil moisture observations leads to improved relationships between model output and crop yield statistics for administrative regions at different administrative levels. Additionally, the innovations of the ensemble Kalman filter can provide some diagnostics that can help to trace deficiencies in the model and/or observations.

The most important conclusion that can be drawn from this work is that the assimilation of soil moisture estimates (SWI) clearly improved the relationship with crop yield statistics for winter-wheat for the majority of regions (66%) where a relationship could be established (i.e. better than the trend only). For grain maize the improvement is less evident because improved relationships

could only be found for 56% of the regions. At national level, the results of the regression only improved for Spain, but not for Germany, France and Italy. Although the results at national level are somewhat disappointing, it is encouraging that the results do improve for Spain where crop production is most affected by water limitations and thus the potential for improvement using SWI is greatest.

A clear limitation of the current analysis is that only the ensemble average was used, thereby excluding important information about uncertainty in the crop yield forecast which was shown to be important for some regions (section 4.4.4). For operational application of probabilistic crop yield forecasting this is highly undesirable, because an important part of the information provided is not utilised and communicated. However, an important bottleneck in using such ensemble information is that the current generation of tools for analysing CGMS output and making crop yield forecasts, is lacking the ability to process, analyse and visualise ensemble based data.

With regard to the performance of the ensemble Kalman filter, it can be concluded that the assumptions underlying the EnKF are not entirely fulfilled, given that the normalised innovations are not Gaussian and that the resulting spatial and temporal patterns show a clear correlation structure. The excessive spread in the distribution of normalised innovations indicates that the sum of the variances on observations and forecasts is underestimated. It was argued that the errors on both the model and the observations are underestimated.

With regard to the observed soil moisture, better modelling and validation of the SWI product may lead to a better understanding and estimates of the error on the SWI. Moreover, it is expected that the accuracy of the SWI derived from the scatterometer onboard METOP will be considerable better due to METOP's improved revisit pattern compared to ERS1/2 (Pellarin et al., 2006). With regard to the modelled soil moisture, additional sources of uncertainty have to be included in the WOFOST simulations. For this purpose, the probabilistic weather inputs could be extended to include radiation and temperature as these variables will influence the evapotranspiration and plant growth rates and consequently add additional variability to the soil moisture state. Additionally, a Gaussian noise term could be added to the model states during simulation in order to take into account unknown errors or deficiencies in the model structure itself.

## 6.3 Reflection

The innovative aspect of the presented approach is the use of the probabilistic approaches and data assimilation for crop growth models and their applica-

tion at regional scale. Within this approach the ensemble is the centrepiece in two ways: first of all it supports the crop growth modelling system enabling a probabilistic approach and data assimilation. Secondly, it plays an important role in the generation of the final product through statistical post-processing, visualisation and finally in the decision making process. Although this last aspect was only marginally treated within this thesis, the potential applications that come within reach through such an approach are beyond what is commonly available in crop yield forecasting systems.

In section 1.4 three operational constraints were identified: algorithms should be applicable at regional scale, satellite data continuity should be warranted and local ancillary data should not be used. The first operational constraint mainly applies to chapters 4 and 5 where algorithms were developed and applied that involve some calibration. One example is the use of the ELDAS precipitation dataset in order to calibrate the error distributions in the model. Although ELDAS is not available for regions outside Europe, other methods exist to calibrate such tools and derive the error distributions (see section 4.1). A second example is the ‘calibration’ of the normalized innovations through the appropriate error structure in the observations and simulations. However, this calibration can be carried by making an educated guess about the appropriate error structure and rerunning the simulations until the normalized innovations approximate a Gaussian distribution.

The second operational constraint was addressed in section 1.3 (page 6) where it was concluded that the operational polar-orbiting and geostationary satellite missions provide the best warranties for satellite data continuity. Nevertheless, the majority of instruments onboard these satellites is not tailored for crop monitoring purposes. For example, the spatial resolution of the optical instruments is too low to monitor canopy development for specific crop types. Requirements for a crop monitoring mission would be to obtain frequent (i.e. 2–3 days revisit interval) optical observations with a spatial resolution that matches the scale of the landscape (50 m) over large areas (continents). This cannot be accomplished with a single polar-orbiting satellite and therefore a constellation of satellites will be necessary. However, the funding required for such a continued mission and the corresponding ground segment for near realtime data delivery will be enormous.

Finally, the third operational constraint was addressed by only using land cover products which are available over the entire study domain or even globally (e.g. Global Land Cover 2000 (Bartholomé and Belward, 2005)). However, these land cover products were not designed for crop related applications because the nomenclature (no specific crop types) and update frequency (three monthly at best) are not appropriate. In the ideal situation, the satellite constellation envisaged in the previous paragraph can be used to obtain



within-season maps of specific crop types. However, given the unfeasibility of such a system, an intermediate solution could be to create vegetation continuous fields (Hansen et al., 2003) for specific crop types based on MODIS 250m or MERIS 300m data.

Given that the operational constraints have been met, it can be concluded that the developed approach can potentially be implemented within the European MARS system. From a practical point of view, some software development will be necessary in order to improve the computational efficiency of the existing code and to include additional steps (such as ensemble generation) in the existing processing chain. The experience with the current system has shown that, in terms of processing requirements, the limiting factor is not the running of the coupled WOFOST–ensemble Kalman filter, but it is the database I/O related to retrieving the meteorological ensemble forcings (e.g. the table storing 15 years of ensemble meteorological forcings contains nearly  $1.3 \cdot 10^9$  records).

Database retrieval is necessary because ensemble generation is too computationally intensive to carry out on-the-fly, so precomputed ensembles were used. Although this is currently constraining the processing speed of the application it was already concluded in section 4.5 that large gains in ensemble generation speed could be obtained relatively easy. Moreover, the whole CGMS processing chain is well suited for distributing over multiple processing nodes in a grid or a cluster, particularly if the central database is clustered as well (Dorigo et al., 2006). Additional to adaptations for processing requirements, many tools for visualisation and data analyses will need to be adapted as well, in order to benefit from the additional information that the ensemble can provide. Meanwhile, the ensemble average could be used as a temporary solution.

Besides the implementation in the European MARS system, the methodology has the potential to provide improved crop yield indicators for crop yield forecasting in many areas with major agricultural production of rain-fed crops. These areas are, for example, the North China plain, Russia and Ukraine, Central Asia, the Great Plains of North America, Australia and parts of South America.

Another application field would be the implementation of the developed approach within the framework of the Global Information and Early Warning System on Food Security (GIEWS) from the Food and Agriculture Organisation (FAO). From a practical point of view, the tools and data sources are available to operate such a system as is demonstrated by the Joint Research Centre's Global Water Satisfaction Index (Nieuwenhuis et al., 2006) and the Crop Explorer operated by the United States Department of Agricultural (USDA, 2007). Within such systems, the assimilation of SWI could be an

important tool to compensate for the uncertainty in rainfall, particularly for data scarce areas of the globe such as Africa (Thorne et al., 2001).

However, from a thematic point of view it is doubtful whether a fairly technological innovation alone, as the one presented in this thesis, can make a true advancement in crop and food security monitoring for GIEWS. Currently there are 33 countries listed in GIEWS (situation 30 May 2007) where food security is an issue (FAO, 2007). Out of these 33 countries, there are only five where food security problems are mainly related to weather events (drought, flooding, cold, heat). In the other cases, economic problems, household income, civil strife, refugees or armed conflicts are the main origin of food insecurity. An agrometeorologic system based on weather as the explaining factor in crop yield, will thus only be useful for food security monitoring in a minority of cases.

This conclusion is aggravated by the fact that crop yield forecasting usually takes place by carrying out a statistical analysis between model output and historic time-series of reported crop yield. This approach assumes a stable economic situation which is often not the case in areas with food security problems. In such situations, the statistical analysis becomes the weakest link in the crop yield forecasting chain and it is therefore likely that improved crop yield indicators (as provided by the approach in this thesis) will not improve forecast skill. This situation can only be improved when forecasting models are developed that include spatially distributed socio-economic data to explain the anthropogenic influences on regional crop yield and production and their impact on food security.

## 6.4 Priorities and further research

The following priorities were identified for further development of CGMS:

- Testing and further developing the ensemble Kalman filter approach, leading to improved simulation of drought stress and crop yield prediction;
- Improving estimates of within-season sowing date and sowing date variability, leading to improved simulation of crop phenological development and crop yield prediction;
- Testing the applicability of numerical weather prediction model derived weather variables in CGMS, leading to global application of CGMS;

- Communicating and analysing ensemble-based indicators and crop yield forecasts, leading to improved understanding and use of probabilistic CGMS results with crop analysts and decision makers.

#### **Testing, further developing and implementing the ensemble Kalman filter approach**

The results presented in this thesis demonstrate that further research is needed on the ensemble Kalman filter because the model and observation errors were systematically underestimated. Moreover, the presented approach needs further testing for other crops and other areas in order to verify the results that were obtained so far and to gain confidence in their general applicability. Finally, software developments are necessary to gain computational efficiency and implement the experimental code in an operational framework.

#### **Improving estimates of within-season sowing date and sowing date variability**

In section 1.1 the lack of information about the within-season sowing dates and sowing date variability within a CGMS grid box, was already identified as one of the key uncertainties related to the regional application of WOFOST. Two approaches are envisaged for obtaining within-season sowing dates. In the short term it should be investigated if statistical relationships can be found between vegetation phenological products (not crop specific) derived from AVHRR/VGT/MODIS and phenological observations for specific crops. Such relationships might exist for regions with clearly dominant crops and can be used to update the CGMS crop calendar. Moreover, the ensemble approach is an excellent tool to represent the uncertainty in the retrieved sowing date.

In the longer term, it should be investigated if vegetation continuous fields can be derived for specific crops. For example, based on MODIS 250m and MERIS 300m observations. These vegetation continuous fields can then be used to select pixels with a high percentage of a single crop type. Next, for these pixels a time-series of satellite observations can be derived that describe the canopy development during the vegetative phase. The CGMS sowing date can then be optimised in order to match the observed canopy development. Variability in sowing dates can then be estimated by comparing the retrieved sowing date for clusters of pixels. A drawback of this second approach is that it relies on observations from satellite missions that do not warrant data continuity.

**Testing the applicability of numerical weather prediction model derived meteorological variables in CGMS**

A bottleneck in the implementation of CGMS for other areas is the necessity to have meteorological observations from weather stations in order to derive interpolated meteorological fields. However, long and consistent time-series are already available globally from numerical weather prediction models that could potentially be used to implement CGMS for areas where access to ground meteorological information is difficult.

However, currently it is unclear how limitations in accuracy of NWP-derived meteorological variables influence the crop simulation model output and the yield forecast. Therefore, a sensitivity analysis is necessary for areas where both sources of meteorological variable are available to determine the sensitivity and the influence on the crop yield forecasting performance.

**Communicating and analysing ensemble-based indicators and crop yield forecasts**

The use of ensemble-based indicators and crop yield forecasts provides additional information to crop analysts and decision makers, but also adds complexity to the products that CGMS provides. Therefore, research is necessary on the cognitive aspects of CGMS ensemble-based results so that the information can be conveyed efficiently and succinctly to the respective users. Given the experience with ensemble based modelling that exists in the meteorological community, a review is necessary to determine if similar approaches can be used for CGMS results as well.

## References

- Aggarwal, P. K. (1995). Uncertainties in crop, soil and weather inputs used in growth-models - implications for simulated outputs and their applications, *Agricultural Systems* **48**(3): 361–384.
- Bach, H. and Mauser, W. (2003). Methods and examples for remote sensing data assimilation in land surface process modeling, *IEEE Transactions on Geoscience and Remote Sensing* **41**(7): 1629–1637.
- Bartholomé, E. and Belward, A. (2005). GLC2000: a new approach to global land cover mapping from Earth observation data, *International Journal of Remote Sensing* **26**(9): 1959–1977.
- Bastiaanssen, W. G. M. and Ali, S. (2003). A new crop yield forecasting model based on satellite measurements applied across the Indus Basin, Pakistan, *Agriculture, Ecosystems and Environment* **94**(3): 321–340.
- Bates, B., Charles, S. and Hughes, J. (1998). Stochastic downscaling of numerical climate model simulations, *Environmental Modelling and Software* **13**(3-4): 325–331.
- Beyer, H., Costanzo, C. and Heinemann, D. (1996). Modifications of the heliosat procedure for irradiance estimates from satellite images, *Solar energy* **56**: 207–212.
- Bindi, M. and Maselli, F. (2001). Extension of crop model outputs over the land surface by the application of statistical and neural network techniques to topographical and satellite data, *Climate-Research* **16**(3): 237–246.
- Boegh, E., Thorsen, M., Butts, M. B., Hansen, S., Christiansen, J. S., Abrahamson, P., Hasager, C. B., Jensen, N. O., van der Keur, P., Refsgaard, J. C., Schelde, K., Soegaard, H. and Thomsen, A. (2004). Incorporating remote sensing data in physically based distributed agro-hydrological modelling, *Journal of Hydrology* **287**(1-4): 279–299.
- Boogaard, H., Eerens, H., Supit, I., Diepen, C. v., Piccard, I. and Kempeneers, P. (2002). Description of the MARS crop yield forecasting system (MCYFS), *Technical report*, Joint Research Centre.
- Bouman, B. A. M. (1994). A framework to deal with uncertainty in soil and management parameters in crop yield simulation: A case study for rice,

- Agricultural Systems* **46**(1): 1–17.
- Bouman, B. A. M. (1995). Crop modeling and remote-sensing for yield prediction, *Netherlands Journal of Agricultural Science* **43**(2): 143–161.
- Bouman, B., Keulen van, H., Laar van, H. and Rabbinge, R. (1996). The ‘School of de Wit’ crop growth simulation models: a pedigree and historical overview, *Agricultural Systems* **52**(2/3): 171–198.
- Burgers, G., Jan van Leeuwen, P and Evensen, G. (1998). Analysis scheme in the ensemble Kalman filter, *Monthly Weather Review* **126**(6): 1719–1724.
- Camacho de Coca, F, García-Haro, F. J. and Martínez, B. (2003). An operational strategy for retrieval of vegetation products from SEVIRI & AVHRR-3 data, in EUMETSAT (ed.), *Proceedings of the LSA-SAF training workshop (2002)*, Vol. EUM P38.
- Carbone, G. (1993). Consideration of meteorological time-series in estimating regional-scale crop yield, *Journal of Climate* **6**(8): 1607–1615.
- Carbone, G. J., Kiechle, W., Locke, C., Mearns, L. O., McDaniel, L. and Downton, M. W. (2003). Response of soybean and sorghum to varying spatial scales of climate change scenarios in the southeastern United States, *Climatic Change* **60**(1 - 2): 73–98.
- Carpenter, T. M. and Georgakakos, K. P. (2004). Impacts of parametric and radar rainfall uncertainty on the ensemble streamflow simulations of a distributed hydrologic model, *Journal of Hydrology* **298**(1-4): 202–221.
- Ceballos, A., Scipal, K., Wagner, W. and Martinez-Fernandez, J. (2005). Validation of ERS scatterometer-derived soil moisture data in the central part of the Duero Basin, Spain, *Hydrological Processes* **19**(8): 1549–1566.
- Challinor, A. J., Slingo, J. M., Wheeler, T. R., Craufurd, P. Q. and Grimes, D. I. F. (2003). Toward a combined seasonal weather and crop productivity forecasting system: Determination of the working spatial scale, *Journal of Applied Meteorology* **42**(2): 175–192.
- Challinor, A. J., Wheeler, T. R., Craufurd, P. Q., Slingo, J. M. and Grimes, D. I. F. (2004). Design and optimisation of a large-area process-based model for annual crops, *Agricultural and Forest Meteorology* **124**(1-2): 99–120.
- Charles, S., Bates, B., Smith, I. and Hughes, J. (2004). Statistical downscaling of daily precipitation from observed and modelled atmospheric fields, *Hydrological Processes* **18**(8): 1373–1394.
- Chaubey, I., Haan, C. T., Grunwald, S. and Salisbury, J. M. (1999). Uncertainty in the model parameters due to spatial variability of rainfall, *Journal of Hydrology* **220**(1-2): 48–61.
- Cherchali, S., Amram, O. and Flouzat, G. (2000). Retrieval of temporal profiles of reflectances from simulated and real NOAA-AVHRR data over heterogeneous landscapes, *International Journal of Remote Sensing* **21**(4): 753.
- Clark, M., Gangopadhyay, S., Hay, L., Rajagopalan, B. and Wilby, R. (2004).

- The Schaake shuffle: A method for reconstructing space-time variability in forecasted precipitation and temperature fields, *Journal of Hydrometeorology* **5**(1): 243–262.
- Council of the European Community (1988). Council Decision of 26 september 1988 adopting a pilot project on remote sensing applied to agricultural statistics, *Official Journal of the European Union* **L273**: 12–17.
- Courault, D., Seguin, B. and Oliosio, A. (2005). Review on estimation of evapotranspiration from remote sensing data: From empirical to numerical modeling approaches, *Irrigation and Drainage Systems* **19**(3 - 4): 223–249.
- Crow, W. T. (2003). Correcting land surface model predictions for the impact of temporally sparse rainfall rate measurements using an ensemble Kalman filter and surface brightness temperature observations, *Journal of Hydrometeorology* **4**(5): 960–973.
- Crow, W. T. and Wood, E. F. (2003). The assimilation of remotely sensed soil brightness temperature imagery into a land surface model using ensemble Kalman filtering: a case study based on ESTAR measurements during SGP97, *Advances in Water Resources* **26**(2): 137–149.
- De Wit, A. (1999). The application of a genetic algorithm for crop model steering using NOAA-AVHRR data, in G. Cecchi, E. Engman and E. Zilioli (eds), *Remote sensing for earth science, ocean, and sea ice applications*, Vol. 3868, Bellingham WA (USA), SPIE, Florence, pp. 167–181.
- Deutsch, C. and Journel, A. G. (1998). *GSLIB Geostatistical Software Library and User's Guide*, 2nd edition, Oxford University press, New York.
- Diepen, C.A., v. (1992). An agrometeorological model to monitor the crop state on a regional scale in the European Community: concept, implementation and first operational outputs., in F. Toselli and J. Meyer-Roux (eds), *Conference on application of remote sensing to agricultural statistics*, Vol. EUR 14262 EN, Office for Official publications of the EU, Belgirate, Italy, pp. 269–277.
- Diepen, C.A., v., Wal, T.A., v. d. and Boogaard, H. (1998). Deterministic crop growth modelling fundamentals and application for regional crop state monitoring and yield forecasting, in J. Dallemard and V. Perdigao (eds), *PHARE multi-country environment programme, MARS and environmental related applications (MERA) project*, Vol. EUR 18050 EN, Office for Official publications of the EU, Ispra, pp. 201–227.
- Diepen, C.A., v., Wolf, J. and Keulen, H., v. (1989). WOFOST: a simulation model of crop production, *Soil Use and Management* **5**: 16–24.
- Doraiswamy, P. C., Sinclair, T. R., Hollinger, S., Akhmedov, B., Stern, A. and Prueger, J. (2005). Application of MODIS derived parameters for regional crop yield assessment, *Remote Sensing of Environment* **97**(2): 192–

- 202.
- Dorigo, W., Zurita-Milla, R., De Wit, A. J. W., Brazile, J., Singh, R. and Schaepman, M. (2006). A review on reflective remote sensing and data assimilation techniques for enhanced agroecosystem modeling, *International Journal of Applied Earth Observation and Geoinformation* **9**(2): 165–193.
- Easterling, W. E., Weiss, A., Hays, C. J. and Mearns, L. O. (1998). Spatial scales of climate information for simulating wheat and maize productivity: the case of the US Great Plains, *Agricultural and Forest Meteorology* **90**(1-2): 51–63.
- EUROSTAT (2005). *European regional and urban statistics – Reference guide*, Office for official publications of the European Communities, Luxembourg.
- Evensen, G. (2003). The ensemble Kalman filter: theoretical formulation and practical implementation, *Ocean Dynamics* **53**(4): 343–367.
- Faivre, R. and Fischer, A. (1997). Predicting crop reflectances using satellite data observing mixed pixels, *Journal of Agricultural, Biological, and Environmental Statistics* **2**(1): 87.
- FAO (2007). <http://www.fao.org/GIEWS/english/hotspots/index.htm>, Internet URL.
- Fischer, A. (1994). A model for the seasonal variations of vegetation indices in coarse resolution data and its inversion to extract crop parameters, *Remote Sensing of Environment* **48**(2): 220–230.
- Fodor, N. and Kovacs, G. J. (2005). Sensitivity of crop models to the inaccuracy of meteorological observations, *Physics and Chemistry of the Earth, Parts A/B/C* **30**(1-3): 53–57.
- Frère, M. and Popov, G. (1986). Early agrometeorological crop yield forecasting. FAO plant production and protection paper No. 73, *Technical report*, Food and Agriculture Organisation.
- Genovese, G. (1998). The methodology, the results and the evaluation of the MARS crop yield forecasting system, in D. Rijks, J. Terres and P. Vossen (eds), *Agrometeorological applications for regional crop monitoring and production assessment*, Office for official publications of the EU, EUR 17735 EN, Luxembourg, pp. 67–119.
- Georgakakos, K. P., Seo, D. J., Gupta, H., Schaake, J. and Butts, M. B. (2004). Towards the characterization of streamflow simulation uncertainty through multimodel ensembles, *Journal of Hydrology* **298**(1-4): 222–241.
- Gijsman, A. J., Jagtap, S. S. and Jones, J. W. (2002). Wading through a swamp of complete confusion: how to choose a method for estimating soil water retention parameters for crop models, *European Journal of Agronomy* **18**(1-2): 77–106.
- Goovaerts, P. (1997). *Geostatistics for Natural Resources Evaluation*, Oxford



- university press, New York.
- Gozzini, B. and Paniagua, S. (2000). *Coordination and comparison of several interpolation methods of meteorological data (minimum temperature)*, Office for Official Publications of the EU, Luxembourg.
- Grimes, D. I. F., Coppola, E., Verdecchia, M. and Visconti, G. (2003). A neural network approach to real-time rainfall estimation for Africa using satellite data, *Journal of Hydrometeorology* **4**(6): 1119–1133.
- Guérif, M. and Duke, C. L. (2000). Adjustment procedures of a crop model to the site specific characteristics of soil and crop using remote sensing data assimilation, *Agriculture, Ecosystems and Environment* **81**(1): 57–69.
- Hansen, J. W. and Jones, J. W. (2000). Scaling-up crop models for climate variability applications, *Agricultural Systems* **65**(1): 43–72.
- Hansen, J. W., Potgieter, A. and Tippet, M. K. (2004). Using a general circulation model to forecast regional wheat yields in northeast Australia, *Agricultural and Forest Meteorology* **127**(1-2): 77–92.
- Hansen, M., DeFries, R., Townshend, J., Carroll, M., Dimiceli, C. and Sohlberg, R. (2003). Global percent tree cover at a spatial resolution of 500 meters: First results of the MODIS vegetation continuous fields algorithm, *Earth Interactions* **7**: 1–15.
- Hartkamp, A., White, J. and Hoogenboom, G. (1999). Interfacing geographic information systems with agronomic modeling : A review, *Agronomy Journal* **91**(5): 762–772.
- Hasenauer, S., Wagner, W., Scipal, K., Naeimi, V. and Bartalis, Z. (2006). Implementation of near real time soil moisture products in the SAF network based on METOP ASCAT data, *EUMETSAT Meteorological Satellite Conference*, Helsinki, Finland.
- Hoogenboom, G. (2000). Contribution of agrometeorology to the simulation of crop production and its applications, *Agricultural and Forest Meteorology* **103**(1-2): 137–157.
- Hossain, F. and Anagnostou, E. N. (2006). A two-dimensional satellite rainfall error model, *IEEE Transactions on Geoscience and Remote Sensing* **44**(6): 1511–1522.
- Kerr, Y. H., Waldteufel, P., Wigneron, J. P., Martinuzzi, J. M., Font, J. and Berger, M. (2001). Soil moisture retrieval from space: The soil moisture and ocean salinity (SMOS) mission, *IEEE Transactions on Geoscience and Remote Sensing* **39**(8): 1729–1735.
- King, D. (1990). The available water capacity map compiled from the European Community soils map at scale one to one million, in F. Toselli and J. Meyer-Roux (eds), *Proceedings of conference on the application of remote sensing to agricultural statistics*, Vol. EUR 12581 EN, Office for Official Publications of the EU, Luxembourg, pp. 235–242.

- King, D., Burril, A., Daroussin, J., Le Bas, C., Tavernier, R. and Van Ranst, E. (1995). The EU soil geographic database, in D. King, R. Jones and A. Thomasson (eds), *European land information systems for agro-environmental monitoring*, EUR 16232 EN, Office for Official Publications of the EU, Luxembourg, pp. 43–60.
- Koslowsky, D. (2003). 12 years Mediterranean satellite data set and analyses, in H.-J. Bolle (ed.), *Mediterranean Climate*, Springer-Verlag, Berlin Heidelberg New York, pp. 165–177.
- Koslowsky, D., Billing, H. and Eckardt, M. (2001). Sensor degradation and inter-calibration of the shortwave channels of the AVHRR - NOAA 11/14/16 satellites, *Proceedings of the 2001 EUMETSAT Meteorological Satellite Data Users' Conference*, Antalya, Turkey, pp. 107–113.
- Kraalingen, D. v. and Rappoldt, C. (2000). Reference manual of the FORTRAN utility library TTUTIL v. 4, *Technical report*, Plant Research International.
- Kyriakidis, P. C., Miller, N. L. and Kim, J. (2004). A spatial time series framework for simulating daily precipitation at regional scales, *Journal of Hydrology* **297**(1-4): 236–255.
- Lanza, L. (2000). A conditional simulation model of intermittent rain fields, *Hydrology and Earth System Sciences* **4**(1): 173–183.
- Launay, M. and Guérif, M. (2003). Ability for a model to predict crop production variability at the regional scale: an evaluation for sugar beet, *Agronomie* **23**: 135–146.
- Maas, S. J. (1988). Using satellite data to improve model estimates of crop yield, *Agronomy Journal* **80**(4): 655–662.
- Mackay, N. G., Chandler, R. E., Onof, C. and Wheeler, H. S. (2001). Disaggregation of spatial rainfall fields for hydrological modelling, *Hydrology and Earth System Sciences* **5**(2): 165–173.
- Margulis, S. A., Entekhabi, D. and McLaughlin, D. (2006). Spatiotemporal disaggregation of remotely sensed precipitation for ensemble hydrologic modeling and data assimilation, *Journal of Hydrometeorology* **7**(3): 511–533.
- Margulis, S. and Entekhabi, D. (2001). Temporal disaggregation of satellite-derived monthly precipitation estimates and the resulting propagation of error in partitioning of water at the land surface, *Hydrology and Earth System Sciences* **5**(1): 27–38.
- Mathe-Gaspar, G., Fodor, N., Pokovai, K. and Kovacs, G. J. (2005). Crop modelling as a tool to separate the influence of the soil and weather on crop yields, *Physics and Chemistry of the Earth, Parts A/B/C* **30**(1-3): 165–169.
- Mearns, L. O., Easterling, W., Hays, C. and Marx, D. (2001). Comparison of agricultural impacts of climate change calculated from high and low resolution climate change scenarios: Part I. the uncertainty due to spatial

- scale, *Climatic Change* **51**(2): 131–172.
- Mearns, L. O., Mavromatis, T., Tsvetsinskaya, E., Hays, C. and Easterling, W. (1999). Comparative responses of EPIC and CERES crop models to high and low spatial resolution climate change scenarios, *Journal of Geophysical Research-Atmospheres* **104**(D6): 6623–6646.
- Meetschen, D., van den Hurk, B. J., Ament, F. and Drusch, M. (2004). Optimized surface radiation fields derived from Meteosat imagery and a regional atmospheric model, *Journal of Hydrometeorology* **5**(6): 1091–1101.
- Mellor, D., Sheffield, J., O'Connell, P. E. and Metcalfe, A. V. (2000). A stochastic space-time rainfall forecasting system for real time flow forecasting I: Development of MTB conditional rainfall scenario generator, *Hydrology and Earth System Sciences* **4**(4): 603–615.
- Metzger, M., Bunce, R., Jongman, R.H.G. and Mùcher, C. and Watkins, J. (2005). A climatic stratification of the environment of Europe, *Global Ecology and Biogeography* **14**(6): 549–563.
- Mo, X., Liu, S., Lin, Z., Xu, Y., Xiang, Y. and McVicar, T. (2005). Prediction of crop yield, water consumption and water use efficiency with a SWAT-crop growth model using remotely sensed data on the North China Plain, *Ecological Modelling* **183**(2-3): 301–322.
- Monteith, J. and Unsworth, M. (1990). *Principles of Environmental Physics*, Arnold, London.
- Moulin, S., Bondeau, A. and Delecolle, R. (1998). Combining agricultural crop models and satellite observations: from field to regional scales, *International Journal of Remote Sensing* **19**(6): 1021–1036.
- Moulin, S., Fischer, A., Dedieu, G. and Delecolle, R. (1995). Temporal variations in satellite reflectances at field and regional scales compared with values simulated by linking crop growth and SAIL models, *Remote Sensing of Environment* **54**(3): 261–272.
- Mùcher, C., Champeaux, J., Steinnocher, K., Griguolo, S., Wester, K., Heunks, C., Winiwater, W., Kressler, F., Goutorbe, J., ten Brink, B., van Katwijk, V., Furberg, O., Perdigao, V. and Nieuwenhuis, G. (2001). Development of a consistent methodology to derive land cover information on a European scale from remote sensing for environmental monitoring, the PELCOM report, *Technical Report Alterra-report 178*, Alterra, Green World Research.
- Mùcher, C., Steinnocher, K., Kressler, F. and Heunks, C. (2000). Land cover characterization and change detection for environmental monitoring of pan-Europe, *International Journal of Remote Sensing* **21**: 1159–1181.
- Nemecek, T., Derron, J. O., Roth, O. and Fischlin, A. (1996). Adaptation of a crop-growth model and its extension by a tuber size function for use in a

- seed potato forecasting system, *Agricultural Systems* **52**(4): 419–437.
- Nieuwenhuis, G. J. A., Van der Wal, T., Mucher, C. and De Wit, A. J. W. (1998). Integrated use of high and low resolution satellite data and crop growth models, in D. Rijks, J. Terres and V. P. (eds), *Agrometeorological applications for regional crop monitoring and product assessment.*, Vol. EUR 17735 EN, Joint Research Centre, European Commission, pp. 147–159.
- Nieuwenhuis, G., Wit, A. d., Kraalingen, D. v., Diepen, C. v. and Boogaard, H. (2006). Monitoring crop growth conditions using the global water satisfaction index and remote sensing, *Proceedings of the ISPRS commission VII mid-term symposium: From pixels to processes*, pp. 686–687.
- Nonhebel, S. (1994). The effects of use of average instead of daily weather data in crop growth simulation models, *Agricultural Systems* **44**(4): 377–396.
- Oleson, J., Bøcher, P. and Jensen, T. (2000). Comparison of scales of climate and soil data for aggregating simulated yields of winter wheat in Denmark, *Agricultural, Ecosystems and Environment* **82**: 213–228.
- Olioso, A., Inoue, Y., Ortega-Farias, S., Demarty, J., Wigneron, J. P., Braud, I., Jacob, F., Lecharpentier, P., Ottlé, C., Calvet, J. C. and Brisson, N. (2005). Future directions for advanced evapotranspiration modeling: Assimilation of remote sensing data into crop simulation models and SVAT models, *Irrigation and Drainage Systems* **19**(3 - 4): 377–412.
- Ouaidrari, H., Goward, S., Czajkowski, K., Sobrino, J. and Vermote, E. (2002). Land surface temperature estimation from AVHRR thermal infrared measurements - an assessment for the AVHRR Land Pathfinder II data set, *Remote Sensing of Environment* **81**(1): 114–129.
- Pachepsky, Y. and Acock, B. (1998). Stochastic imaging of soil parameters to assess variability and uncertainty of crop yield estimates, *Geoderma* **85**(2-3): 213–229.
- Pardo-Igúzquiza, E., Grimes, D. I. F. and C.-K., T. (2006). Assessing the uncertainty associated with intermittent rainfall fields, *Water Resour. Res.* **42**.
- Pellarin, T., Calvet, J. and Wagner, W. (2006). Evaluation of ERS scatterometer soil moisture products over a half-degree region in southwestern France, *Geophysical Research Letters* **33**: L17401.
- Pellenq, J. and Boulet, G. (2004). A methodology to test the pertinence of remote-sensing data assimilation into vegetation models for water and energy exchange at the land surface, *Agronomie* **24**(4): 197–204.
- Prevot, L., Chauki, H., Troufleau, D., Weiss, M., Baret, F. and Brisson, N. (2003). Assimilating optical and radar data into the STICS crop model for wheat, *Agronomie* **23**(4): 297–303.
- Qin, Z. and Karnieli, A. (1999). Progress in the remote sensing of land surface

- temperature and ground emissivity using NOAA-AVHRR data, *International Journal of Remote Sensing* **20**(12): 2367–2394.
- Reichle, R. H. and Koster, R. D. (2005). Global assimilation of satellite surface soil moisture retrievals into the NASA catchment land surface model, *Geophysical Research Letters* **32**(2): –.
- Reichle, R. H., McLaughlin, D. B. and Entekhabi, D. (2002). Hydrologic data assimilation with the ensemble Kalman filter, *Monthly Weather Review* **130**(1): 103–114.
- Reichle, R. H., Walker, J. P., Koster, R. D. and Houser, P. R. (2002). Extended versus ensemble Kalman filtering for land data assimilation, *Journal of Hydrometeorology* **3**(6): 728–740.
- Roebeling, R. A., Van Putten, E., Genovese, G. and Rosema, A. (2004). Application of Meteosat derived meteorological information for crop yield predictions in Europe, *International Journal of Remote Sensing* **25**(23): 5389–5401.
- Rubel, F., Brugger, K., Skomorowski, P. and Kotteck, M. (2004). Daily and 3-hourly quantitative precipitation estimation for ELDAS, in P. Viterbo and B. Van den Hurk (eds), *ECMWF/ELDAS Workshop on Land Data Assimilation*, ECMWF - Proceedings, European Centre for Medium-range Weather Forecasts, Reading, pp. 19–32.
- Rubel, F. and Hantel, M. (2001). BALTEX 1/6-degree daily precipitation climatology 1996-1998, *Meteorol. Atmos. Phys.* **77**: 155–166.
- Russel, G. and Gardingen, P.R., v. (1997). Problems with using models to predict regional crop production, in v. Gardingen, P.R., M. Foody and P. Curran (eds), *Scaling up: from cell to landscape*, Cambridge University Press, Cambridge, pp. 273–294.
- Salisbury, J. and D'Aria, D. (1992). Emissivity of terrestrial materials in the 8-14  $\mu\text{m}$  atmospheric window, *International Journal of Remote Sensing* **35**: 141–148.
- Schneider, K. (2003). Assimilating remote sensing data into a land-surface process model, *International Journal of Remote Sensing* **24**(14): 2959–2980.
- Semenov, M. A. and Porter, J. R. (1995). Non-linearity in climate change impact assessments, *Journal of Biogeography* **22**(4-5): 597–600.
- Seo, D. J., Perica, S., Welles, E. and Schaake, J. C. (2000). Simulation of precipitation fields from probabilistic quantitative precipitation forecast, *Journal of Hydrology* **239**(1-4): 203–229.
- Sharman, M. (1992). Action II: Monitoring vegetation with AVHRR: purpose, principles and products, in F. Toselli and J. Meyer-Roux (eds), *Conference on application of remote sensing to agricultural statistics*, Vol. EUR 14262 EN, pp. 145–158.

- Sobrino, J. A., Coll, C. and Caselles, V. (1991). Atmospheric correction for land surface temperature using NOAA-11 AVHRR channel 4 and 5, *Remote Sensing of Environment* **38**: 19–34.
- Soltani, A., Meinke, H. and de Voil, P. (2004). Assessing linear interpolation to generate daily radiation and temperature data for use in crop simulations, *European Journal of Agronomy* **21**(2): 133–148.
- Supit, I. (1997). Predicting national wheat yields using a crop simulation and trend models, *Agricultural and Forest Meteorology* **88**(1-4): 199–214.
- Supit, I., Hooijer, A. and Diepen van, C. (1994). System description of the WOFOST 6.0 crop simulation model implemented in CGMS, volume 1: Theory and algorithms., *Technical Report EUR 15956 EN*, Joint Research Center, Commission of the European Communities.
- Supit, I. and van Kappel, R. R. (1998). A simple method to estimate global radiation, *Solar Energy* **63**(3): 147–160.
- Syed, T., Lakshmi, V., Paleologos, E., Lohmann, D., Mitchell, K. and Famiglietti, J. (2004). Analyses of process controls in land surface hydrological cycle over the continental United States, *Journal of Geophysical Research* **109**(D22105).
- Thorne, V., Coakely, D., Grimes, D. and Dugdale, G. (2001). Comparison of TAMSAT and CPC rainfall estimates with raingauges, for southern Africa, *International Journal of Remote Sensing* **22**(10): 1951–1974.
- Thornton, P. K., Bowen, W. T., Ravelo, A. C., Wilkens, P. W., Farmer, G., Brock, J. and Brink, J. E. (1997). Estimating millet production for famine early warning: an application of crop simulation modelling using satellite and ground-based data in Burkina Faso, *Agricultural and Forest Meteorology* **83**(1-2): 95–112.
- USDA (2007). <http://www.pecad.fas.usda.gov/cropexplorer/>.
- van Ittersum, M. K., Leffelaar, P. A., van Keulen, H., Kropff, M. J., Bastiaans, L. and Goudriaan, J. (2003). On approaches and applications of the Wageningen crop models, *European Journal of Agronomy* **18**(3-4): 201–234.
- Verdin, J. and Klaver, R. (2002). Grid cell based crop water accounting for the famine early warning system, *Hydrological Processes* **16**: 1617–1630.
- Vinnikov, K., Robock, A., Qui, S., Entin, J., Owe, M., Choudhury, B., Hollinger, S. and Njoku, E. (1999). Satellite remote sensing of soil moisture in Illinois. USA., *J. Geophys. res.* **104**: 4145–4168.
- Vinnikov, K. Y., Robock, A., Speranskaya, N. A. and Schlosser, C. A. (1996). Scales of temporal and spatial variability of midlatitude soil moisture, *J. Geophys. res.* **101**: 7163–7174.
- Voet, P., v. d., Diepen, C.A., v. and Oude Voshaar, J. (1994). Spatial interpolation of daily meteorological data: a knowledge based procedure for

- the regions of the European Community, *Technical Report SC report 53/3*, DLO Winand Staring Centre.
- Vossen, P. (1992). Forecasting national crop yields of E.C. countries: the approach developed by the agriculture project, in F. Toselli and J. Meyer-Roux (eds), *Conference on application of remote sensing to agricultural statistics*, Vol. EUR 14262 EN, Office for Official publications of the EU, Belgirate, Italy, pp. 159–176.
- Vossen, P. (1995). Early crop production assessment of the European Union, the systems implemented by the MARS-STAT project, in J. Dallemand and P. Vossen (eds), *Workshop for Central and Eastern Europe on agrometeorological models: theory and applications in the MARS project*, Vol. EUR 16008 EN, Office for Official Publications of the EU, Ispra, Italy, pp. 21–51.
- Vossen, P. and Rijks, D. (1995). Early crop yield assessment of the E.U. countries: the system implemented by the Joint Research Centre, *Technical Report EUR 16318*, Publication of the Office for Official Publications of the E.C.
- Wagner, W., Lemoine, G. and Rott, H. (1999). A method for estimating soil moisture from ERS scatterometer and soil data, *Remote Sensing of Environment* **70**(2): 191–207.
- Wagner, W., Scipal, K., Pathe, C., Gerten, D., Lucht, W. and Rudolf, B. (2003). Evaluation of the agreement between the first global remotely sensed soil moisture data with model and precipitation data, *Journal of Geophysical Research D: Atmospheres* **108**(19).
- Wilks, D. S. and Wilby, R. L. (1999). The weather generation game: a review of stochastic weather models, *Progress in Physical Geography* **23**(3): 329–357.
- Wit, A. J. W. d., Boogaard, H. L. and Diepen, C. A. v. (2004). Using NOAA-AVHRR estimates of land surface temperature for regional agrometeorological modelling, *International Journal of Applied Earth Observation and Geoinformation* **5**(3): 187–204.
- Wit, A.J.W., d., Boogaard, H. and Diepen, C.A., v. (2005). Spatial resolution of precipitation and radiation: The effect on regional crop yield forecasts, *Agricultural and Forest Meteorology* **135**(1-4): 156–168.
- Wit, A.J.W., d. and Bruin, S., d. (2006). Simulating space-time uncertainty in continental-scale gridded precipitation fields for agrometeorological modelling, in M. Caetano and M. Painho (eds), *Accuracy 2006*, Instituto Geográfico Português, Lisbon, Portugal, pp. 367–376.
- Wit, A.J.W., d., Bruin, S., d. and Torfs, P. (2007). Representing uncertainty in continental-scale gridded precipitation fields for agrometeorological modelling, *Journal of Hydrometeorology* **revised version submitted**.

- Wit, A.J.W., d. and Diepen, C.A., v. (2007). Crop model data assimilation with the ensemble Kalman filter for improving regional crop yield forecasts, *Agricultural and Forest Meteorology* **in press**.
- Yang, C., Chandler, R. E., Isham, V. S. and Wheeler, H. S. (2005). Spatial-temporal rainfall simulation using generalized linear models, *Water Resources Research* **41**(W11415): 1–13.
- Yun, J. I. (2003). Predicting regional rice production in South Korea using spatial data and crop-growth modeling, *Agricultural Systems* **77**(1): 23–38.



## Extended summary

Information on the outlook of yield and production of crops over large regions is essential for government services dealing with import and export of food crops, for agencies with a role in food relief, for international organisations with a mandate in monitoring the world food production and trade, as well as for commodity traders. In Europe, such information is provided by the MARS (Monitoring Agriculture with Remote Sensing) Crop Yield Forecasting System operated by the Joint Research Centre. Since 1994, this system provides objective crop yield forecasts early in the season for all European Union member states. In recent years, the system has been extended to cover other areas of interest such as the Horn of Africa and Central Asia as well as a dedicated system with global coverage.

An important component in the MARS Crop Yield Forecasting System is the so-called Crop Growth Monitoring System (CGMS) which employs a crop growth model to determine the influence of soil, weather and management on crop yield. For this purpose, soil, management and weather data are gathered over Europe on a  $50 \times 50$  km grid and the WOFOST crop growth model (World Food Studies) is applied to each grid to simulate the growth of specific crops. The simulation results per crop type are stored in a database and spatially aggregated to provinces and countries to be used as predictors for crop yield.

Although CGMS is being applied successfully within the framework of the MARS crop yield forecasting system, there are large uncertainties related to applying crop growth models over such large areas. Examples of these uncertainties are the generally unknown within-season sowing dates, the uncertainty in the effect of drought due to limited weather station density and poorly known soil parameters, the lack of information about irrigation and the weighting of individual simulation results to administrative regions. This thesis focuses on developing and testing methods for quantifying and reducing uncertainty on the crop model simulations that are used for crop yield forecasting. The ultimate goal is to improve the accuracy and timeliness of regional crop yield forecasts.

The basis for quantifying uncertainty is to use an ensemble of models

where the variability in the outcome of the individual models within the ensemble is an indication of the uncertainty in the final crop yield forecast. Reducing uncertainty is attempted by combining crop model simulations with satellite-derived information through an ensemble Kalman filter (EnKF).

A key aspect in this approach is that the uncertainty of the different components of the system can be estimated properly. It was argued on both theoretical and practical grounds that the interpolated meteorological forcings which are driving the crop growth model are the main uncertainty in the system. The main argument for the dominant effect of uncertainty in weather is that crop yield forecasting systems do not predict crop yield directly, but merely aim to capture the year-to-year pattern of crop response to weather variability. In such a system, the influence of relatively stable factors like soil and management is secondary to factors that generate the year-to-year variability in simulated crop yield (mainly variability in weather).

Based on the results from chapters 2 and 3 it was indeed demonstrated that the uncertainty in the interpolated meteorological forcings is important. In particular uncertainty in the temporal and spatial distribution of precipitation has a strong effect on the results of the crop growth model because it determines the amount of moisture in the soil that is available for the plant. Uncertainty in precipitation was found to be particularly important in areas which are marginal for crop growth. This dominant role of precipitation is in agreement with results from hydrological land surface models where precipitation is generally acknowledged to be the key variable. Additionally, it was demonstrated that when local ( $50 \times 50$  km) crop simulation results are aggregated to large areas, the effect of uncertainty in precipitation strongly diminishes and its influence on the yield forecast for Germany and France was found to be small.

In chapter 4 a method was developed to operationally quantify and visualise uncertainty due to precipitation forcings. This method works by creating ensembles of equiprobable realisations of precipitation inputs which can be used as input in the crop simulation model in order to obtain an ensemble of crop simulation results. The variability in the ensemble of crop simulations results is a measure for the influence of uncertainty in precipitation.

The conclusions from this work were that the statistical properties of the precipitation field were reproduced reasonably well in the realisations that the method produces. Moreover, the deviations from the target statistics that were found are of minor importance for crop simulation models. Finally, it was demonstrated that the uncertainty in input precipitation fields and the resulting variability in crop model simulation results considerably influence the yield forecast for a region in South-France.

In chapter 5 the WOFOST model was coupled to an ensemble Kalman filter

which enabled assimilating satellite observations of soil moisture. The goal of this procedure is reducing the uncertainty in the WOFOST simulated soil moisture as a result of uncertainty in precipitation. This approach was tested for Spain, France, Germany and Italy for winter-wheat and grain maize. For these regions and crops, the WOFOST model was applied and root-zone soil moisture estimates based upon the satellite-derived Soil Water Index (SWI) over the period 1992–2000 were assimilated into the WOFOST model. Validation was carried out by checking if 1) the approach lowered the error on a linear regression model between crop simulation model output and EUROSTAT crop yield statistics for administrative regions, and 2) the regression model performed better than a model based on a trend only. Additionally, the innovations of the ensemble Kalman filter provided diagnostics that were used to trace deficiencies in the model.

With regard to the relationship with EUROSTAT crop yield statistics, our results demonstrate that the assimilation of SWI has lowered the error with crop yield statistics for winter-wheat for the majority of regions (66%) where a relationship could be established (i.e. better than the trend only). For grain maize the improvement was less evident because improved relationships could only be found for 56% of the regions. At national level, the results of the regression only improved for Spain, but not for Germany, France and Italy. Although the results at national level were somewhat disappointing, it is encouraging that the results did improve for Spain where crop production is most affected by water limitations and thus the potential for improvement using SWI is greatest.

With regard to the innovations of the ensemble Kalman filter, the results demonstrated that the assumptions underlying the EnKF were not entirely fulfilled, given that the normalised innovations were not Gaussian and that the resulting spatial and temporal patterns showed clear correlation structures. This indicates that the innovations made to the model water balance were not the result of pure random noise, but included systematic deviations in the model dynamics and/or a poorly known error structure in the satellite-derived soil moisture estimates. Based on the excessive spread in the distribution of normalised innovations, it was concluded that errors on both model simulations and satellite observations were underestimated. This demonstrates that additional sources of error need to be included in the simulations and observations.

Finally, in chapter 6 it was concluded that the developed approach is operationally feasible because the algorithms are applicable at continental scale, the satellite data applied will be available at least until 2018 and the method does not rely on site-specific data. Therefore, the approach presented in this thesis could be applied within the European MARS system and has the po-

tential to provide improved crop yield indicators for crop yield forecasting in many areas with major agricultural production of rainfed crops. On the other hand, its application for food security monitoring was deemed useful only when combined with a more advanced analyses which should include spatially distributed socio-economic data to explain the anthropogenic influences on regional crop yield and production and their impact on food security.

# Samenvatting

Vroegtijdige informatie over de opbrengst en productie van landbouwgewassen voor regio's en landen is essentieel voor het functioneren van een groot aantal organisaties en diensten. Voorbeelden hiervan zijn overheidsdiensten die import en export van landbouwproducten reguleren, organisaties die in voedselhulp voorzien, internationale organisaties die de globale voedselproductie en handel monitoren, maar ook voor handelaren in agrarische producten. In Europa wordt, ten behoeve van het EU beleid, dergelijke informatie verzameld en verstrekt door het MARS oogstvoorspellingssysteem dat door het Joint Research Centre wordt beheerd. Sinds 1994 voorziet dit systeem de Europese Commissie van vroegtijdige oogstvoorspellingen van een aantal belangrijke gewassen voor alle Europese lidstaten en aangrenzende regio's. In de afgelopen jaren is het systeem uitgebreid naar andere, voor de EU belangrijke, regio's zoals de Hoorn van Afrika en Centraal Azië.

Een belangrijk onderdeel van het MARS oogstvoorspellingssysteem is het zogenaamde CGMS (Crop Growth Monitoring System). CGMS gebruikt een gewasgroeimodel om het effect van bodem, weer en teeltmaatregelen op de groei van het gewas te bepalen. Hiervoor worden relevante gegevens verzameld over Europa, waarna ze worden geïnterpoleerd en opgeslagen in een grid structuur met een grid grootte van  $50 \times 50$  km. Het WOFOST (WORLD FOOD STudies) gewasgroeimodel wordt vervolgens toegepast voor ieder  $50 \times 50$  km grid om de groei van een aantal belangrijke gewassen te simuleren. De simulatie resultaten worden ruimtelijk geaggregeerd naar provincies en landen en gebruikt als indicatoren in een statistisch model dat de uiteindelijke oogst voorspelt.

Hoewel CGMS een zeer succesvol onderdeel is van het MARS oogstvoorspellingssysteem zijn er toch grote onzekerheden met betrekking tot het toepassen van gewasgroeimodellen over dergelijke grote gebieden. Voorbeelden van deze onzekerheden zijn het gebrek aan kennis over de actuele zaaidatum van gewassen, onzekerheid in het effect van droogte door de beperkte dichtheid van weerstations en beperkte kennis van de bodemfysische eigenschappen, gebrek aan inzicht over het toepassen van irrigatie, en onzekerheden in

de aggregatie van individuele simulatieresultaten naar regio's en landen. Het werk dat in dit proefschrift wordt beschreven is er op gericht methoden te ontwikkelen en te testen om het effect van deze onzekerheden te kwantificeren en waar mogelijk te verkleinen. Het ultieme doel is om de nauwkeurigheid van de oogstvoorspellingen die met behulp van CGMS worden gemaakt te verbeteren.

Om de onzekerheid in de uitkomsten van CGMS te kwantificeren is er voor gekozen om gebruik te maken van een ensemble van gewasgroei simulaties. Bij een dergelijke aanpak wordt er niet één simulatie uitgevoerd, maar wordt er een groot aantal simulaties uitgevoerd waarbij de variabiliteit in de uitkomsten een maat is voor de onzekerheid in het systeem en de uiteindelijke oogstvoorspelling. Om de onzekerheid in de uitkomsten van CGMS te verkleinen is gebruik gemaakt van satellietwaarnemingen van het bodemvocht die het gesimuleerde bodemvochtgehalte bij kunnen sturen. Hiervoor is een Ensemble Kalman filter gebruikt en deze techniek wordt 'data-assimilatie' genoemd.

Een belangrijk aspect bij deze aanpak is dat de onzekerheid in de verschillende onderdelen (weer, modelparameters, bodem, teeltmaatregelen) goed kan worden geparаметeriseerd. In dit proefschrift wordt op praktische en theoretische gronden beargumenteerd dat de onzekerheid in het weer de bepalende factor is voor onzekerheid in de WOFOST simulaties. Dit komt omdat de weersgegevens afkomstig zijn van een beperkt aantal weerstations over Europa en met deze reeks is het niet mogelijk om de daadwerkelijke ruimtelijke en temporele variabiliteit in het weer (neerslag, straling en temperatuur) te beschrijven. Daarnaast is het zo dat oogstvoorspellingssystemen de opbrengst van gewassen niet direct voorspellen, maar er op gericht zijn om variabiliteit in opbrengst tussen jaren goed te voorspellen. In een dergelijk systeem zijn statische factoren zoals bodem en teeltmaatregelen minder belangrijk dan een dynamische factor zoals het weer die uiteindelijk de variabiliteit in opbrengst tussen jaren genereert.

Op basis van de resultaten in hoofdstukken 2 & 3 kon inderdaad worden gedemonstreerd dat de onzekerheid in het geïnterpoleerde weer belangrijk is. Met name de onzekerheid in de temporele en ruimtelijke variabiliteit van de neerslag heeft een grote invloed op de simulatieresultaten van het WOFOST gewasgroei-model en vooral in gebieden die marginaal geschikt zijn voor landbouw. Naarmate de simulatieresultaten voor individuele  $50 \times 50$  grid cellen verder werden geaggregeerd naar grotere gebieden dan werd de invloed van de onzekerheid in neerslag echter snel kleiner. Op het niveau van landen als Frankrijk en Duitsland kon worden aangetoond dat de invloed van de onzekerheid in neerslag op de voorspelling voor maïs uiteindelijk klein was.

In hoofdstuk 4 wordt een methode beschreven om de onzekerheid in neerslag op een operationele manier te kunnen kwantificeren en visualiseren. Het

idee achter deze methode is om niet één ‘versie’ van de dagelijkse neerslag gegevens te gebruiken in WOFOST, maar om een ensemble aan versies (realisaties) te gebruiken waarbij iedere versie (realisatie) anders is, maar wel even plausibel binnen de grenzen van de onzekerheid die er is. Het ensemble aan neerslagrealisaties kan vervolgens worden gebruikt om een ensemble van WOFOST simulaties te genereren. De variabiliteit in de uitkomsten van de WOFOST simulaties is dan een maat voor de invloed van de onzekerheid in de neerslag.

Uit de resultaten van hoofdstuk 4 kan worden geconcludeerd dat de ontwikkelde methode voor het genereren van neerslagrealisaties voldoet. De statistische eigenschappen van de waargenomen neerslagverdeling worden vrij goed gereproduceerd door de realisaties van de neerslag en de afwijkingen die zijn geconstateerd hebben weinig invloed op de resultaten van het WOFOST gewasgroeimodel. Het gebruik van deze neerslagrealisaties is uiteindelijk gedemonstreerd voor een provincie in Zuid-Frankrijk waar kon worden aangetoond dat de onzekerheid in neerslag een aanzienlijke invloed had op de oogstvoorspelling voor deze regio.

In hoofdstuk 5 is het WOFOST model gekoppeld met een Ensemble Kalman filter om assimilatie van door satellieten waargenomen bodemvocht mogelijk te maken. Het doel van deze aanpak is om de simulatie van het bodemvocht te verbeteren, waardoor ook de uiteindelijke oogstvoorspelling kan worden verbeterd. Deze aanpak is uitgevoerd voor Spanje, Italië, Frankrijk en Duitsland voor winter-tarwe en maïs. Voor deze regio’s en gewassen is het WOFOST model toegepast en zijn bodemvocht schattingen geassimileerd die zijn afgeleid van satellietwaarnemingen over de periode 1992-2000. De resultaten zijn gevalideerd door te bepalen of de methode met assimilatie van bodemvocht resulteerde in betere regressiemodellen tussen WOFOST simulatieresultaten en EUROSTAT opbrengst statistieken, dan de klassieke methode zonder data-assimilatie.

De validatie met de EUROSTAT statistieken toonde aan dat de nieuwe methode met data-assimilatie voor winter-tarwe in 66% van de regio’s leidde tot betere regressiemodellen dan de klassieke methode. Voor maïs waren de resultaten iets minder positief omdat slechts voor 56% van de regio’s een verbetering kon worden vastgesteld. Op nationaal niveau verbeterden de regressiemodellen alleen voor Spanje en niet voor de overige landen. Hoewel dit resultaat enigszins teleurstelt, is het bemoedigend dat verbetering kon worden vastgesteld voor Spanje waar het effect van droogte doorgaans het grootst is en waar dus het potentieel voor verbetering d.m.v. data-assimilatie het grootst is.

In het laatste hoofdstuk wordt geconcludeerd dat de methoden die in dit proefschrift ontwikkeld en getest zijn operationeel kunnen worden toegepast

omdat ze voldoen aan een aantal operationele randvoorwaarden, zoals gegarandeerde data beschikbaarheid van satellieten en schaalbaarheid in tijd en ruimte. De ontwikkelde aanpak kan dus operationeel worden geïmplementeerd in het Europese MARS oogstvoorspellingssysteem, maar kan in principe globaal worden toegepast in gebieden met niet-geïrrigeerde landbouw. Verder wordt geconcludeerd dat de ontwikkelde methoden minder bruikbaar zijn voor toepassingen op het gebied van monitoring van hongersnoden.



# Curriculum vitae

Allard Johannes Wilhelmus de Wit was born on July 3 1973 in Alkmaar, The Netherlands. He holds an MSc degree from the Free University of Amsterdam which he finished in 1996 with specialisations in Hydrology, Physical Geography and Remote Sensing.

He was employed for one year at the Survey Department of the Ministry of Transport, Public Works and Water Management where he focussed on the use of remote sensing change detection techniques for updating road network databases. In 1997 he started working for the Centre for Geoinformation at Alterra Green World Research.

From 1997 to 2000 he was project leader of the National land use database (LGN) which aimed at maintaining and improving LGN. Since 2000 he is involved in several projects on the use of agrometeorological and remote sensing techniques for operational crop yield forecasting in Europe and China, as well as other national and EU activities.

His current research focuses on improving the regional application of crop models and the uncertainties involved in moving from point scale to regional scale. His interests focus in particular on the use of remote sensing to improve the output of crop models by applying data assimilation techniques.



## Selected publications

- Bruin, S. d., Wit, A.J.W. d., Van Oort, P.A.J. and Gorte, B.G.H., 2004. Using quadtree segmentation to support error modelling in categorical raster data. *International Journal of Geographical Information Science*, **18**(2): 151-168.
- Bruin, S. d. and Wit, A.J.W. d., 2005. Stochastic simulation of large grids using free and public domain software. *Computers and Geosciences*, **31**(7): 828-836.
- Dorigo, W.A., Zurita-Milla, R., Wit, A.J.W. d., Brazile, J., Singh, R. and Schaepman, M.E., 2007. A review on reflective remote sensing and data assimilation techniques for enhanced agroecosystem modeling. *International Journal of Applied Earth Observation and Geoinformation*, **9**(2): 165-193.
- Van Oort, P.A.J., Bregt, A.K., Bruin, S. d., Wit, A.J.W. d. and Stein, A., 2004. Spatial variability in classification accuracy of agricultural crops in the Dutch national land-cover database. *International Journal of Geographical Information Science*, **18**(6): 611-626.
- Wit, A.J.W. d., 1999. Application of a genetic algorithm for crop model steering using NOAA-AVHRR data, *Proceedings of SPIE - The International Society for Optical Engineering*, pp. 167-181.
- Wit, A.J.W. d., Boogaard, H.L. and Diepen, C.A. v, 2004. Using NOAA-AVHRR estimates of land surface temperature for regional agrometeorological modelling. *International Journal of Applied Earth Observation and Geoinformation*, **5**(3): 187-204.
- Wit, A.J.W. d. and Clevers, J.G.P.W., 2004. Efficiency and accuracy of per-field classification for operational crop mapping. *International Journal of Remote Sensing*, **25**(20): 4091-4112.
- Wit, A.J.W. d. and Su, B., 2004. Deriving phenological indicators from SPOT-VGT data using the HANTS algorithm. In: F. Veroustraete, E. Bartholomé and W.W. Verstraeten (Editors), *Proceedings of the 2nd international VEG-ETATION user conference*. Office for Official Publications of the European

---

Communities, Antwerp, pp. 195-202.

- Wit, A.J.W.d., Boogaard, H.L. and Diepen, C.A. v., 2005. Spatial resolution of precipitation and radiation: The effect on regional crop yield forecasts. *Agricultural and Forest Meteorology*, **135**(1-4): 156-168.
- Wit, A.J.W. d. and Diepen, C.A. v., 2006. Crop Growth Modelling And Crop Yield Forecasting Using Satellite-Derived Meteorological Inputs. In: J. van Genderen (Editor), *ISPRS Technical Commission VII Symposium: Remote Sensing, from Pixels to Processes*. ITC, Enschede, pp. 667-671.
- Wit, A.J.W. d. and Bruin, S. d., 2006. Simulating space-time uncertainty in continental-scale gridded precipitation fields for agrometeorological modelling. In: M. Caetano and M. Painho (Editors), *Accuracy 2006*. Instituto Geográfico Português, Lisbon, Portugal, pp. 367-376.
- Wit, A.J.W. d. and Diepen, C.A. v., 2007. Crop model data assimilation with the Ensemble Kalman filter for improving regional crop yield forecasts. *Agricultural and Forest Meteorology*, In press.



Netherlands Research School for the  
Socio-Economic and Natural Sciences of the Environment

## CERTIFICATE

The Netherlands Research School for the  
Socio-Economic and Natural Sciences of the Environment  
(SENSE), declares that

*Allard de Wit*

Born on: *3 July 1973* at: *Alkmaar The Netherlands*

has successfully fulfilled all requirements of the  
Educational Programme of SENSE.

Place: *Wageningen* Date: *19 October 2007*

the Chairman of the  
SENSE board

Prof. dr. R. Leemans

the SENSE Director  
of Education

Dr. C. Kroeze



The SENSE Research School declares that Mr. Allard de Wit has successfully fulfilled all requirements of the Educational PhD Programme of SENSE with a work load of 36 ECTS, including the following activities:

PhD courses:

- Techniques for Writing and Presenting a Scientific Paper
- Bayesian Statistics
- IDL advanced programming
- Omgaan met opdrachtgever

Other Activities:

- Writing accepted research proposals accepted by a variety of programmes (EC-FP5/6, GO, NRSP, LNV, Tender-contracts)
- Board member of the Dutch Society for Remote Sensing and Geo-informatics (GIN)
- Organization of GIN workshops
- Guesteditorship for a special issue of the International Journal of Applied Remote Sensing and Geo-information

Oral Presentations:

- VGT user Conference, March 2004, Antwerp, Belgium
- EARSel Conference, July 2004, Dubrovnik, Croatia
- ECMWF Workshop on Land data assimilation, November 2004, Reading, England
- ISPRS commission 7 Conference, May 2006, Enschede, The Netherlands
- Accuracy 2006 Conference, July 2006, Lisbon, Portugal
- CGMS expert meeting, October 2006, Arlon, Belgium
- MARS Workshop remote sensing support to crop yield forecasting, November 2006, Stresa, Italy

Poster Presentations:

- IGARRS conference, July 2003, Toulouse, France
- FP Geoland Forum 3 Conference, February 2006, Vienna, Austria

Deputy director SENSE

Dr. A. van Dommelen